ISRN LUTMDN/TMHP—11/5231—SE
ISSN 0282-1990

Freezing in Fire Sprinkler Systems During Activation at Low Temperatures

Kamil Oskar Bialas

Thesis for the Degree of Master of Science

Division of Heat Transfer
Department of Energy Sciences
Faculty of Engineering, LTH
Lund University
P.O. Box 118
SE-221 00 Lund
Sweden

Freezing in Fire Sprinkler Systems During Activation at Low Temperatures

Kamil Oskar Bialas

21 March 2011

© Kamil Oskar Bialas

Division of Heat Transfer
Department of Energy Sciences
Faculty of Engineering, LTH
Lund University
P.O. Box 118
SE-221 00 Lund
Sweden

Acknowledgements

Firstly of all, I would like to express my gratitude to Magnus Arvidson who took initiative to this thesis. Magnus Arvidson is a fire protection engineer and technical officer at Department of Fire Technology at SP Technical Research Institute of Sweden. He has contributed greatly with help related to general description of sprinkler systems and hydraulic design. Magnus was also a talented organizer of all practical details linked to my time at SP in Borås and was thus a perfect supervisor.

I am indebted to Leif Hanje for defining the subject of this thesis together with Magnus. Leif Hanje is managing director and founder of Ultra Fog AB in Gothenburg, which develops, manufactures and constructs water mist sprinkler systems. I am also grateful to the skilful and inspiring designer from Ultra Fog, Anders Kjellberg for providing much valuable information regarding water mist systems.

At Lund University, I have been very lucky to work with my supervisor and Associate Professor, Christoffer Norberg, to whom I owe pleasant obligation for helping me to find much of literature to this thesis, indefatigability in reading proofs of the report and providing many valuable remarks.

I appreciate kindness of my compatriots at Depratment of Energy Sciences, Associate Professor Janusz Wollerstrand and University Teacher Teresa Hankala-Janiec for providing help in translating abstract to Polish.

Finally I would like to thank my examiner, Professor Bengt Sundén, my reviewers, Erdzan Hodzic and Konrad Tarka and not least the crowd of friends for attending the oral presentation and providing the final remarks.

Preface

This thesis for degree of Master of Science in Mechanical Engineering was conducted at Department of Energy Sciences at Lund University in cooperation with SP Technical Research Institute of Sweden and Ultra Fog AB. The author who beside mechanical engineering studied fire protection engineering as well, will also use this thesis to graduate as Bachelor of Science in Fire Protection Engineering.

Abstract

The subject of this thesis is theoretical examination of freezing phenomena inside fire sprinkler systems during activation at low temperatures in the surroundings. Many sprinkler systems are installed in environments such that they must be operable at subfreezing temperature conditions. During activation of such a system, water is assumed to penetrate a significant distance and without interruption through cooled piping to the sprinkler. The motivation for this study is to investigate whether this is a reasonable assumption.

The objective of this thesis is therefore to present calculation methods that can be used to predict whether system failure due to flow stoppage caused by ice growth at activation is to be feared and to make general observations, whenever possible. Our attention is directed mainly towards high pressure water mist sprinkler systems of dry pipe type. In order to find as far as possible analytical calculation procedures that can be customized to our problem, the approach was literature studies in the field.

The result of this work shows that a sprinkler system during activation may experience complete blockage in two distinctive ways; either due to dendritic or (more unlikely) annular ice growth. The dendritic ice formation mode is characteristic for rather moderate subfreezing temperatures in proximity of 0 °C and is associated with the phenomenon of supercooling of the flowing volume of water which leads to sudden slush ice growth when nucleation starts. On the other hand, at the annular ice growth mode characteristic for lower temperatures, an ice shell at the pipe wall is created immediately in contact with water but is continuously melted away on its upstream-side by gradually warmer water (due to heat up of the system by incoming water).

At the same time, the existing models have been found unsatisfactory to provide complete quantitative description of these phenomena to an extent sufficient to solve our problem. This means that complete blockage of a sprinkler system at activation still cannot be predicted with certainty. Nevertheless, we believe that we have sufficient grounds to claim that in a high pressure water mist system, flow stoppage in the piping (and piping only) due to ice formation (dendritic or annular) should be considered as unlikely. However, this cannot be generalized to high pressure nozzles in these systems. For conventional sprinkler systems, annular ice growth is not believed to cause complete flow blockage until the surroundings temperatures are considerably lower than –30 °C but at the same time, these systems are probably vulnerable for complete blockage due to dendritic ice growth.

Hence, we propose experimental activities in order to provide a base for future development of the existing models towards our application.

Sammanfattning

Syftet med det här arbetet är en teoretisk undersökning av frysningsfenomen i utlösande sprinklersystem vid låga temperaturer. Det finns många sprinklersystem installerade i sådan miljö att de är tänkta att fungera under vattnets fryspunkt. Vid utlösning, förutsättes att vatten färdas en ofta betydande sträcka fram till sprinkler genom nedkylda rör och vi vill undersöka huruvida det är rimligt.

Målet är därför att komma fram till beräkningsmetoder som kan användas för att förutsäga huruvida ett visst sprinklersystem kan fallera genom att en fullständig blockering av flödet inträffar på grund av isbildning inne i systemet tillika att möjligast mån göra generella iakttagelser. Arbetet fokuserar huvudsakligen på högtrycksystem av typen vattendimma av torrörstyp. Tillvägagångssättet var litteraturstudier inom området med syftet att finna beräkningsmodeller som kan tillämpas till den här problematiken.

Resultat av detta arbete visar att ett utlösande sprinklersystem kan erfara en fullständig blockering på två olika sätt, antingen genom dendritisk eller, vilket är mindre troligt, annulär isbildning. Den dendritiska isbildningen är karaktäristiskt för ganska måttliga negativa temperaturer i förhållandevis närhet till 0 °C och är kopplad till underkylning av den flödande vattenvolymen vilket leder till en plötslig bildning av issörja i flödet när väl isbildning startar. Å andra sidan, den annulära isbildningen som är typisk för lägre starttemperaturer ger sig till känna av ett skal av is som bildas på rörväggen direkt vid kontakt med det penetrerande vattnet (utan någon underkylning av hela vattenvolymen) men som dock kontinuerligt smälts på sin uppströmssida av det allt varmare flödet (i och med att röret värms upp av flödet).

Samtidigt visade sig de existerande modellerna otillfredsställande för att kunna fungera som grund för en kvantitativ beskrivning av dessa fenomen till en grad tillräcklig för att lösa vårt problem vilket innebär att fullständig blockering av ett sprinklersystem vid utlösning fortfarande inte kan förutsägas med säkerhet. Icke desto mindre ger de tillräckligt för att vi ska hävda att blockering av ett högtrycksystem på grund av isbildning i rören måste anses som osannolik. Märk dock väl, att detta inte kan sägas om munstycken i dessa högtrycksystem eller om konventionella sprinklersystem som troligen är känsliga för blockering på grund av dendritisk isbildning. Samtidigt tros inte det annulära isbildningssättet kunna leda till en fullständig blockering av ett konventionellt sprinklersystem förrän vid temperaturer betydligt lägre än –30 °C.

Med anledning av detta, föreslår vi experimentella undersökningar som förhoppningsvis kan ge data som kan användas för att utveckla de existerande modellerna till att bättre lämpa sig för vår problemställning.

Streszczenie

Tematem niniejszej pracy jest teoretyczne zbadanie zjawisk zamarzania zachodzących w przeciwpożarowych systemach tryskaczowych w momencie ich uruchamiania przy niskiej temperaturze otoczenia. Systemy tego typu muszą sprawnie funkcjonować niekiedy przy temperaturach znacznie poniżej zera. Przy uruchomieniu systemu, zakłada się, że woda jest w stanie napełnić schłodzony system i bez przeszkód dotrzeć do poszczególnych tryskaczy. Celem tej pracy jest zbadanie czy powyższe założenie jest realistyczne.

Celem pracy jest przedstawienie metod obliczeniowych, które pozwolą przewidzieć czy dany system tryskaczowy może ulec awarii na skutek niedrożności spowodowanej zamarzaniem wody w fazie uruchamiania systemu oraz przedstawienie obserwacji o charakterze ogólnym. Główna uwaga poświęcona jest wysokociśnieniowym systemom mgły wodnej. Zastosowana metoda to obszerne studia literatury fachowej w poszukiwaniu modeli obliczeniowych dających się zastosować do przedmiotu niniejszej pracy.

Rezultatem pracy jest wniosek, że system tryskaczowy może ulec blokadzie w trakcie uruchamiania na dwa różne sposoby – poprzez dendrytyczne albo, co mniej prawdopodobne, pierścieniowe tworzenie się lodu. Dendrytyczny przyrost lodu jest charakterystyczny dla umiarkowanych, ujemnych temperatur otoczenia i występuje w wodzie przechłodzonej, gdy spontaniczna nukleacja przechodzi w gwałtowne tworzenie się kryształków lodu w całej jej objętości. Pierścieniowy przyrost lodu jest typowy dla niższych temperatur i polega na tworzeniu się pierścieniowej warstwy lodu na ściance wyziębionej rury, gdy woda napełnia system. Warstwa ta topi się jednak stopniowo w miarę dalszego napływu cieplejszej od ścianki rury wody „podążając" tym samym za awansującym frontem wody.

Zidentyfikowane metody obliczeniowe okazały się być niewystarczające dla pełnego, kwantytatywnego opisu badanych zjawisk. Wynika stąd, że przewidzenie, czy wystąpi blokada danego systemu tryskaczy w zadanych warunkach, nie jest jeszcze możliwe. Da się wykazać, że niezależnie od sposobu tworzenia się lodu blokada rur systemu tryskaczowego wysokiego ciśnienia jest bardzo mało prawdopodobna, ale stwierdzenie to nie obejmuje samych dysz. Konwencjonalne systemy tryskaczowe nie wydają się zagrożone blokadą lodem pierścieniowym o ile temperatura otoczenia nie jest dużo niższa niż –30 °C, jednak systemy te mogą być podatne na blokadę lodem dendrytycznym.

W związku z powyższym, autor pracy proponuje przeprowadzenie eksperymentów mogących dać podstawę do dalszego rozwoju omawianych metod obliczeniowych w zakresie tematyki niniejszej pracy.

Nomenclature

Abecedarium Latinum

A	pipe cross section area, [m^2]
B	freezing parameter, eq. (5.12), [-]
c_p	specific heat capacity at constant pressure, [J/(kgK)]
C	C-factor i.e. Hazen-Williams wall roughness coefficient, [-]
C_f	friction coefficient, [-]
d	pipe inner diameter, [m]
D	pipe inner diameter, [m]
f	friction factor, [-]
Gr	Grashof number, [-]
g	gravity, [m/s^2]
h_f	wall friction head loss, [m]
h_i	heat transfer coefficient inside pipe, [W/(m^{2}K)]
h_{if}	latent heat of fusion, [J/kg]
h_o	heat transfer coefficient outside pipe, [W/(m^{2}K)]
h_m	minor head loss, [m]
h_{pump}	pump head input delivered to water, [m]
h_{tot}	total head loss, [m]
k	thermal conductivity of pipe material, [W/(mK)]
k_f	thermal conductivity of fluid, [W/(mK)]
k_s	thermal conductivity of solid phase, [W/(mK)]
K	K-factor of a sprinkler, eq. (3.12), [(l/min)/(kPa)^{0,5}]
K_{bar}	K-factor, [(l/min)/(bar)^{0,5}]
K_m	minor loss coefficient, [-]
K_{US}	K-factor in US customary units, [(gal/min)/(psi)$^{0.5}$]
l	total pipe length between sprinkler and pump, branched system,[m]
l_g	design pipe length between sprinkler and pump, gridded system, [m]
L	pipe length, [m]
L_{ip}	length of hypothetical solid ice plug, [m]
$\dot{m}$	mass flow rate, [kg/s]
n	number of ice band in the freezing section, [-]
$\mathrm{Nu_d}$	Nusselt number, [-]
$\overline{\mathrm{Nu_d}}$	mean Nusselt number, [-]
p	pressure, [Pa]
p_{pump}	pressure provided by the pump, [Pa]
p_1	pressure at the most remote sprinkler, Figure 3.6,[Pa]
$\dot{q}$	heat flux, [W]
Q	flow rate, [m^3/s]
Q_1	flow rate from the most remote sprinkler, [m^3/s]
Pr	Prandtl number, [-]
r	radial coordinate, [m]
R	radial location of solid-liquid interface inside pipe, [m]

R_0	inner radius of the pipe, [m]
R_i	inner radius of the pipe, [m]
R_o	outer radius of the pipe, [m]
R_{total}	thermal resistance, [Km/W]
R^*	dimensionless solid-liquid interface radius, [-]
$\mathrm{Re_d}$	Reynolds number, [-]
S	spacing between two neighboring ice bands at steady state, [m]
t	time, [s]
T_0	ambient temperature, [K]
T_c	interface (contact) temperature, [K]
T_m	liquid equilibrium freezing/melting temperature, [K]
T_n	nucleation temperature, [K]
T_f	fluid bulk temperature, [K]
T_p	initial pipe temperature, [K]
T_{ref}	reference temperature, eq. 4.24, [K]
V	average velocity, [m/s]
x	axial pipe coordinate, [m]
x	instantaneous penetration length of liquid, Figure 5.4, [m]
x_P	penetration length at pipe blockage, [m]
$\dot{x}$	velocity of penetrating liquid front, [m/s]
X	length of the adiabatic pipe section, Figure 5.12,[m]
z	height, eq. (3.1), [m]
z	axial coordinate in freezing section, [m]
Z	length of the freezing section, Figure 5.12,[m]
Z^*	dimensionless freezing section length, equation (5.54),[-]

Ελληνικό αλφάβητο

α	thermal diffusivity, eq. 5.1, [-]
β	volumetric thermal expansion coefficient, $1/T_\infty$ for ideal gases, [-]
β_p	thermal effusivity of pipe material, eq. 5.1, [$J/(m^2Ks^{1/2})$]
β_f	thermal effusivity of water, eq. 5.1, [$J/(m^2Ks^{1/2})$]
δ^*	dimensionless radius of the solid-liquid interface, R/R_0, [-]
δ_E^*	δ^* at the freezing section exit, [-]
Δp	pressure drop, [Pa]
$\Delta p_{f,tot}$	design pressure loss, [Pa]
θ	cooling temperature ratio, [-]
ν	kinematic viscosity, [m^2/s]
ρ	density, [kg/m^3]
τ	wall shear stress, [Pa]
τ_{bond}	shear strength of bond between ice and pipe wall, [Pa]
Υ_β	effusivity ratio, eq. 5.1, [-]
$\chi_{mass,i,d}$	mass fraction dendritic ice, [-]
$\chi_{vol,i,d}$	volume fraction dendritic ice, [-]

Indices, superscripts and subscripts

c	contact, coolant
f	friction, fluid
i	inner, ice
i, a	annular ice
i, d	dendritic ice
l	liquid
lam	laminar
m	melting, minor loss
min	minimal
n	nucleation
o	outer
p	at constant pressure, pipe
s	solid phase
$super$	supercooling
tot	total
vol	volume
w	wall, water
0	initial, prior to solidification
$*$	dimensionless quantity

Table of contents

1. Introduction

Fire sprinkler systems for controlling or suppressing fire dates back to nineteenth century. Continuous technical development of these systems together with introduction of new areas of operation is linked to new emerging issues. This thesis will be devoted to such an issue.

1.1 Background

Fire protection of many heritage buildings in Sweden, especially old wooden churches, has been improved greatly by installation of fire detection and suppression systems (Arvidson, 2006). Of the latter, fire sprinkler systems are prevailing. The great historical, cultural and religious values that are related to heritage premises as well as the fact that furnishings traditionally associated with interiors of such spaces often consists of great concentration of wooden, upholstered furniture, paintings etcetera renders use of conventional "raining" sprinkler system problematic, due to vulnerability to water damage, which becomes especially unjustifiable if the system activates unintentionally. For this reason, installation of water mist sprinkler systems in such premises experiences increasing popularity.

In water mist systems, water is atomized to a spray (mist) in special nozzles not totally unlike the function of an aerosol spray. Use of water mist for fire suppression offers plenty of benefits, of which perhaps the most important is reduced water consumption due to more efficient use of water which in turn diminishes water damage. Additional advantage in this context is of aesthetical nature – reduced water flow gives impact on piping dimensions so that more discreet installation can be made. This makes water mist systems very good alternative for heritage premises but this does not mean that design, installation and maintance become trouble-free. There are many challenges and questions associated with these activities irrespectively of whether the system is conventional sprinkler systems or water mist systems. Arvidson (2006) provides a comprehensive review of these questions based on experiences from many Swedish wooden churches where fire sprinkler systems have been installed.

One of these questions is coupled to the fact that many old churches are unheated wherefore freezing temperatures can be reached. As sprinkler systems are usually throughout pre-filled with water, measures against freezing must be taken. One of these measures is adding antifreeze to the standing water but this approach is associated with a number of disadvantages, among others: increased system complexity, increased risk for leakage, potential flammability of the solution, health aspects and destructive potential in contact with materials e.g. permanents spots on wood. These problems can be avoided by modification of the system design so that the part of the system inside the cold space is filled with compressed air which evacuates upon activation and after some delay gives space for water arriving from a room with more temperate conditions. This is called dry pipe sprinkler system.

The question that finally arises and is to be answered in this thesis is whether such arrangement really constitutes adequate security against freeze-off of the system that possibly may occur if the advancing water front is cooled down enough for ice formation to start.

1.2 Objective

The objective of this thesis is to theoretically examine freezing phenomena that may occur during activation of dry pipe sprinkler systems in general and water mist systems in particular

at low temperatures and find analytical methods making it possible to predict complete blockage of a sprinkler system during start-up.

The ultimate goal of this activity is to present calculation procedures that can be implemented in sprinkler design to prevent complete blockage of the system during activation. These should make it possible to design a sprinkler system so that operation at some lowest design temperature is secured. Similarly, for an existing sprinkler system the lowest operational temperature without additional measures should be predicted. It seems obvious that work beginning with this thesis cannot be considered as completed until in some way quantified freeze-off perspective is natural part of sprinkler design activities for systems aimed to be operable at freezing temperatures alternatively until such risk can be totally rejected as non-existing. We will endeavour to have this practical outlook always in mind.

In greater detail, cooling of the water flow followed by solidification process and possible complete blockage during filling of a dry pipe sprinkler system is to be described and quantified. With implementation in sprinkler design in mind, as uncomplicated calculation procedures as possible should be preferred, however, without sacrificing validity. If limping or unsatisfactory models are used in absence of others, a careful discussion on impact on the results should follow.

1.3 Method

As approach we chose an attempt to analytically describe the interesting freezing process based on literature studies followed by extraction of the interesting information and its adaptation to our problem. If not a fully satisfactory solution can be found, some attention should be paid to description of appropriate experimental set-ups and the possibility of numerical approach.

We will to reasonable extent try to have an approach characterized by systematic description from basic principles so that the thesis easily can be a platform for future investigations.

1.4 Limitations

Our attention in this thesis will be mainly directed towards high pressure water mist systems of the dry-pipe type. The task of quantitative as well as qualitative description of freezing phenomena inside pipes will be given priority over calculations on existing systems and discussions of measures that can be taken to prevent system freeze-off.

2. Fire sprinkler systems

The aim of a fire sprinkler system (referred to as simply sprinkler system thenceforward) is either to control or suppress a fire (NFPA, 2007). Originating in fire safety efforts in factories of the 19th century, the sprinkler system experienced broadening of its primary usage to application in offices, hotels, ships, residences etc (Bryan, 1990).

A sprinkler system consists of sprinklers attached to piping providing water. Water of desirable flow and pressure for the system is provided by a fire pump which can be connected to local water supply system or a tank, depending on water demand.

2.1 Piping arrangements

Common for all sprinkler systems is a piping consisting of feed mains, cross mains, branch lines and sprinklers. Feed mains supply the cross mains, cross mains in turn supply the branch lines and finally the branch lines supply the sprinklers with water (see Figure 2.1). Piping design, sprinkler used and operational details may however differ and the sprinkler systems can be divided with respect to these differences (Bryan, 1990).

2.1.1 Branched sprinkler system

The traditional branched piping arrangement is a tree-like structure with cross mains as a trunk and branch lines as branches. Depending on the location of the cross main relative to the branches and the feed main in relation to the cross main, a number of sub-arrangements are possible (Figure 2.1). In all of them particular sprinkler can be fed with water from only one direction.

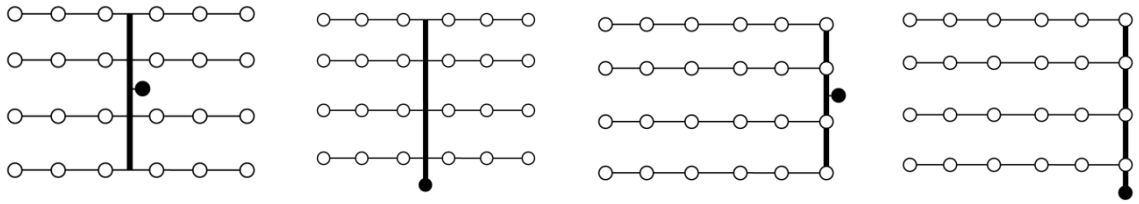

Figure 2.1 *Branched sprinkler arrangements (from left): center central feed, central end feed, side central feed, side end feed. Feed mains marked as dots, cross mains as bold lines, branch lines as thin lines and sprinkler as circles.*

2.1.2 Gridded sprinkler system

A gridded sprinkler system consists of parallel cross mains that are connected by multiple branch lines so that an operating sprinkle can receive water from two directions, from both cross mains, see Figure 2.2.

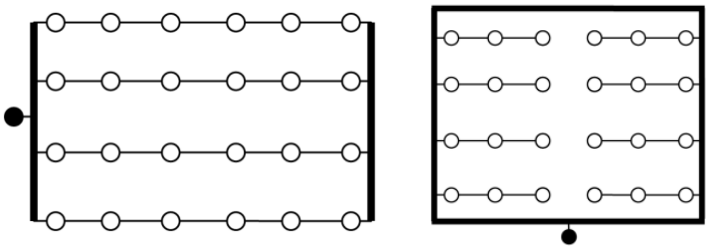

Figure 2.2 *Gridded and looped sprinkler systems*

2.1.3 Looped sprinkler system

In a looped system, cross mains are tied together to a loop to which branches are connected. Hereby more than one path for flow of water to an operating sprinkler is possible (Figure 2.2).

The presented basic piping arrangements may in a sprinkler system also be combined so that different arrangements are found in different sections of the structure.

2.2 Fire sprinklers

All traditional sprinklers consist of a frame and a deflector discharging water. Depending on orientation, they can be divided in pendant (water stream directed down towards the deflector) and upright sprinklers (Figure 2.3). Further differences give rise to distinct types of sprinkler systems.

Figure 2.3 *Pendant and upright sprinklers*

2.2.1 Automatic sprinkler system

The most widespread type of sprinkler system is the automatic sprinkler system. An automatic sprinkler is equipped with some kind of heat-activated element that operates the sprinkler independently of other sprinklers in a system after achieving a certain predefined temperature. This is done by utilizing a fusible link or (which is dominating) a frangible glass bulb containing liquid as device blocking water flow through the sprinkler (Figure 2.4). When the hot fire plume or resulting ceiling jet reaches the fusible-link sprinkler, the link melts and water flow is released. In the case with the bulb, the liquid in the bulb expands at the expense of a small air pocket, as the bulb is not completely filled with the liquid. When the air pocket is annihilated, the pressure rise in the bulb is extremely fast and the bulb is broken allowing water to flow.

Figure 2.4 *Sprinkler with fusible link and sprinkler equipped with glass bulb*

Depending on mass and heat capacity of the heat-activated element, sprinklers with the same activation temperature placed in the same environment will experience different times to activation. To classify this, Response Time Index (RTI) is used; the higher the RTI, the longer the time to response (Bryan 1990; NFPA, 2007). Depending on desirable response time, bulbs of different dimensions can be chosen as can be seen in Figure 2.3 and 2.4.

One disadvantage of the automatic sprinkler systems is the possibility of accidental activation of the system caused by e.g. unintentional mechanical destruction of the bulb.

Wet and dry pipe sprinkler systems

Most commonly in an automatic sprinkler system, the sprinklers are attached to a piping system containing water thus discharging water immediately after activation of sprinkler by heat of fire. Such system is called wet pipe sprinkler system (NFPA, 2007). This set-up may however be undesirable if the system is installed in spaces in which temperature may fall below 0 °C with risk of freezing the water and making the system inoperable.

One of solutions to this problem is the dry pipe sprinkler system in which the part of the system aimed for the cold space is filled with air or nitrogen under pressure. This pressure balances water pressure on the other side of so called dry pipe valve keeping the valve closed. An activation of sprinkler will release entrapped air, allow water to open the valve and reach the sprinkler with some delay. Is this system a sufficient guarantee that freezing will not block the water flow not even under rather extreme temperature conditions of Scandinavian winter? This question is supposed to be answered by this thesis.

Wet pipe sprinkler systems are simple, robust, reliable and least expensive. A dry pipe system requiring supply of compressed air and additional control equipment increases the complexity (thus decreasing reliability by creating more failure points) and costs of both installation and maintenance. The time delay between activation and discharging of water is also disadvantageous.

2.2.2 Deluge sprinkler system

Using open sprinklers without any heat-activated blocking mechanisms gives a deluge sprinkler system. The piping system that they are attached to is connected to water supply through a deluge valve opened by either a detection system or an operator. Thus the water discharges from all sprinklers attached to the system (yet after some delay). This set-up may be chosen in environments where fire can spread extremely fast. If a sprinkler system is installed in a wooden church, there is always a deluge system for external roof and facade protection present, Figure 2.5. Indeed it is often pointless to equip a wooden church with internal sprinkler system if fire can spread unrestrictedly outside having in mind that majority of such fires in Sweden are started by arsonists (Arvidson, 2006).

Figure 2.5 *Left: functional test of a deluge water mist sprinkler system for external roof and facade protection of Älgarås church in Sweden. Right: deluge and dry pipe valve assembly for similar system in Habo church, Sweden. (Arvidson, 2006)*

2.2.3 Preaction sprinkler system

Principles of activation of automatic and deluge sprinkler systems may be combined if additional precautions against unintentional activation of the system are desirable due to for example extraordinary sensitivity for water damage. In a preaction sprinkler systems, both sprinkler activation and detection of fire by separate detection system is required for water to be discharged from the sprinklers. Two types of preaction systems are used for this purpose.

In single-interlock systems, a valve allowing water to fill the piping is opened by a fire detection system. Water will however not be discharged until one or more sprinklers activates because of heat of fire.

In a double-interlock system not even piping will be filled unless fire is detected in two independent ways. The system is very similar to standard dry pipe system. However in a double-interlock system a dry pipe valve will not open untill both fire detection system and an automatic sprinkler activate. The double-interlock strategy is used in application where accidental filling of the system due to false alarm may have fatal consequences as in cold spaces where the water will freeze blocking the system and making it inoperable until the ice is allowed to melt away.

2.3 Water mist systems

Water mist is defined as a water spray in which 99 % of total volume is contained in droplets up to 1 mm in diameter at the minimum operating pressure of the water mist nozzle creating it (NFPA, 2003). Water mist as extinguishing agent is a relatively new concept. The commercial break-through occurred as late as in the beginning of 1990's mainly thanks to gradual abandoning of halons which seemed to be perfect extinguishing media for fixed extinguishing systems until their ozone-depleting effect was paid attention to (Arvidson, 2008).

2.3.1 Advantages of water mist

Non-toxicity and cheapness are characteristic for water as extinguishing agent regardless whether leather bucket or water mist nozzle is used. Further advantages of water mist are:

- In many cases significantly lower water flow rates compared to traditional sprinkler systems reducing risk of water damage making water mist suitable for especially sensitive spaces e.g. heritage premises

Explanation: The most important extinguishing mechanisms are gas-phase cooling of flame (with intention to cool it to a degree making existence of flame impossible) and cooling the fuel surface (decreasing amount of emission of combustible volatiles). Evaporation of water demands huge amount of energy which will be taken from the flame, playing important role in cooling it. As the rate of evaporation is proportional to available liquid surface area which is inversly proportional to the size of the droplet, evaporation increases with decreasing droplet size rendering effective utilization of water in extinguishing process instead of flooding the building (Särdqvist, 2006).

- Applicability against pool and spray fires

Explanation: Inappropriate use of water against pool fires may cause explosive phenomenon of boil over as heavier water is deposited on the bottom displacing quickly the fuel out of the vessel after achieving boiling temperature. However, the small droplets of water mist will most likely evaporate before penetrating the flame, cooling it effectively instead.

- Applicability as inerting or explosion suppression systems
- Blocking of transfer of radiant heat
- Providing greater cooling of the protected equipment than its gaseous counterparts
- Low electrical conductivity if deionized water is used

2.3.2 Piping

Although the same basic pipe arrangement may be used in water mist system as for traditional sprinkler systems, branched systems are most widespread. The big difference compared to traditional systems is dimension of pipe being smaller due to much smaller water flows.

2.3.3 Sprinklers

Just like traditional sprinkler system, water mist systems can be designed as automatic (wet pipe or dry pipe), deluge and preaction systems. While the task of a traditional sprinkler is to evenly discharge water in its entourage, a water mist sprinkler (more often denoted as nozzle) has to produce water mist. This is mostly done by combining high pressure in the system with very small openings for water to pass (Figure 2.6 and 2.7), not very unlike fuel injectors in diesel engines. A technique useful in creating water mist if combined with high pressure and small openings is to make two or more water streams to collide at the opening (Figure 2.7).

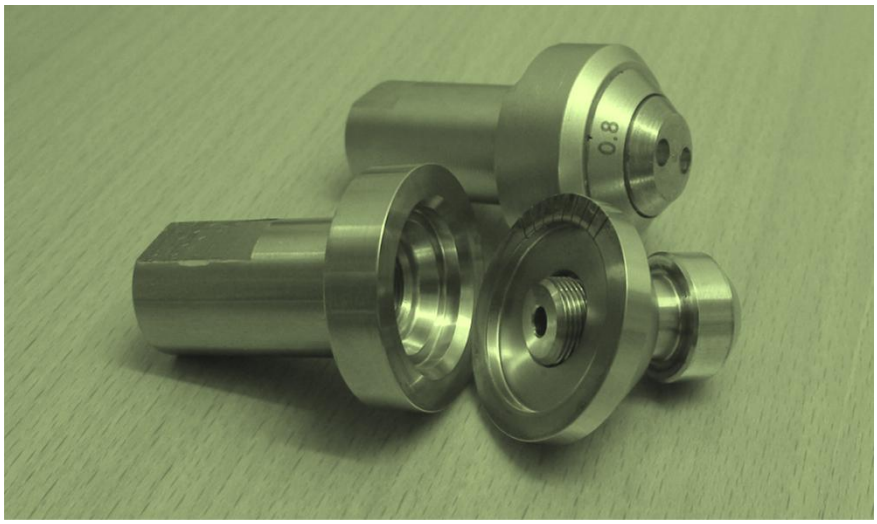

Figure 2.6 *Open water mist nozzle (disassembled and assembled state) in which water mist is created by letting water leave the nozzle through radial incisions seen on the top of the disassembled nozzle*

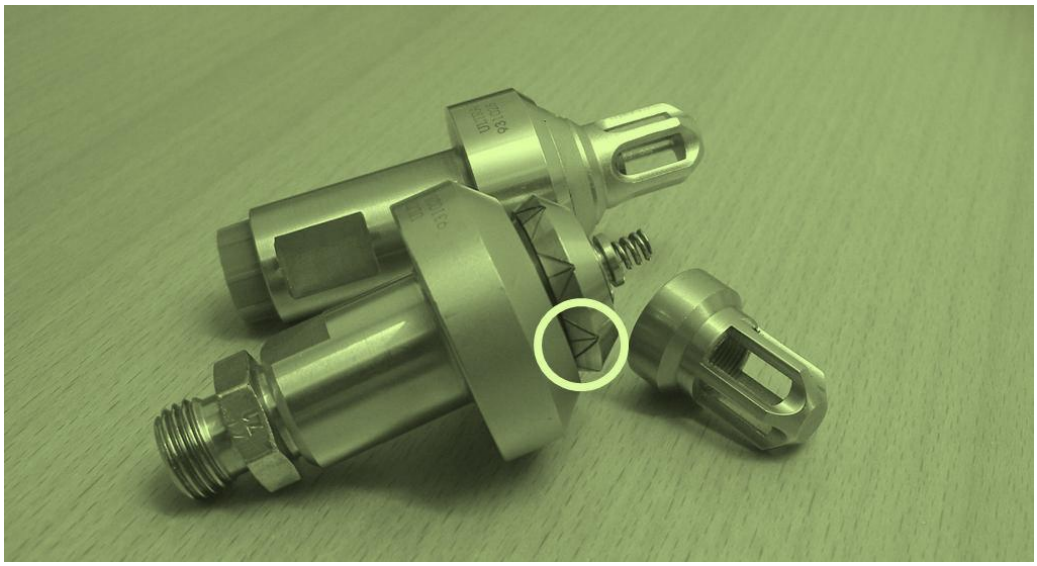

Figure 2.7 *Automatic, bulb containing water mist nozzle (in partly disassembled and assembled state) in which three water streams are directed through showed incisions in such way that they collide at the opening helping create water mist*

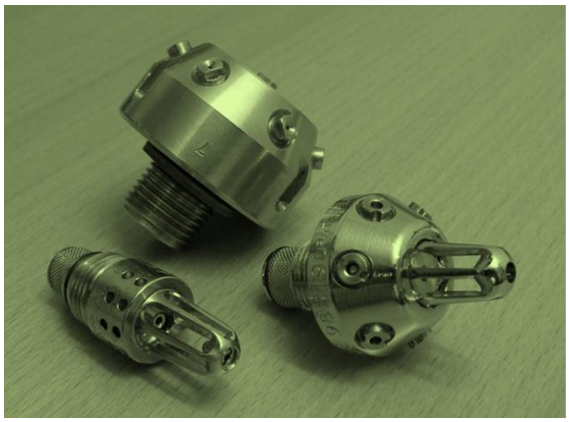

Figure 2.8 *A little bit older water mist nozzles*

Addition of compressed air in the nozzle is another way to atomize water. The atomization of water to water mist may also be done without any use of high pressure using special type of deflector. Depending on the highest pressure a piping is exposed to, the water mist system may be divide into high, intermediate and low pressure systems. High pressure is defined as exceeding 34.5 bar, low pressure defined as not-exceeding 12.1 bar while pressures of other magnitude turn to be intermediate (NFPA, 2003).

2.3.4 Common dimensions

Higher surface-area-to-volume ratio gives more effective cooling of water inside the pipe. Approximating the pipe with an at both ends insulated cylinder, this ratio can be found to be inversely proportional to the diameter making small pipe dimensions not surprisingly more sensitive for freezing and more interesting to study in this case.

The smallest pipe dimensions in a sprinkler system are these of branch lines followed by cross mains. In a traditional sprinkler system with copper piping 28 x 1.2 (outer diameter x wall thickness) is common branch line dimension while cross mains often consists of dimensions 35 x 1.5 or 42 x 1.5. Water mist systems consist mostly of stainless steel piping where the most common dimensions are 12 x 1, 22 x 2 and 28 x 2. See Table 2.1 for summary.

Table 2.1 *Common pipe dimensions in sprinkler systems and water mist systems*

Designation	Inner diameter [mm]	Outer diameter [mm]
12 x 1	10	12
22 x 2	18	22
28 x 1.2	25.6	28
28 x 2	24	28
35 x 1.5	32	35
42 x 1.5	39	42

3. Pipe flow

From a fluid mechanical point of view a sprinkler system represents a multiple-pipe system or piping network (if gridded or looped) which allows it to be handled in accordance with the classical branch of fluid mechanics – pipe flow.

3.1 Essential expressions

The usual quantitative description of pipe flow originates in the energy equation applied to a control volume (White, 2008). With common assumptions for pipe flow, i.e. steady flow, one inlet and one outlet (both one-dimensional) and incompressible flow, the energy equation will take the following form:

$$\left(\frac{p}{\rho g}+\frac{V^2}{2g}+z\right)_{in}=\left(\frac{p}{\rho g}+\frac{V^2}{2g}+z\right)_{out}+h_f+\sum h_m-h_{pump} \qquad (3.1)$$

p	pressure, [Pa]
ρ	density, [kg/m^3]
V	average velocity, [m/s]
g	gravity, [m/s^2]
z	height, eq. (3.1), [m]
h_f	wall friction head loss, [m]
h_{pump}	pump head input delivered to the water, [m]
h_m	minor head loss, [m]

It is worth noting that equation (3.1) is written in such a form that every term is of dimension length and called head.

To solve pipe flow problems the friction head loss or pipe resistance h_f has to be specified closer. This has been done by Julius Weisbach in the 19th century who proposed the following empirical correlation:

$$h_f=f\frac{L}{d}\frac{V^2}{2g} \qquad (3.2)$$

f	Darcy friction factor, [-]
L	pipe length, [m]
d	pipe inner diameter, [m]

Equation (3.2) is often referred to as Darcy-Weisbach equation. Henry Darcy was the first to establish the effect of wall roughness on pipe resistance. His friction factor is hence a function of roughness but also the Reynolds number and the duct shape. The influence of wall roughness on friction factor is however significant only if the flow is turbulent. For fully developed, laminar flow, the friction factor can be derived analytically and turns out to be exclusively a function of Reynolds number:

$$f_{lam}=\frac{64}{\mathrm{Re_d}} \qquad \mathrm{Re_d}<2300 \qquad (3.3)$$

$$\mathrm{Re_d}=\frac{Vd}{\nu} \qquad (3.4)$$

ν kinematic viscosity, [m²/s]

Expressions for the friction factor in the fully developed turbulent flow are based on empirical, experimental data. The most famous of such expressions (especially in plotted form known as the Moody chart) is the iteration formula of Colebrook, also known as the Colebrook-White equation which covers even transitional regime:

$$\frac{1}{f^{1/2}} = -2\log\left(\frac{\epsilon/d}{3{,}7} + \frac{2{,}51}{f^{1/2}\mathrm{Re_d}}\right) \qquad \mathrm{Re_d} > 2300 \qquad (3.5)$$

ϵ roughness, [m]

With these equation friction losses in pipe seems to be quantified. The wall friction is nevertheless not the only source of pressure drop in pipes. Pipe entrances and exits, expansions and contractions, bends and valves (open or partially closed) will all contribute to the total system loss and are denoted as minor losses h_m, each specified by a loss coefficient K_m in such a way that:

$$h_m = K_m \frac{V^2}{2g} \qquad (3.6)$$

This allows the total system loss to be expressed as follows:

$$h_{tot} = h_f + \sum h_m = \frac{V^2}{2g}\left(\frac{fL}{d} + \sum K_m\right) \qquad (3.7)$$

3.2 Pipe flow problems

The expressions (3.1)-(3.7) allow solving four basic types of pipe flow problems which are summarized in Table 3.1, (White, 2008).

Table 3.1 *Types of pipe flow problems*

To compute	Given
h_f	d, L, V (or flow rate Q), ν, g, ε
V	d, L, h_f, ν, g, ε
L	Q, d, h_f, ν, g, ε
d	Q, L, h_f, ν, g, ε

Computing h_f or L is straightforward as f can be directly evaluated from equation (3.3) or from equation (3.5) if the flow is turbulent, either by iteration or using Moody chart. This cannot however be done so easily for turbulent flow if we want to compute V or d because $\mathrm{Re_d}$ becomes unknown when V or d is not known besides the fact that d is included in (3.5) not only in $\mathrm{Re_d}$ but also explicitly. For these problems solution can be obtained in an iterative manner.

To get started, f is guessed, this value is then used to compute the unknown quantity (i.e. V or d and $\mathrm{Re_d}$) after which a new f can be calculated from (3.5). The process is repeated until convergence of the searched quantity is obtained.

The problem when d is requested is known as the sizing problem and represents actually the essence of sprinkler system design. A sprinkler system consist of sprinklers aimed to discharge a certain prescribed water quantity per time unit (Q) and piping system is to be designed in such

way (appropriate pipe diameters among others) that this is guaranteed. Further information on sprinkler system design will is provided in section 3.4.

3.3 Multiple-pipe systems

With certain rules in mind, solving the equations for multiple-pipe systems need not be much more complicated than solving them for a one-pipe system (White, 2008).

3.3.1 Pipes in series

At stationary, incompressible flow conditions, it is obvious that condition of continuity for pipes in series (Figure 3.1) implicates the same flow rate in all pipes:

$$Q_1 = Q_2 = Q_3 = constant \tag{3.8}$$

The total head loss must be sum of the head losses in each pipe, inclusively minor losses:

$$h_{tot} = \sum_i \frac{V_i^2}{2g}\left(\frac{fL}{d}\right)_i + \sum_j \frac{V_j^2}{2g}(K_m)_j \tag{3.9}$$

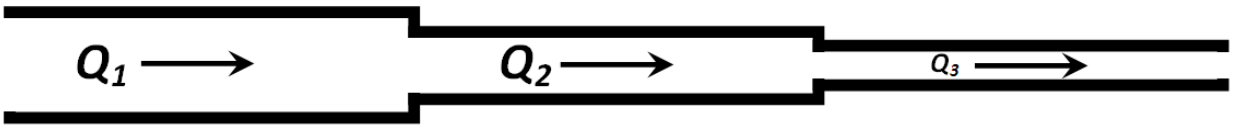

Figure 3.1 *Pipes in series*

Minor losses in system in Figure 3.1 arise due to contractions of pipe diameter. While evaluating corresponding K_m from tables one must be care whether it is defined with respect to velocity before or after the contraction i.e. which of them is to be used in second term in equation (3.9).

3.3.2 Pipes in parallel

For pipes in parallel (Figure 3.2), the total flow must be a sum of the individual flows in the pipes:

$$Q_{tot} = Q_1 + Q_2 + Q_3 \tag{3.10}$$

The pressure drop must be the same in all pipes, since pressure in A (Figure 3.2) as well as in B must have only one value.

$$\Delta h_{A\to B} = \Delta h_1 = \Delta h_2 = \Delta h_3 \tag{3.11}$$

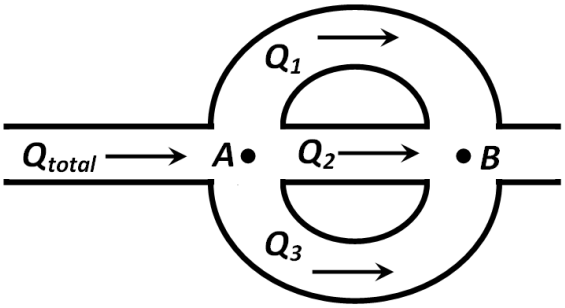

Figure 3.2 *Pipes in parallel*

3.3.3 Piping network

A piping network is a multiple-pipe system with numerous loops, see schematic representation in Figure 3.3. Regardless of the complexity of certain piping networks, they all follow same basic rules:

- The net flow into all junctions must be zero
- The net pressure change around any closed loop in the system must be zero as pressure at each junction must have only one value
- The pressure changes must satisfy friction loss and minor-loss correlations

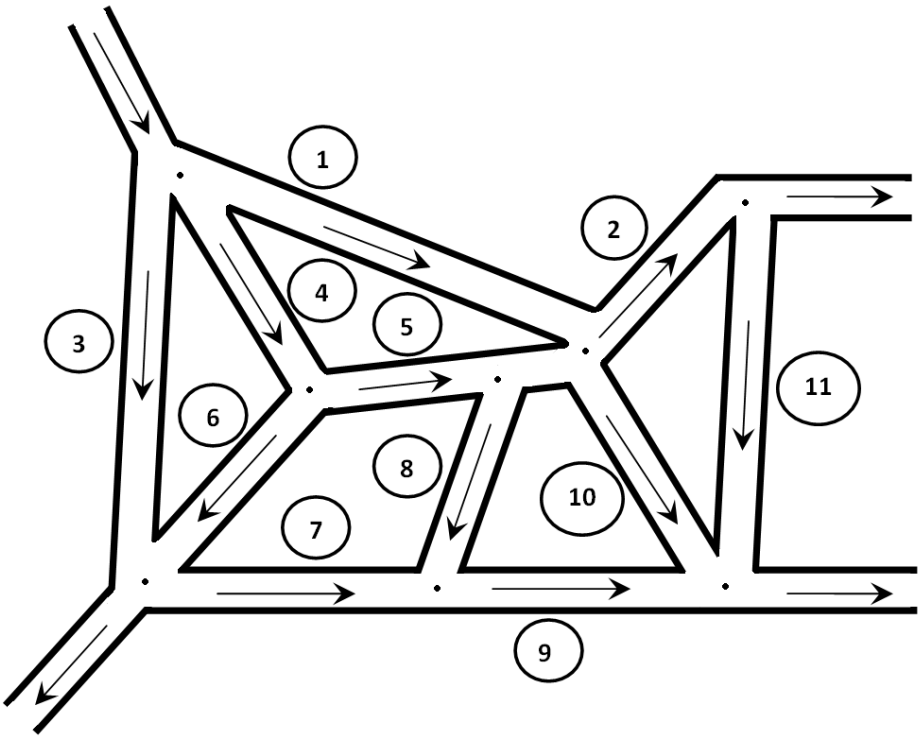

Figure 3.3 *Piping network*

To determine flow rates in the pipes and pressures at the junctions (indicated as points in Figure 3.3) one should apply these rules to each junction and independent loop in the piping network so that a set of simultaneous equations is obtained. Solution can be obtained by iteration which does the problem suitable for computer approach.

3.4 Hydraulic sprinkler system design

Type of occupancy, quantity and combustibility of the furnishing and commodity stored constitutes the base for designing a sprinkler system of appropriate potential (NFPA, 2007).

3.4.1 Organizations providing prescriptions on sprinkler systems

The recommendations on the design of sprinkler systems on land are developed by often non-governmental organizations e.g. National Fire Protection Association (NFPA) in United States, European Committee for Standardization (CEN) in Europe or the Swedish Fire Protection Association (SFPA) in Sweden. When an authority having jurisdiction enforces a presence of a sprinkler system in certain type of buildings and/or activities, most commonly it even enforces fulfilment of the recommendations of some such organization as well. In some countries there may be a complete lack of sprinkler requirements by the authorities (Sweden). In these cases insurance companies represents main driving force for sprinkler installation as they offer lower prices for customers if a sprinkler system fulfilling certain recommendations is installed.

On the contrary, the design of sprinkler systems in marine applications is subject of regulations provided by one organization alone, the International Maritime Organization under the United Nations which assembles all maritime nations.

3.4.2 Design of automatic sprinkler systems

In contrast to deluge sprinkler systems, automatic sprinkler systems are not designed to discharge prescribed water flow from all sprinklers simultaneously. Instead, only a fraction of total number of sprinklers, represented by design area of sprinkler operation, is assumed to activate (NFPA, 2007).

Design area of sprinkler operation

The design area of sprinkler operation can be seen as an operation floor area of activated sprinklers of a certain size in relation to the expected fire. Also the shape of the design area is aimed to correspond to the shape of a growing fire making it rather compact. The designed area can be further divided in areas associated with operation of individual sprinklers (usually 3 x 3 m) as showed in Figure 3.4.

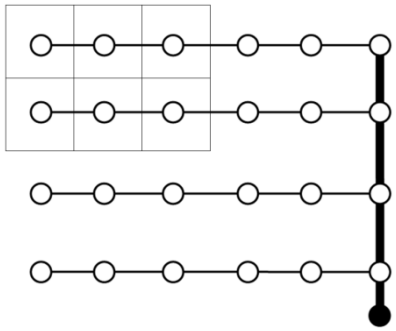

Figure 3.4 *The concept of design area of sprinkler operation*

The sprinkler system is hydraulically designed to supply sprinklers in the design area with a water flow prescribed by the regulations. The hydraulic sprinkler design calculations are usually performed on only one area of sprinkler operation. The design area in the calculations is however chosen to be the most unfavourably placed one from a hydraulic point of view

(practically at a longest distance from feed main as in Figure 3.4). This ensures that sprinkler flows in equivalent area located at arbitrary place in the system are at least those prescribed.

Practically it is of course possible to activate more sprinklers than those in the design area (i.e. more than 6 in Figure 3.4) and even all sprinklers simultaneously, however without guaranty that the individual sprinkler flows will be those prescribed. If simultaneous action of all sprinklers is desirable, the deluge sprinkler system should be used.

Prescriptions on system performance

The occupancies may be classified in accordance to fire hazard depending on quantity and combustibility of material inside. The fire hazard class of the occupancy induces requirements on the existence and performance of the sprinkler system.

The desirable performance of the system is specified in terms of the design area of sprinkler operation. This means that for a certain fire hazard class, the dimensions of the design area of sprinkler operation, the flow rate of sprinklers and durations of the system operation are given. Depending on hazard class, the design area may range from couple of tens of square meters and only four sprinklers activated to hundreds of square meters and tens of sprinklers activated.

Further, the required flow of the sprinklers is specified by so called ceiling sprinkler density. Ceiling sprinkler density describes the sprinkler system action in terms of millimetre water per minute (equal to $l/(m^2 \cdot min)$). As every sprinkler has a certain area as its operational domain (usually 3 x 3 m), this value can be directly converted to flow discharged from the individual sprinkler.

Moreover the regulations usually enable some flexibility in choosing the size of the design area and ceiling sprinkler density. This means that for a certain hazard class, a smaller ceiling sprinkler density may be compensated by a larger design area and vice versa in accordance with strict rules.

After choosing a sprinkler type appropriate for the prescribed flow, the size of its operational domain will implicate certain arrangement of the sprinklers. The next step is to decide whether branched, gridded or looped system will be use to supply the sprinklers with water. When this is done, all the arrangement details as lengths are known and the only remaining unknowns are the diameters. The hydraulic design of a sprinkler system consists of determining these diameters.

Design of branched sprinkler systems

Step 1: determining pressure drop over hydraulically most remote sprinkler

The design calculation procedure is started from hydraulically the most unfavourably placed sprinkler. This means usually an outer sprinkler at a longest distance from the feed main as it is the most difficult one to supply with a certain flow rate due to the pressure losses in the piping. This is in turn due to the fact that sprinkler flow rate and pressure drop can be related as follows (Jensen, 2001):

$$\Delta p = \left(\frac{Q}{K}\right)^2 \qquad (3.12)$$

Δp pressure drop over the sprinkler, [kPa]
Q flow rate from the sprinkler, [l/min]
K K-factor of a sprinkler, [(l/min)/(kPa)^{0,5}]

Equation (3.12) is one of the most fundamental in the sprinkler industry and is presented together with commonly used dimensions. There are however K-factors defined with other units in usage i.a. with bar instead of kPa. It is trivial to show that: $K_{bar} = K \cdot 10$. It is not unusual to see K-factors defined in US customary units i.e. (gal/min)/(psi)$^{0.5}$. The corresponding conversion formula can be easily derived: $K_{US} = K \cdot 1.44$.

K-factor in equation (3.12) should not be confused with the non-dimensional minor loss coefficient K_m from equation (3.7) which is the proper way of correlating the component pressure drop and the flow in fluid mechanics. By writing equation (3.7) in fashion of equation (3.12) these two different coefficients can be related to each other:

$$\Delta p = \frac{\rho V^2}{2} K_m = \frac{\rho Q^2}{2A^2} K_m = \frac{Q^2}{\frac{2A^2}{\rho K_m}} = \left(\frac{Q}{\sqrt{\frac{2}{\rho K_m}} A} \right)^2 \Leftrightarrow K = \sqrt{\frac{2}{\rho K_m}} A \qquad (3.13)$$

As seen in (3.13) the K-factor is density-dependent and lacks generality of the constant K_m which in contrast to K-factor can be straightforwardly used for e.g. calculation on the initial air or nitrogen flow through the sprinkler in dry pipe systems. The equation (3.12) constitutes however a standard in describing sprinkler performance. Figure 3.5 shows a collection of sprinklers and water mist nozzles with different K-factors.

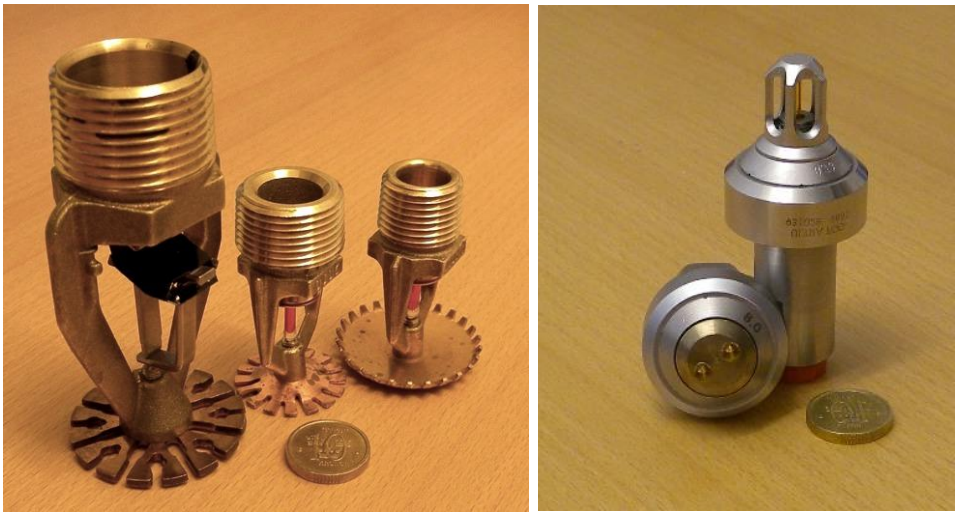

Figure 3.5 *Sprinklers and water mist nozzles with different K-factors, from left: K = 17.3, K = 11.5, K = 8, K = 0.08, K = 0.073*

As the flow rate from the sprinkler is known and equal to the prescribed one and the K-factor of the chosen sprinkler type is known as well, the pressure in the pipe at the location of the hydraulically most remote sprinkler can be calculated. This pressure is denoted as p_1 in Figure 3.6 and is simply equal to Δp if the atmospheric pressure is defined as zero-pressure.

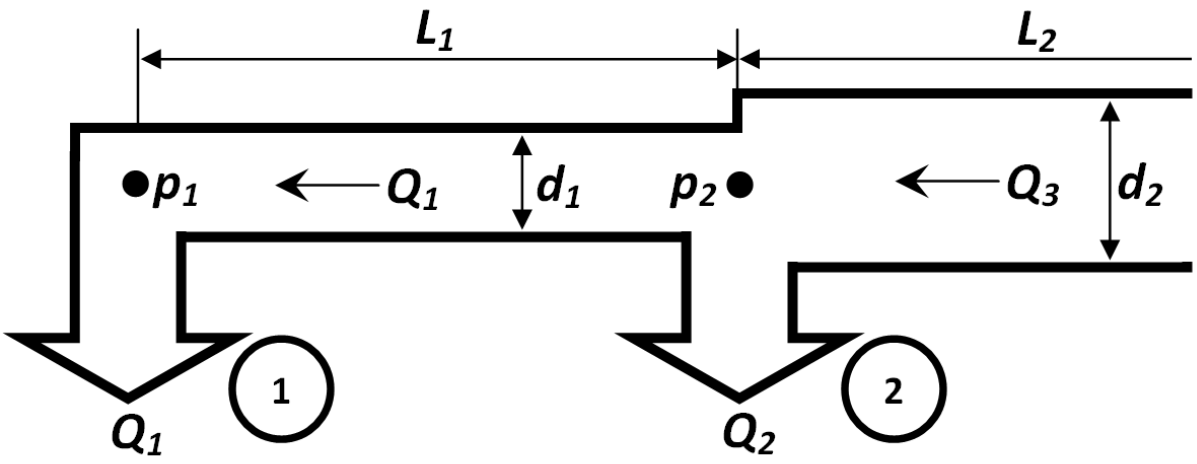

Figure 3.6 *Hydraulically most remote sprinkler (1), the adjacent piping and next sprinkler (2)*

Step 2: Determining design pressure loss

As outlined earlier, all lengths in the sprinkler systems (such as L_1 in Figure 3.6) are chosen prior to the hydraulic design that aims to determine appropriate diameters of the piping. In other words, diameter d_1 is now to be selected so that the flow Q_1 will be at least the one prescribed.

One method is to calculate the design pressure loss per unit length of the pipe and use this value for sizing the pipes. To do this, the energy equation (3.1) is utilized.

Let us consider sprinkler (1) in Figure 3.6. The pressure provided by the pump must overcome the height difference between pump and the sprinkler and the sum of friction and minor losses in the piping system. The pressure "remaining" after these pressure losses is p_1. After including the common approximation of insignificance of velocity differences between pump and the sprinkler (Jensen, 2001), equation (3.1) provides:

$$\left(\frac{p}{\rho g}\right)_{pump} = \left(\frac{p}{\rho g} + z\right)_1 + \sum h_m + \sum h_f \qquad (3.14)$$

After multiplying with gravity g and density ρ one obtains an expression in terms of pressure:

$$p_{pump} = (p + z\rho g)_1 + \sum p_m + \Delta p_{f,tot} \qquad (3.15)$$

Let us move pressure loss due to friction to the right hand side of the equation:

$$\Delta p_{f,tot} = p_{pump} - z_1\rho g - p_1 - \sum p_m \qquad (3.16)$$

By dividing both sides of this equation with distance to the pump l, one obtains a friction pressure loss per length unit, as follows.

$$\frac{\Delta p_{f,tot}}{l} = \frac{p_{pump} - z_1\rho g - p_1 - \sum p_m}{l} \qquad (3.17)$$

The left-hand side quantity in eq. (3.17) is also the searched design pressure loss which can be evaluated if the right-hand side of the expression is known. The pressure provided by the pump is assumed to be known and so are z_1 and l. Pressure at the most remote sprinkler p_1 is

calculated according to eq. (3.12) so to provide the prescribed flow rate (Q_1) and is therefore also known. However, the minor loss term Σp_m is not known and it is velocity-dependent, see eq. (3.6). This means also diameter dependence (through known flow rate) while we actually want to use design pressure loss to determine diameters in the system.

Therefore, to not complicate the procedure too much, the minor loss term is initially neglected and control calculations are made afterwards to see if the flows from the sprinklers are at least those prescribed.

Step 3: Sizing the pipe section between sprinklers (1) and (2)
To size the pipe section, the design pressure loss per length unit is multiplied with the length of this pipe section L_1. The resulting friction loss term can be also expressed in accordance with equation (3.2) i.e. the Darcy-Weisbach equation:

$$\frac{\Delta p_{f,tot}}{l} L_1 = \Delta p_f = \frac{\rho V_1^2}{2} \frac{f L_1}{d_1} = \frac{8 \rho {Q_1}^2}{\pi^2 d_1^4} \frac{f L_1}{d_1} \tag{3.18}$$

A manipulation of equation (3.18) gives an expression for the friction factor.

$$f = \frac{\Delta p_f \pi^2 d_1^5}{8 \rho Q_1^2 L_1} \tag{3.19}$$

From the expression above d_1 can be calculated (at least numerically) for a guessed initial value of f. Then, a new value of f can be obtained, either through Colebrook formula (equation (3.5)) or Moody chart and the procedure can be repeated until convergence in obtained values is observed. This is known as a sizing problem outlined earlier (last line in Table 3.1).

Step 4: Sizing the rest of the branch line
The calculation procedure continues and d_2 is obtained in similar way using L_2, Q_3 and $\Delta p_f = \Delta p_{f,tot} \cdot L_2/l$ in eq. (3.19). It is worth to note that:

$$Q_3 = Q_1 + Q_2 = K\sqrt{p_1} + K\sqrt{p_2} = K\sqrt{p_1} + K\sqrt{p_1 + \Delta p_f} \tag{3.20}$$

As Q_2 is higher than Q_1, this shows that the sprinkler (2) fulfils the requirements of prescribed flow rate.

The procedure is then repeated until the last operating sprinkler in the design area within this branch line is reached. In Figure 3.4 it is the third sprinkler from the left. When the pipe section supplying this sprinkler is sized (d_3 following the notation in Figure 3.6), one ensures function of the least favoured sprinklers on this branch. If this diameter is maintained all the way to the cross main and a sequence of more favoured sprinklers on the branch activates instead, the flow rates of these sprinklers will be ensured automatically. This is because lower distance to the pump and larger diameter in comparison to the least favoured design area will guarantee higher pressures at the sprinklers. In consequence, the first branch line has been designed.

From the practical point of view it is of course not realistic to construct the sprinkler system using precisely the calculated diameters. As indicated in Table 2.1, manufactured pipes usually have standardized diameters and thus a calculated diameter is a lower limit for what can be

chosen. The chosen diameter is consequence always larger, which is desirable creating a margin of safety needed among others for ensuring the "space" for the minor losses.

Step 5: Sizing the remaining branch lines
The easiest way to complete designing the system is to make all branch lines identical with the first one sized. As the first branch line was sized for from hydraulically most unfavourable conditions, the flow requirements will be fulfilled automatically. Now the cross main can be sized.

Step 6: Sizing the cross main
The cross main section from the uppermost branch line in Figure 11 to the next one is sized for the flow in this hydraulically most remote branch line. The next pipe section is then sized for both this flow and flow in the second branch line from above. Observe that the procedure is analogous with designing the branch line; the difference is that the branch line has been replaced by the cross main and the sprinklers with the branch lines. If this is the last branch line in the design area as indicated in Figure 3.4, this diameter is maintained through the whole residual cross main to guarantee the prescribed flow rates for an arbitrary placed design area. This is entirely in analogy with designing branch line in Step 4. Just like branch line diameter may be held constant between cross main and the last sprinkler in the design area (third from left on uppermost branch in Figure 3.4), the cross main may as well have constant cross section from feed main to the last branch line in the design area (second from above, Figure 3.4).

Design of gridded sprinkler systems
Hydraulic design of gridded sprinkler systems has as a purpose of supplying sprinklers in a design area of sprinkler operation (hydraulically most remote one) with prescribed flows which is in complete analogy with procedure for branched sprinkler systems.

The position of the design area is not as obvious as in a branched system due to fact that every area can be fed from both sides. It can be shown that for a side end fed gridded system as in Figure 3.7, the design area of sprinkler operation is located centrally on the branch lines and as far away from the feed main as possible (Jensen, 2001). This is based on assumption that the number of activated branches (two uppermost in Figure 3.7) is small in comparison to the number of inactive branches, wherefore Figure 3.7 should only be viewed as a schematic representation.

Further, the design requires knowledge or assumption of flow pattern in the system. The assumption made for gridded systems is that flow to the design area is equal from both sides and that the inactive branches equally contribute in supplying water from feed side to the opposite one. The resulting design flow pattern is presented in Figure 3.7.

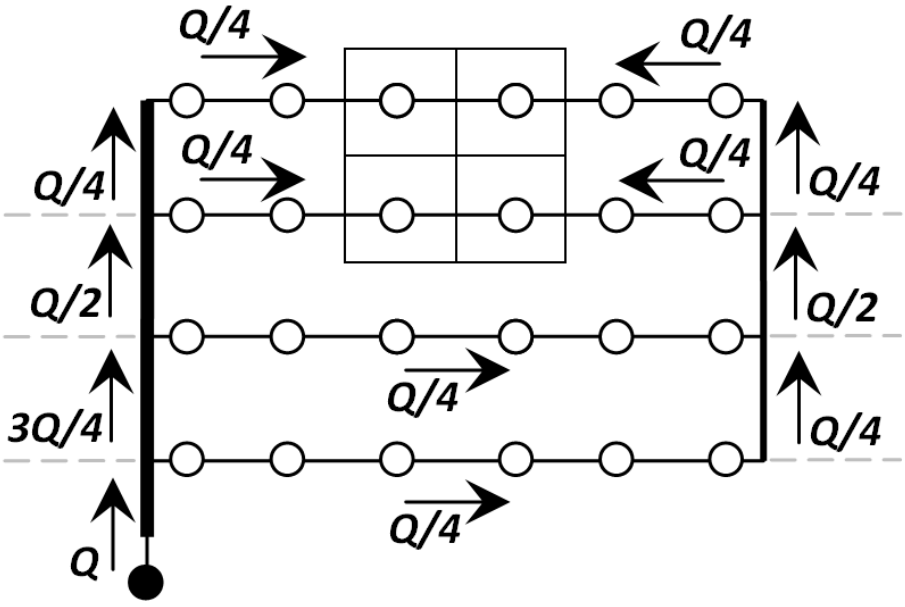

Figure 3.7 *Design flow pattern in a gridded system*

A general description (for arbitrary number of branch lines) of flow pattern can be done if the number of active branch lines is denoted as *n* and number inactive as *m*. Then, the largest flow in cross main on feed side will be *Q*, *Q/2* in the cross main on the opposite side, *Q/(2m)* in the inactive branches and *Q/(2n)* in the active ones. The approach used is to size all branch lines for *Q/(2n)*, the cross main on feed side for *Q* and the cross main on opposite side for *Q/2* i.e. the largest flows occurring in respective pipe.

To do this, design pressure drop in the system is calculated in analogy with branched systems. This time, it is not that obvious how length in equation (3.17) is to be chosen as there are more than one way for the flow to the sprinklers. An appropriate expression of design distance is derived by Jensen (2001):

$$l_g = \frac{x+y}{2} \tag{3.21}$$

x	length of branch line, [m]
y	length of cross main, [m]

By adding the length of feed main to l_g one obtains the length l to be used in equation (3.17).

3.4.3 Design of deluge sprinkler systems

With the information outlined above, the only thing a reader needs to know is that hydraulic design of deluge sprinkler systems is simply design of branched or gridded system for a design area of sprinkler operation containing all sprinklers.

3.4.4 Design of water mist systems

Hydraulic design of water mist systems does not differ much from that of traditional sprinkler systems. The main difference is that designers do not need to follow any general ceiling sprinkler densities. Instead the densities followed are based on certain standardized performance tests. Thus the ceiling sprinkler densities may vary between different manufacturers and different nozzles for same type of occupancy.

3.4.5 Comments on methodology

The hydraulic sprinkler design methodology outlined above is to be viewed as systematic guide to chose reasonable pipe diameters rather than a stringent sizing problem. The assumptions which may seem unsupported and doubtful if considered isolated are easy to justify in this case; as long as a final control calculation is made and confirms that the flow rates are larger (but not unreasonably larger) than those prescribed, these assumptions are of lesser importance.

3.4.6 Use of Hazen-Williams equation in sprinkler design

The above described methods are consistent with general pipe flow theory (White, 2008). However, it is a simplified formula of Hazen-Williams that is most often used as a standard in traditional sprinkler systems design (Jensen, 2002):

$$\Delta p_f = 6.05 \cdot 10^{10} \frac{(Q/C)^{1.85} L}{d^{4.87}} \qquad (3.22)$$

C C-factor (wall roughness coefficient)

It is easily seen that the sizing problem using this equation is limited to simply solving for d. There is no need of iteration procedure as no implicit Colebrook formulas is present, however there are factors making use of eq. (3.22) very doubtful.

Although Hazen-Williams equation is often presented in textbooks along with Darcy-Weisbach equation, it is absolutely not a tantamount expression. This empirical expression lacks dimensional homogeneity and, what is more important, if improperly used may result in errors as high as 40 %. The problem with the expression is that the C-factor intended and tabulated as a coefficient describing wall roughness is rather comparable to friction factor f in equation (3.2) and can easily be shown to be a strong function of relative roughness and Reynolds number, and in consequence also function of diameter and viscosity (Liou, 1998).

This makes the equation valid in quite a narrow range of Reynolds numbers in neighbourhood of those present at the experiments performed to determine C. With this in mind it is not surprising that a general definition of what a proper use of the Hazen-Williams equation means is somewhat controversial. Williams and Hazen (1933) themselves proposed 0.05 m < d < 1.85 m and $8 \cdot 10^3$ < Re < $2 \cdot 10^6$. More recently proposed limits include 10^4 < Re <10^7 & C > 100 and 10^5 < Re <10^8 (Quentin et al., 2007).

Unfortunately this background information is typically passed over in silence in tables containing C-factors while the fact that diameter appears separately in the Hazen-Williams equation makes an incautious user even more sure that diameter dependence is fully accounted for (Liou, 1998) while actually it is not.

A possible explanation for Hazen-Williams equations to be still broadly used is the presence of extensive databases of C-factors for different pipe materials compared to the relatively small database of corresponding relative roughness values (ϵ/d) required by Colebrook equation (Quentin et al., 2007). To remedy this Liou (1998) presents expression for converting C to ϵ/d assuming that experimental conditions in terms of d and Re used in determination C are known. Such detailed historical information is however typically absent and therefore Quentin et al. (2007) presents a model requiring only knowledge or sound assumption of diameter used. The apparent cumbersome nature of implicit Colebrook formula can neither be used as argument for

choosing Hazen-Williams equation. Not only can it easily be dealt with most graphing calculators of today but there are also several explicit formulas approximating that of Colebrook available (Liu, 1998; White, 2008) making the calculations easy and accurate.

Use of the Hazen-Williams equation has hardly any justification and is strongly discouraged (Liou, 1998). In light of this, it is even more remarkable that the Hazen-Williams equation is prescribed to be used by all significant providers of sprinkler recommendations as National Fire Protection Association (NFPA, 2003; NFPA, 2007) and European Committee of Standardization (CEN, 2004).

There are many equations in engineering praxis that are deficient just as equations (3.22) and (3.12) but remains in use despite efforts of more orthodox professionals to replace them with scientifically more correct expressions. It is not easily done considering that K-factors are used in describing sprinkler performance almost from the beginning, while Hazen-Williams equation with its C-factor dates to 1901. With this time perspective, papers of Liou and Quentin are very recent and it seems that the sprinkler branch has not yet paid attention to them, *vide* e.g. Isman (2010).

For high and intermediate pressure water mist systems, NFPA (2003) actually prescribes usage of Darcy-Weisbach equation, while the Hazen-Williams is permitted for diameters larger than 20 mm and flow velocities lower than 7.6 m/s and recommended for low pressure systems.

3.4 Essential pump theory

To make a sprinkler system functional, water flow must be created in some way. The easiest way would be if the sprinkler system could be connected to the bottom of a large reservoir. Presuming that the reservoir is large enough for the height of the free water surface to be assumed constant, such a solution would provide the sprinkler system with a constant driving pressure head i.e. pressure drop through the system independent of the flow rate. In other word, the flow rate through the activated system will adjust itself to a level giving sum of minor losses and friction losses equal to the pressure head. Such a configuration seems however unpractical and pumps are used instead.

Pumps i.e. machines that add energy to the fluid are usually classified according to their working principle in two main categories: positive-displacement pumps and dynamic pumps (White, 2008). Positive-displacement pumps represent a principle opposite to that of constant head system as here the flow rate is constant. This can be achieved easiest by a reciprocating piston pump.

In a piston pump, the pumped fluid is sucked into a liquid cylinder through a suction valve when piston moves upwards and is thereafter forced out of the cylinder through a discharge valve by downward motion of the piston which increases pressure of the liquid. This is in complete analogy with mass flow rate in a reciprocating piston engine and it is actually possible to use piston engine as liquid pump by driving on crankshaft and connecting intake to a water source. The author has seen this, but do not claim that this is general feature of all reciprocating engines.

In a dynamic pump, closed volumes similar as cylinders in piston pumps are absent and energy is added to the liquid by e.g. fast-rotating impellers or vanes (White, 2008). The most distinguished representative of the dynamic pump family is a centrifugal pump (with impeller); nearly standard in fire engines and together with piston pump the most prevalent pump type in

sprinkler context. The pump characteristic, defined as relation between pressure provided as a function of extracted flow from the pump, is more complicated for centrifugal pumps than for flow- and pressure-creating devices discussed earlier with pressure and flow rate usually related in parabolic fashion, right diagram in Figure 3.8.

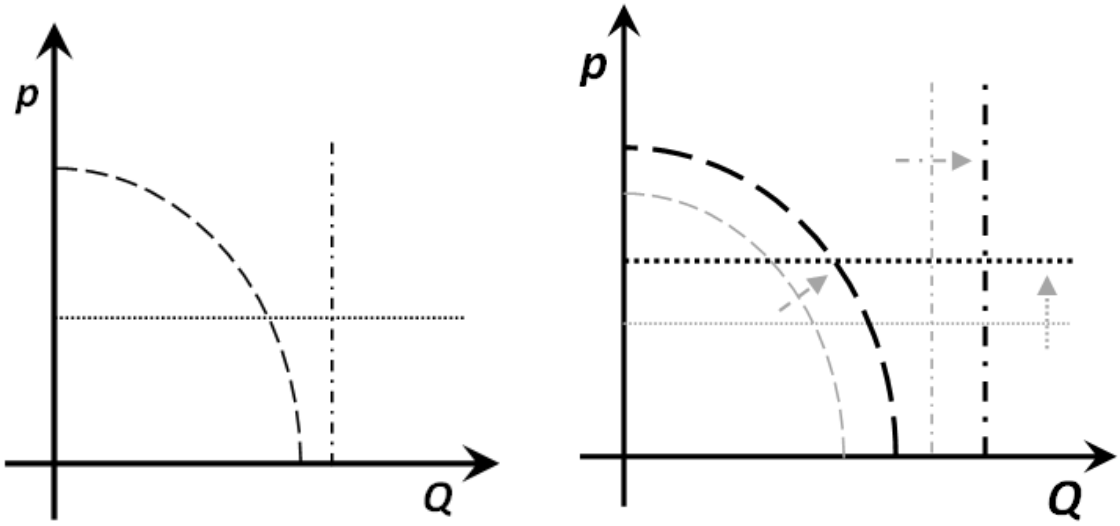

Figure 3.8 *Principal pump characteristic (performance) curves for large reservoir (dotted line), reciprocating piston pump (dot-dashed line) and centrifugal pump (dashed) (left) and impact on curves due to increased pump speed or water height in the reservoir*

The interpretation of the dashed pump performance curve in Figure 3.8 is that the highest pump head is obtained if no flow is extracted from the pump. A centrifugal pump can be driven without any flow extract as there are no closed volumes present during working cycle and the pump is therefore open between low and high pressure side, so that no forced motion of the fluid can occur and this is in this configuration the highest pressure head of the pump is observed. Thereafter, the head achieved by the centrifugal decrease as the flow extracted increase. Finally, a maximal flow rate that can be extracted is reached and in this point the pump head is zero.

It should be mentioned that just like characteristic pump for large reservoir presumes some height to free liquid surface, the pump performance pumps for piston and centrifugal pump in Figure 3.8 presumes some constant pump speed. Performance may be of course improved by increasing pump speed or height to free surface in the reservoir, which gives impact on the characteristic as indicated in right diagram in Figure 5.8.

The pressure losses in a system can also be related to flow rate according to eq. (3.7) so that so-called system curve can be obtained and plotted in same diagram as pump performance curve. The actual flow rate will be given as the intersection between the pump characteristic and the system curve, Figure 3.9.

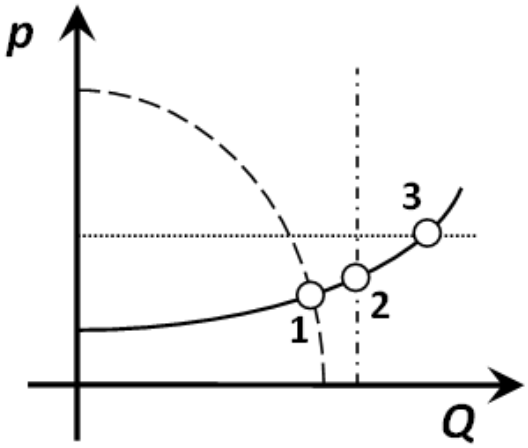

Figure 3.9 *System curve (solid line) and actual flow rates in the system if connected to large reservoir (3), piston pump (2) or centrifugal pump (1)*

In Figure 3.9, the system curve is represented by the solid line and operational points for different pump types are marked. If the system curve does not start at origin, as in Figure 3.9, static height difference in the system is indicated i.e. pump lies at lower altitude than the system.

Centrifugal pumps can deliver huge amounts of water; however the pressure that can be achieved is of course limited due to connection between fluid on high and low pressure side. On contrary, great pressures can be achieved by piston pumps, but the flow is rather limited by reciprocating movement of the piston. These differences make centrifugal pumps ideal for conventional and other low pressure sprinkler systems while a piston pump is obvious choice for high pressure water mist systems, Figure 3.10.

Figure 3.10 *Electrical centrifugal pumps supplying a conventional sprinkler system with water, (Arvidson, 2006)*

4. Heat transfer in pipes

A sprinkler pipe containing water will be subjected to heat transfer as soon as a difference in temperature between the water and ambient air outside is present.

4.1 Radial heat transfer in pipe

If the pipe is long in comparison to the diameter, it may be assumed that the heat transfer occurs only in radial direction and hence is one-dimensional. The expression of heat flux water and ambient air can be expressed as (Sundén, 2006):

$$\dot{q} = \frac{2\pi L(T_f - T_0)}{\frac{1}{h_i R_i} + \frac{1}{k} ln\frac{R_o}{R_i} + \frac{1}{h_o R_o}} \tag{4.1}$$

$\dot{q}$	heat flux, [W]
L	pipe length, [m]
T_f	water bulk temperature, [K]
T_0	ambient temperature, [K]
h_i	heat transfer coefficient between water and pipe, [W/(m²K)]
h_o	heat transfer coefficient between pipe and air, [W/(m²K)]
k	thermal conductivity of pipe material, [W/(mK)]
R_i	inner radius of the pipe, [m]
R_o	outer radius of the pipe, [m]

Equation (4.1) is often written in the following form:

$$\dot{q} = \frac{L(T_f - T_0)}{R_{total}} \tag{4.2}$$

Where R_{total} is so called thermal resistance defined as:

$$R_{total} = \frac{1}{2\pi}\left(\frac{1}{h_i R_i} + \frac{1}{k} ln\frac{R_o}{R_i} + \frac{1}{h_o R_o}\right) \tag{4.3}$$

Temperature distribution in pipe itself may be interesting as well and can be expressed as follows (Sundén, 2006):

$$\frac{T(r) - T(R_o)}{T(R_i) - T(R_o)} = \frac{\ln(r/R_o)}{\ln(R_i/R_o)} \tag{4.4}$$

r	radial coordinate, [m]

4.2 Cooling of water flowing in a pipe

Statement of the problem of water flowing in a pipe with radial heat transfer can be summarized by Figure 4.1.

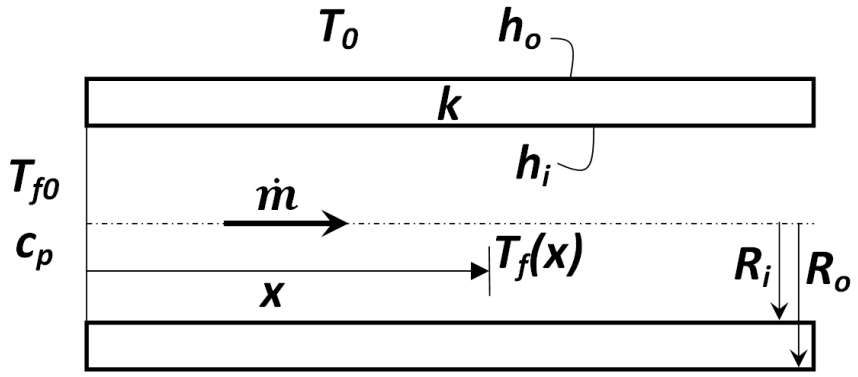

Figure 4.1 *Heat transfer in pipe with a main flow*

This problem is treated appropriately by setting up an energy balance on an infinitesimal pipe element and using that heat conducted through the wall (equation (4.2)) must be balanced by water enthalpy flux (Sundén, 2006):

$$\frac{dx(T_f - T_0)}{R_{total}} = d\dot{q} = -\dot{m}c_p \frac{dT_f}{dx} dx \tag{4.5}$$

$\dot{m}$ mass flow rate, [kg/s]
c_p heat capacity at constant pressure, [J/(kgK)]

Solution to (4.5) in terms of bulk temperature T_f as functions of coordinate x is given by Sundén (2006):

$$T_f(x) = T_0 + \left(T_{f0} - T_0\right) e^{\frac{-x}{\dot{m}c_p R_{total}}} \tag{4.6}$$

For the special case of constant wall temperature, equation (4.5) can be simplified by realizing that constant wall temperature can be modelled by setting $h_o = k = \infty$ and $T_0 = T_w$ in expressions (4.3) and (4.6), this gives:

$$T_f(x) = T_w + \left(T_{f0} - T_w\right) e^{\frac{-2k_f h_i x}{\rho c_p V R_i}} \tag{4.7}$$

k_f heat conductivity of fluid, [W/(mK)]

Approximate solution to the constant wall temperature problem can be derived by setting up the heat balance directly on the whole interesting length x at once, which is frequently done in Holman (1997):

$$\dot{q} = h_i \pi d_i x \left(T_w - \frac{T_f(x) + T_{f0}}{2}\right) = \dot{m}c_p\left(T_f(x) - T_{f0}\right) \tag{4.8}$$

The temperature can be then easily solved:

$$T_f(x) = \frac{T_{f0}\left(\frac{\dot{m}c_p}{h_i \pi R_i x} - 1\right) + 2T_w}{\frac{\dot{m}c_p}{h_i \pi R_i x} + 1} \tag{4.9}$$

The difference between (4.9) and (4.7) is that in (4.8) it is assumed that $(T_f(x) + T_{f0})/2$ represents the mean bulk temperature which imposes a solution fulfilling this assumption. In reality, the temperature varies exponentially and approaches asymptotically T_0 or T_w in (4.6) and (4.7) respectively. In (4.9) there is no such mathematical barrier preventing $T_f(x)$ become lower than T_w which is unphysical and requires careful usage of this expression.

All the expressions (4.6)-(4.9) are derived assuming constant c_p and R_{total} i.e. also constant heat transfer coefficients. As c_p varies with temperature and h_i depends both on temperature and coordinate (which will be showed soon), this means that appropriate average values are to be used.

Recalling definition of thermal resistance and assuming that other quantities are known, the water bulk temperature at some certain location *x* can be calculated from (4.6) or (4.7) if heat transfers coefficients h_i and h_o (or only h_i in (4.7) or (4.9)) can be determined. Heat transfer coefficients are usually calculated from definition of a dimensionless quantity called Nusselt number:

$$\mathrm{Nu_d} = \frac{hd}{k_f} \tag{4.10}$$

$\mathrm{Nu_d}$ Nusselt number, [-]

To solve h from (4.10), the Nusselt number must be known. Nusselt numbers are calculated using empirical or semi-empirical correlations. These will take different forms dependent on whether convection is forced or natural.

4.2.1 Modes of convection

The heat transfer equations presented until now are valid regardless of whether fluids of interest (water inside pipe and air outside) are at rest or in motion. The influence of this is accounted for by convective heat transfer coefficients h_i and h_o which are calculated in different ways depending on type of convection. There are three types of convection: forced, natural and mixed forced and natural convection.

Forced convection can be described as a phenomenon of enhanced heat transfer due to main flow of fluid close to the surface of interest.

Natural convection, in similarity with forced convection, occurs due to motion of fluid close to surface at different temperature. However, in natural convection process there is no main flow of fluid or it is insignificant. Instead the flow is driven by mass forces due to density variation between ambient air and warmer air close to the surface (if $T_w > T_\infty$).

If the magnitude of mass forces associated with natural convection and inertial forces of the main flow are similar, a mixed convection mode occurs with natural convection and forced convection contributing simultaneously. Thus by relating mass and inertial forces, convection mode present can be identified. This can be done using the ratio $\mathbf{Gr/Re^2}$.

$\frac{\mathbf{Gr}}{\mathbf{Re^2}} \ll \mathbf{1}$ forced convection

$\frac{\mathbf{Gr}}{\mathbf{Re^2}} \gg \mathbf{1}$ natural convection

$\frac{\mathbf{Gr}}{\mathbf{Re^2}} \approx \mathbf{1}$ mixed forced and natural convection

Grashofs number defined according to (4.11) and Re are evaluated at characteristic velocity i.e. free stream or bulk velocity in external and internal flow respectively.

$$\mathrm{Gr} = \frac{g\beta(T_w - T_\infty)L^3}{\nu^2} \tag{4.11}$$

β volumetric thermal expansion coefficient, $1/T_\infty$ for ideal gases, [-]

In the present problem, convection will be most likely forced inside the pipe and natural outside the pipe (i.e. ambient air assumed being at rest).

4.2.2 Forced convection inside pipe

Convection is very dependent on whether the flow is laminar or turbulent as turbulence enhances greatly the convective transfer. Thus, separate correlation for Nusselt number exists for these two flow modes.

Laminar flow

For fully developed thermal conditions in laminar pipe flow at constant wall temperature, the Nusselt number is equal to 3.656 (Sundén, 2006), which can be used directly to calculate heat transfer coefficient in (4.7). In reality, the value of 3.656 is asymptotically approached as distance from the pipe entrance x increases due to the fact that there exist a thermal entrance section where the thermal conditions i.e. the temperature profile is not fully developed. To take account for this, an expression for so called mean Nusselt number can be used (Sundén, 2006), equation (4.12).

$$\overline{\mathrm{Nu}}_\mathrm{d} = 3.656 + \frac{0.0668\mathrm{Re_d Pr}\cdot d/x}{1+0.04(\mathrm{Re_d Pr}\cdot d/x)^{2/3}} \tag{4.12}$$

Pr Prandtl number, $\nu\rho c_p/k$, [-]

Expressions (4.6), (4.7) and (4.9) are all derived assuming constant h_i and h_o which are however coordinate dependent as Nusselt number is. Therefore, if possible, mean Nusselt number expressions as (4.12) should always be used to calculate heat transfer coefficients. Temperature dependence through presence of temperature dependent $\mathrm{Re_d}$ and Pr is handled by evaluating physical properties at estimated mean bulk temperature.

If not wall temperature but heat flux is constant, Nusselt number approaches 4.364 instead of 3.656. A set of equation analogical to expression (4.12) can be used to express mean Nusselt number which includes thermal entrance effects (Sundén, 2006):

$$\overline{\mathrm{Nu}}_\mathrm{d} = 1.953\left(\frac{x/d}{\mathrm{Re_d Pr}}\right)^{-1/3} \quad \text{if} \quad \frac{x/d}{\mathrm{Re_d Pr}} < 0.03 \tag{4.13}$$

$$\overline{\mathrm{Nu}}_\mathrm{d} = 4.364 + \frac{0.0722}{x/d}\mathrm{Re_d Pr} \quad \text{if} \quad \frac{x/d}{\mathrm{Re_d Pr}} > 0.03 \tag{4.14}$$

Turbulent flow

For turbulent flow in smooth pipe, fully developed thermal conditions and constant wall temperature or constant heat transfer rate through the pipe wall, the Nusselt number can be calculated using (Sundén, 2006):

$$\mathrm{Nu_d} = \frac{\mathrm{Re_d Pr}(f/8)}{1.07+12.7\sqrt{f/8}\left(\mathrm{Pr}^{2/3}-1\right)} \tag{4.15}$$

The friction factor f in above equation is recommended to be evaluated using the friction law of Prandtl, i.e.:

$$\frac{1}{\sqrt{f}} = 2\log\left(\mathrm{Re_d}\sqrt{f}\right) - 0.8 \tag{4.16}$$

Expression (4.15) has also been modified to better agree with reality at lower Re which gives Gnielinski formula:

$$\mathrm{Nu_d} = \frac{(f/8)(\mathrm{Re_d}-1000)\mathrm{Pr}}{1+12.7\sqrt{f/8}\left(\mathrm{Pr}^{2/3}-1\right)} \tag{4.17}$$

$0.5 < \mathrm{Pr} < 2000$
$2300 < \mathrm{Re_d} < 5\cdot10^6$

This time f should is recommended to be calculated from:

$$f = (0.79\ln \mathrm{Re_d} - 1.64)^{-2} \tag{4.18}$$

For constant wall temperature and smooth pipe, following equation can be used:

$$\mathrm{Nu_d} = 0.023\mathrm{Re_d}^{0.8}\mathrm{Pr}^{1/3} \tag{4.19}$$

$\mathrm{Re_d} > 10^5$
$0.7 < \mathrm{Pr} < 160$
$L/D > 60$

To take account for the thermal inlet section where the temperature profile is not fully developed (above correlations do not) the following expression for mean Nusselt number can be used:

$$\overline{\mathrm{Nu_d}} = 0.036\mathrm{Re_d}^{0.8}\mathrm{Pr}^{1/3}\left(\frac{d}{x}\right)^{0.055} \tag{4.20}$$

$10 < x/d < 400$

4.2.3 Natural convection outside the pipe

A pipe warmed up by an internal water flow and exposed to ambient air will be subjected to convection on outside, a natural one, assumed that the air is at rest. Dependent on whether the pipe is placed vertically or horizontally, different expressions for the Nusselt number are valid.

Vertical pipe

A convective heat transfer from vertical pipe to ambient air does not differ principally from convection from vertical plate. For laminar boundary layer ($Gr \cdot Pr < 10^9$), mean Nusselt number with respect to pipe length is given by (Sundén, 2006):

$$\overline{\mathrm{Nu}} = 0.6728 \left(\frac{\mathrm{Gr}_{x=L}}{4}\right)^{1/4} \quad (4.21)$$

It should be mentioned that eq. (4.21) is only valid for air in temperature range approximately between – 50 °C and 0 °C as the original expression present in (Sundén, 2006) included a Prandtl number dependent function which we have evaluated for temperatures interesting for us. Pr for air expects only weak variation with temperature and equals ca 0.72 in this temperature range.

If instead the boundary layer is turbulent ($Gr \cdot Pr > 10^9$), the corresponding expression, after inserting $\mathrm{Pr} = 0.72$, becomes (Sundén, 2006):

$$\overline{\mathrm{Nu}} = 0.0184(\mathrm{Gr}_{x=L})^{2/5} \quad (4.22)$$

Horizontal pipe

The case with a horizontally placed pipe cannot be reduced to the "plate problem" as the pipe surface is not constantly parallel to the gravitation vector. Mean value of Nusselt number over the pipe surface can be calculated from (Sundén, 2006):

$$\overline{\mathrm{Nu}_\mathrm{D}} = 0.3955\mathrm{Gr}_\mathrm{D}{}^{1/4} \quad (4.23)$$

Just like equations (4.21) and (4.22), expression (4.23) is presented in simplified form utilizing that $\mathrm{Pr} = 0.72$ for ambient air of temperatures interesting for us.

4.2.4 Commentary on fluid properties

A number of temperature dependent fluid properties are present in equations used to obtain Nusselt number: heat conductivity, viscosity and Prandtl number.

These properties for use in equation (4.20) are recommended to be evaluated at the mean bulk temperature while those for use in equation (4.19) at mean value of wall temperature and bulk temperature (Sundén, 2006). However, the mean bulk temperature understand as $(T_{f0} + T_f(x))/2$ is not known at the beginning, actually $T_f(x)$ is the searched quantity. This problem can be solved by iterative procedure: fluid properties are evaluated at initial bulk temperature T_{f0} and the obtained $T_f(x)$ is then used to calculate mean bulk temperature for which fluid properties can be evaluated once more so that new $T_f(x)$ can be calculated (Holman, 1997).

In formulas regarding natural convection, a reference temperature defined as mean value between ambient temperature and wall temperature is used:

$$T_{ref} = \frac{T_w + T_\infty}{2} \quad (4.24)$$

5. Ice formation in pipes

Much attention has been paid to ice formation in residential pipes with resulting complete pipe blockage and risk for bursting. These studies are usually limited to cases with no main bulk flow in a pipe (Gilpin, 1977 a & b; Gordon, 1996). Note that this only mean an absence of a main direction of flow – secondary convective flows will of course be present. In contrast, the subject of interest for this thesis is ice formation occurring during activation of a sprinkler system and hence with main pipe flow.

An activated dry pipe sprinkler system can experience flow stoppage due to ice formation inside a pipe at initial subfreezing temperature, most likely during the filling process. This is because the temperature of the system is lowest at the beginning, prior to experiencing heating due to contact with warmer water. In a wet pipe sprinkler system filled with antifreeze added to water, the solution initially filling the pipe will not be vulnerable for freezing but one can imagine situation when all antifreeze is consumed and ordinary water enters the piping with risk of freezing and stoppage at the moment when the flow throughout the system to the sprinkler has been already established.

Even if the latter scenario is rather exotic and goes beyond limitation of this thesis, we will both consider complete flow blockage during filling process and complete flow blockage at an established flow. The reasons are that there is much more extensive literature regarding ice formation at an established flow and that, as it will be seen later, it provides general insights that can be also applied to the filling process.

5.1 Ice formation and flow blockage during filling of a pipe

Gilpin (1981 b) conducted a series of experiments aimed to clarify modes of ice formation and probability of complete blockage during filling of an initially empty cold pipe.

The experimental set-up consisted of a large water tank where water was cooled to approximately 1 °C, a pump and a 30 m long pipe coil of steel or polyvinylchloride (plastic) in a cold room where the temperature could be varied between 0° and –40 °C. The pipes used had inner diameters of 10 mm and 12.7 mm (steel respectively plastic) and corresponding pipe wall thicknesses of 0.6 mm and 3.2 mm respectively. During the tests, the pre-cooled water was pumped into the test coil in the cold room with mean velocity of 0.6 m/s, reached the pipe exit and was finally collected in a bucket (Figure 8.1).

The output included traces of the pressure at the entrance of the pipe (which as will be seen later can be directly related to the ice formation mode) and visual observations of the ice formation when the transparent plastic pipe was used.

5.1.1 Ice formation modes during filling of a pipe

During his plastic pipe experiments, three ice formation modes were visually observed by Gilpin (1981 b): annular, dendritic and mixed.

In the first mode, the annular mode, solidification occurs only at the inside wall of the pipe creating there a thin shell of ice (A in Figure 16). The pipe is gradually warmed up by incoming water which leads to increasing water temperature as function of time at some fixed location along pipe. This in turn causes continual melting of the rear edge of the annular ice shell. Hence, at certain time, only a part of the total pipe length was occupied by the ice shell which extended back from the leading edge of the incoming water.

The dendritic ice growth mode that occurred in Gilpin's experiments was in all respects similar to the dendrite formation during a solidification process in quiescent supercooled liquids (liquids at a temperature below its ordinary freezing point). This dendritic ice formation is characterized by tree-like solid structures growing from the walls into the liquid. The dendrites observed in the experiments were occasionally broken off by the flow and carried away leading to a slush ice at the leading edge of the flow as seen in Figure 5.1 (Mode D).

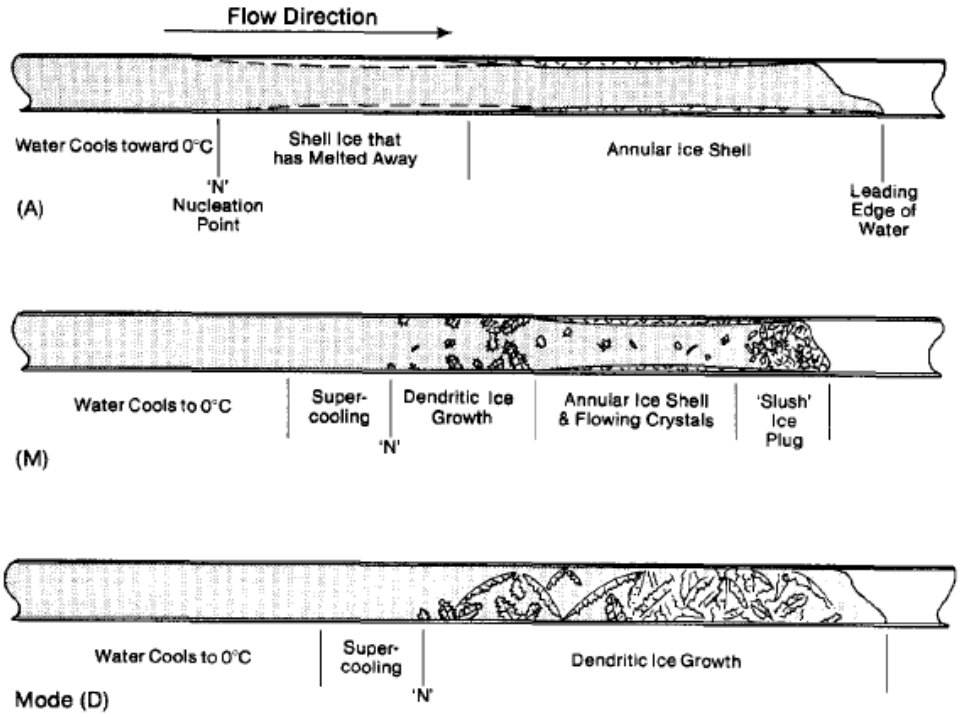

Figure 5.1 *Ice formation modes: annular (A), mixed (M) and dendritic (D) (Gilpin, 1981 b)*

Finally, a mixed mode of ice formation was observed (M in Figure 5.1). In this mode, initial formation of dendritic ice is followed by an annular ice shell with a slush ice plug present at the leading edge of the flow just like in mode D.

The observed ice formation modes in plastic pipe were connected to the entrance pressure traces that were registered during filling of the pipe (Figure 5.2). The first trace (a) represents a normal, smooth entrance pressure build-up during a filling process without any ice formation, observed at T_p = –3.5 ˚C. Here we use T_p to denote initial temperature of the pipe in accordance with the nomenclature of Gilpin (1981 b). This can even be expressed as: $T_p = T_w(x, t = 0)$.

During the test with the same pipe at T_p = –5.5 ˚C, the water flow reached the pipe exit without any ice formation which explains the same appearance of curves (a) and (b) between S and E, Figure 5.2. Dendritic ice started to form first after the establishment of the flow through the pipe causing a pressure rise seen in (b) after E. The subsequent pressure drop to normal exit level at E could in turn be connected to the fact that the dendrites were broken and melted by the continuing flow until no ice remained in the pipe (Gilpin, 1981 b).

T pressure trace (c) in Figure 5.2 documents a complete blockage of the pipe by dendritic ice growth with T_p = –10 ˚C that occurred before the flow front reached the pipe exit. A dendritic ice

slush plug was created in the pipe after which it stuck and was released several times giving rise to the observed pressure fluctuations in (c). Finally it stuck so much that not even a pump pressure of 340 kPa (P_{max} in Figure 17) was able to dislodge the ice.

Mixed ice formation mode was associated with pressure traces (d) and (e). The pressure rise, just like earlier, corresponds to dendritic ice growth. If the dendritic ice was melted before the flow reached the pipe exit, the pressure trace returned to normal as can be observed in (e). No complete pipe blockage was encountered for this mode.

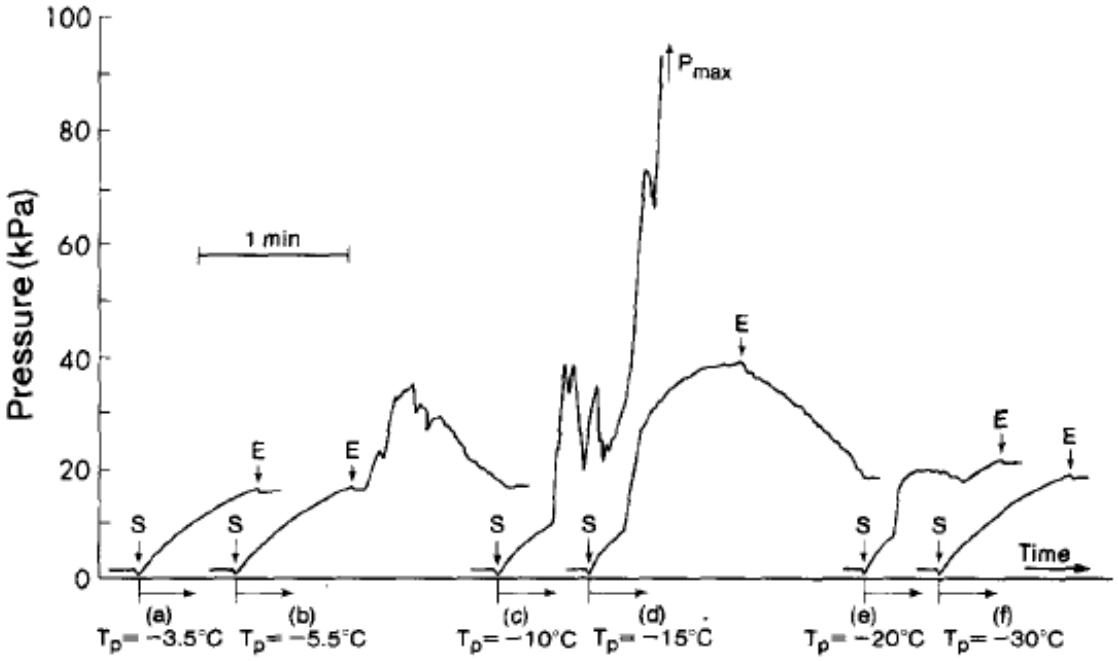

Figure 5.2 *Time traces of pressure at the entrance (plastic pipe) for different pipe temperatures; S – the flow into the pipe is started, E – the flow reaches the pipe exit (Gilpin, 1981 b)*

Pure annular ice formation mode was observed at the lowest temperatures with (f) as a representative pressure trace. This pressure trace is similar to (a) with pressure magnitude as the only difference. This is expected as annular ice shell represents a minor loss which demands a higher entrance pressure to maintain the same flow rate. No flow stoppage occurred.

The time traces of pressure at the entrance of the steel pipe (Figure 5.3) exhibit the same principal appearances as those of the plastic pipe. Thus, it was possible to draw conclusions on ice formation inside the pipe even without direct visibility of action inside.

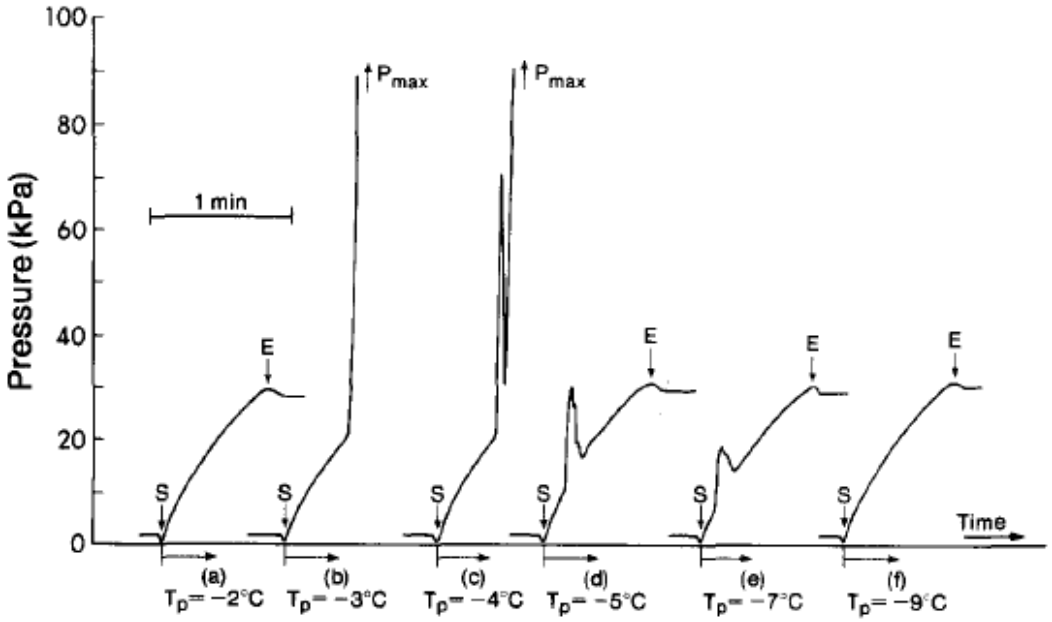

Figure 5.3 *Time traces of pressure at the entrance (steel pipe) for different pipe temperatures; S – the flow into the pipe is started, E – the flow reaches the pipe exit (Gilpin, 1981 b)*

Figure 5.3 reveals that the characteristic pressure traces from experiments with plastic pipe are present but displaced toward higher temperatures. A complete pipe blockage occurred at T_p –3 ˚C to –4 ˚C while the annular ice formation took place for initial temperatures of the pipe lower than –9 ˚C. Of ice formation modes present, just like in experiments with plastic tube, only dendritic ice managed to completely block the flow.

As mentioned, the average flow velocity in experiments with both steel and plastic pipe was 0.6 m/s. Additional tests in the steel pipe for velocities up to 1.2 m/s were done by Gilpin (1981 b) but the results were unaffected. Velocities up to 3.3 m/s were used in additional tests in the plastic pipe and for these highest velocities, no complete blockage of the pipe was observed.

5.1.2 Prediction of ice formation mode

As outlined earlier, dendritic solidification is a characteristic feature of supercooled liquids. In contrast if the bulk water temperature T_f is above 0 ˚C when solidification starts, the ice growth is located to a clearly defined single interface between liquid and solid extending from a cold surface with annular ice growth in pipes as an example. Thus, depending on whether supercooling of the bulk water occurs or not, these two different ice formation modes are to be expected (Gilpin, 1981 b).

For solidification to start, stable nuclei of solid must be formed. This occurs at some supercooling, at a temperature called nucleation temperature. Even if no supercooling of the bulk water appears, at least a local supercooling is therefore required. Thus, rather than the bulk temperature of water as such, the interface temperature between the water and the pipe will determine whether nucleation starts or not. The interface temperature between two semi-infinite solids is described by the contact temperature problem (Eckert and Drake, 1972) and given from:

$$T_f - T_c = \frac{\beta_p}{\beta_f + \beta_p}\left(T_f - T_p\right) = \Upsilon_\beta\left(T_f - T_p\right) \qquad \Upsilon_\beta \leq 1 \qquad (5.1)$$

T_f bulk water temperature, [K]
T_c interface temperature, [K]
T_p initial pipe temperature, [K]
β_p thermal effusivity for pipe material, $\beta = \left(\rho c_p k\right)^{1/2} = \frac{k}{\sqrt{\alpha}}$, [J/(m²Ks$^{1/2}$)]
β_f thermal effusivity for water, [J/(m²Ks$^{1/2}$)]

It can be seen from equation (5.1) that the lower the pipe temperature, the lower interface temperature T_c for a certain water bulk temperature T_f and certain Υ_β. For a very cold pipe it is likely that the interface temperature is lower than the nucleation temperature and thus an annular ice shell will form almost instantaneously. If the pipe is warmer (but of course still below the freezing point of water) the bulk water may be supercooled before interface temperature is low enough for spontaneous nucleation to occur. Then, the dendrites will form and rapidly grow into the supercooled water.

At the same time, a general nucleation temperature of water is impossible to predict accurately due to its great dependence on properties of impurities present. Water supplied for domestic use has been found to usually nucleate in the temperature range from –7 ˚C ($T_{n,lower}$) to –4 ˚C ($T_{n,higher}$). Hence, if the interface temperature is $T_{n,lower}$ or lower, there is a high probability of immediate ice nucleation resulting in annular ice without any supercooling of bulk water. This criterion can be written as:

$T_f \geq 0$°C & $T_c \leq T_{n,lower}$ – annular ice formation mode

By inserting $T_c = T_{n,lower}$ in equation (44), one obtains:

$$T_f - T_{n,lower} = \Upsilon_\beta\left(T_f - T_p\right) \tag{5.2}$$

$$T_f\left(1 - \Upsilon_\beta\right) = T_{n,lower} - \Upsilon_\beta T_p \tag{5.3}$$

Now, $T_f \geq 0$°C is used:

$$T_f = \frac{T_{n,lower}}{1-\Upsilon_\beta} - \frac{\Upsilon_\beta}{1-\Upsilon_\beta} T_p \geq 0°C \tag{5.4}$$

This allows the final criterion for annular ice growth mode to be set up:

$$\boldsymbol{T_p \leq \frac{T_{n,lower}}{\Upsilon_\beta}} \quad (°C) \tag{5.5}$$

Be aware that equation (5.5) imposes use of Celsius scale as initial criterion to derive it is set up in Celsius.

If instead the interface temperature is $T_{n,higher}$ (–4 ˚C) or higher, there is low probability that immediate nucleation occurs. Therefore, it is very likely that the water will be supercooled during its flow through the pipe before nucleation occur which will give dendritic ice formation. The criterion can be written as:

$T_f < 0$°C & $T_c \geq T_{n,higher}$ – dendritic ice formation mode

This can be used in equation (5.1) but using equation (5.4), a "dendritic" counterpart of it can be set up directly:

$$T_f = \frac{T_{n,higher}}{1-\gamma_\beta} - \frac{\gamma_\beta}{1-\gamma_\beta} T_p \leq 0\text{°C} \qquad (5.6)$$

The final criterion for dendritic ice growth mode becomes:

$$\boldsymbol{T_p \geq \frac{T_{n,higher}}{\gamma_\beta}} \qquad (\text{°C}) \qquad (5.7)$$

Pipes temperatures in between those given by criteria (5.5) and (5.7) are assumed to result in the mixed ice formation mode, explicitly:

$$\boldsymbol{\frac{T_{n,lower}}{\gamma_\beta} < T_p < \frac{T_{n,higher}}{\gamma_\beta}} \qquad (\text{°C}) \qquad (5.8)$$

Using criteria (5.5), (5.7) and (5.8) ice formation mode as function of temperature for pipe materials used in experiments can be predicted, see Table 5.1.

Table 5.1 *Predictions of ice formation modes ($\beta_f = 1.54 \cdot 10^3$), after Gilpin (1981 b)*

Pipe material	Thermal effusivity	γ_β	Annular mode	Mixed mode	Dendritic mode
Steel	$11.6 \cdot 10^3$	0.88	$T_p \leq -7.9$ °C	-7.9 °C $< T_p \leq -4.5$ °C	-4.5 °C $< T_p$
Plastic	$0.64 \cdot 10^3$	0.29	$T_p \leq -23.8$ °C	-23.8 °C $< T_p \leq -13.6$ °C	-13.6 °C $< T_p$

There is no upper temperature limit for dendritic ice formation present in Table 5.1 as Gilpin's model does not explicitly predict such limit. It is reasonable to assume that $T_p < T_{n,higher}$ must be such a limit as it is presumed that no nucleation occurs above this temperature. However, initial pipe temperatures slightly above $T_{n,higher}$ would require tremendously long piping for supercooling water to $T_{n,higher}$ thus making this limit hardly applicable in reality.

Gilpin (1981 b) found values presented in Table 5.1 to be in good agreement with results of his experiments summarized by Figure 5.2 and 5.3 which confirms reasonability of assumptions made during derivation of criteria (5.5) and (5.7) e.g. that solution to the contact temperature problem (5.1) is suitable for describing interface temperature between water and pipe wall.

Results in Table 5.1 help us to understand physical meaning of thermal effusivity β and ratio γ_β, where: $0 < \gamma_\beta < 1$. Equation (5.1) shows that the contact temperature between the two materials is closer to the temperature of material with higher thermal effusivity. The larger domination of one β over another, the closer is the contact temperature to the temperature of the material with dominating β. Thermal effusivity β of water in the interesting temperature range is $1.54 \cdot 10^3$ which is more than two times higher than that of plastic (Table 5.1). On other side, thermal effusivity of steel is more than seven times higher than that of water. Therefore, to obtain contact temperature interesting for nucleation, the steel pipe does not need to be cooled to that extent as the plastic pipe. Thermal effusivity can thus be said to measure ability of a material to exchange thermal energy with its surrounding.

Concluding, Gilpin (1981 b) performed a series of experiments which show that the risk for a complete pipe blockage during filling of a pipe is connected to dendritic ice formation and most

apparent at temperatures –3 ˚C to –4 ˚C in steel pipe. A method for determining ice growth mode as a function of initial pipe temperature and material was derived. In the experiments with steel tube, diameter and flow velocities used are representative for especially water mist systems.

5.1.3 Quantification of annular ice growth mode

In Gilpin's experiments, the annular ice formation mode did not manage to completely block the steel pipe even at – 30 ˚C which gives strong support to the thesis that complete annular ice blockage is not very probable. Of course, this cannot be generalized to all possible conditions. Pipe blockage due to annular solidification of a liquid during filling of a pipe has been subject of theoretical and experimental studies by Epstein and co-workers (Epstein et al., 1977; Epstein and Hauser, 1977). The result in the form of a penetration length of the liquid front at the time for pipe blockage has been derived for conditions summarized by Figure 5.4.

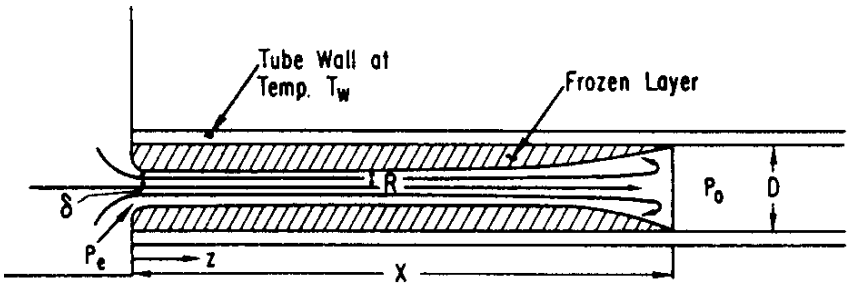

Figure 5.4 *Problem analyzed by Epstein et al. (1977)*

The problem concerns filling of an initially empty pipe by an arbitrary liquid at its freezing temperature resulting in an annular solidification at the inside of the pipe. The pressure at the entrance p_e and the wall temperature T_w are constant. Epstein is aware of the fact that if supercooling with possible dendritic solidification mode occurs, his theory becomes not applicable for the penetration problem. Therefore he assumes that wall temperature is low enough to prevent supercooling of the bulk liquid volume.

Several assumptions are made in order to simplify the problem:

- Most of the penetration occurs in a turbulent flow regime
- Smooth interface between liquid and solid so that friction factor given by Blasius formula can be used
- Constant temperature of solid-liquid interface equal to freezing temperature
- All physical properties constant
- Equal density of liquid and frozen layer
- No minor loss at the entrance
- Flat liquid front (i.e. with a normal parallel to pipe wall)
- Heat conduction only in radial direction

For detailed discussion of the assumptions, see Epstein et al. (1977).

The equation of fluid motion within the frozen layer is derived by Epstein et al. (1977) from continuity and momentum equations and takes the following form:

$$\dot{x}^2 = 12.64 \frac{R_0 \Delta p}{\rho} \left(\frac{2R_0 \dot{x}}{\nu}\right)^{1/4} \int_0^x \left(\frac{R_0}{R}\right)^{19/4} \mathrm{dz} \qquad (5.9)$$

x	instantaneous penetration length of liquid (see Figure 5.4), [m]
$\dot{x}$	velocity of penetrating liquid front, [m/s]
R_0	radius of the pipe, $D/2$ (see Figure 5.4), [m]
Δp	difference between entrance pressure and initial pressure in empty tube, [Pa]
$R = R(z,t)$	radial location of solid-liquid interface (see Figure 5.4), [m]
z	axial coordinate in the freezing section (see Figure 5.4), [m]

To solve this second order nonlinear integro-differential equation, the profile of the solid annulus materialized as *R(z, t)* must be known. As the latent heat of fusion released at the solid-liquid interface upon solidification must be conducted through the solid, $R(z,t)$ can be determined from the one-dimensional conduction equation applied to the solidified layer. Epstein et al. (1977) use an approximate solution to this problem, given by:

$$\frac{4\alpha_s B}{R_0^2}(t-t') = 2\left(\frac{R}{R_0}\right)^2 \ln\left(\frac{R}{R_0}\right) - \left(\frac{R}{R_0}\right)^2 + 1 \tag{5.10}$$

α_s in expression (5.10) is thermal diffusivity of solid defined as:

$$\alpha = \frac{k}{\rho c_p} \approx \frac{k}{\rho c} \tag{5.11}$$

The last simplifying step is done utilizing fact that heat capacities c_p and c_v are almost equal for media and temperature range of interest for us and thus can be denoted as c_l for liquid and c_s for solid (Liley, 2005).

In equation (5.10), B is a solidification parameter defined by:

$$B = \left[1 + \frac{2c_s(T_f - T_w)}{h_{if}}\right]^{1/2} - 1 \tag{5.12}$$

h_{if}	latent heat of fusion, [J/kg]

Finally, t and t' in equation (5.10) denote time (starting at $t = 0$ where $x = 0$) and time of arrival of the flow front at location z respectively. The time of arrival can be expressed by following implicit relation:

$$x(t') = z \tag{5.13}$$

It is worth to emphasize that equation (5.10) is derived for a quiescent liquid. However, as no convective heat transfer can occur between liquid and solid surface, both assumed maintained at the same freezing temperature, Epstein et al. (1977) judge that (5.10) can be used with t' as the only velocity dependent parameter, representing simply arrival of water.

Consequently, to solve R from equation (5.10), t' and hence x which must be solved from equation (5.9), must be known which requires simultaneous solution of equations (5.9) and (5.10). To reduce computational effort, Epstein et al. (1977) made an assumption on solid annulus profile and proved its reasonability by a sensitivity analysis. Equation (5.10) was only used at the entrance (t' known) and constituted a frame for profile of the frozen layer i.e. with solid crust profile as a function of time known at the entrance (5.10) and at x (no solid at x i.e.

$R_0 = R$, see Figure 5.4), only the exact shape in between was subject for approximation. The final result is:

$$\frac{x_P}{D} = 0.155\mathrm{Re}^{8/11}\left(\frac{\mathrm{Pr}\frac{\alpha_l}{\alpha_S}}{B}\right)^{7/11} \tag{5.14}$$

x_P penetration length at pipe blockage, [m]
D tube diameter, [m]

Reynolds number in equation (5.14) is defined as:

$$\mathrm{Re} = \left(\frac{2\Delta p}{\rho}\right)^{1/2}\frac{D}{\nu} \tag{5.15}$$

As seen, Reynolds number is evaluated using velocity calculated from equation (3.1) set up between entrance and location x where all pressure losses are neglected. In reality, both the velocity (expressed by equation (5.9)) and flow diameter ($2R$) vary (meanwhile constant d is used in (5.15)). Reynolds number in equation (5.15) is hence only an approximate one and aimed to be good representation of mean Re. It is required in order to express the result in a simple and explicit way, equation (5.14).

Epstein and Hauser (1977) devoted a separate paper to numerical, simultaneous solution of (5.9) and (5.10), and showed good agreement with previous approximation, obtaining 0.141 instead of 0.155 in equation (5.14).

By inserting properties of water and ice evaluated at freezing point, from Fukusako and Yamada (1993) and Liley (2004), expression (53) can be simplified and adapted to our problem of concern, which gives:

$$\frac{x_P}{D} = 0.2028\frac{\mathrm{Re}^{8/11}}{B^{7/11}} \tag{5.16}$$

The same can be done with equation (5.12):

$$B = \left[1 + 0.0124\left(T_f - T_w\right)\right]^{1/2} - 1 \tag{5.17}$$

Conformity between expression (5.14) and experiments have been controlled with a set-up in correspondence to system from Figure 5.4. The pipe coil used was immersed in a bath of coolant in effort to maintain constant, predefined wall temperature. The results are summarized by Figure 20.

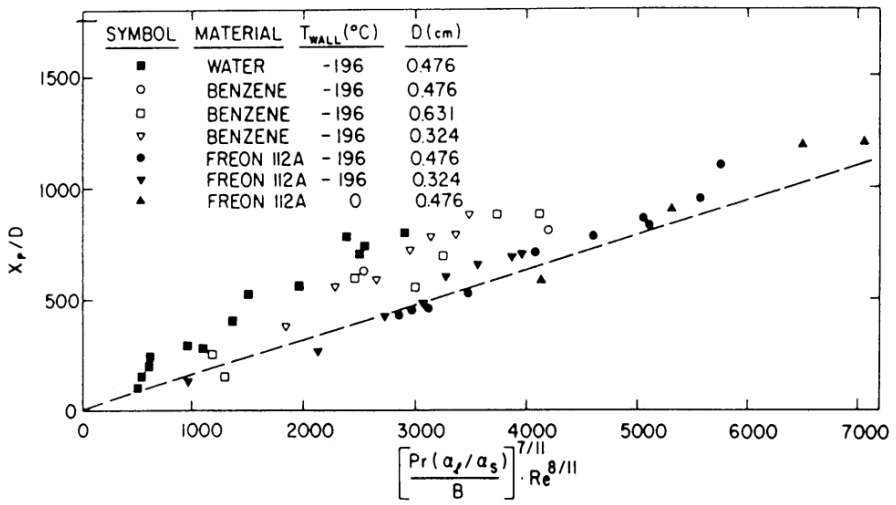

Figure 5.5 *Experimental data compared to equation (5.14) (Epstein et. al, 1977)*

Experimental results plotted in Figure 5.5 show quite good agreement with the theoretical model. As can be seen, water exhibits largest deviation from the model of liquids tested which has been related by Epstein et al. (1977) to difficulties in maintaining constant wall temperature with water streaming inside. Thus, penetration lengths of water have been underestimated.

Relevance for treated problem

The research of Epstein and his associates was restricted to constant wall temperatures and liquid at freezing temperatures. The first of the restrictions seems reasonable for short times of start up of a cold sprinkler system. Regarding the latter one, water filling a sprinkler system will not initially be at its freezing temperatures. It can of course be cooled down to freezing point after travelling a distance which could be calculated e.g. with equation (4.7). A simple calculation procedure would then be to add the penetration length calculated with Epstein's method to this distance, which would give total penetration length before complete blockage. Correctness of this procedure is however questionable because it neglects ice formation in pipe previous to reaching the freezing temperature. This is in conflict with Gilpin's (1981 b) experimental observations which reveal that annular ice growth is actually a mode characteristic for cases with bulk volume of liquid above freezing point. This makes any attempts to directly apply Epstein's method to problem of ice formation in sprinkler systems during filling suspicious, at least until such a procedure is confirmed experimentally for inlet water temperature higher than the freezing point.

Calculated penetrations lengths in accordance with Epstein's method with input data representative for sprinkler systems will however be presented in chapter 7.

5.1.4 Quantification of dendritic ice growth mode

Gilpin (1981 b) identified experimentally the dendritic ice formation mode as one with a greatest potential of achieving complete pipe blockage during filling of an initially empty, cold pipe. Risk for complete blockage was most obvious at temperatures between – 4 °C and – 3 °C. As Gilpin had an identification of ice formation mode as his main subject of interests, he did not attempt to quantify dendritic ice growth mode. For our problem such quantifying is however required, as it is not enough to make a statement that risk for complete blockage due to dendritic ice formation is highest in some temperature range. Given an unheated space, we cannot prevent

that the temperature at some time is within the dangerous range. However it is not stated in Gilpin (1981 b) that a steel pipe of arbitrary length and arbitrary water flow in it, will always experience complete blockage if a start-up is performed in the dangerous temperature range between – 4 °C and – 3 °C. He just states that such a blockage is "probable". Any more detailed assessment must be specific for certain system and originate in a quantitative description of morphology of dendritic ice growth.

Quantification of ice formation in pipe with quiescent water

During a process of supercooling, water will be cooled to temperature beneath its ordinary freezing point of 0 °C. Solidification of supercooled water will then proceed in a fashion of tree-like solid structures (dendrites) growing rapidly from the walls into the supercooled liquid. This process will continue until the bulk water temperature returns to 0 °C after being heated up by the latent heat of fusion released by the forming dendrites. Thus, we can set up an energy balance (Gilpin, 1977 b) for the system that originally consists of some volume of supercooled water:

$$m_{w,0} c_w \Delta T_{super} = m_{i,d} h_{if} \tag{5.18}$$

$m_{w,0}$	initial mass of water, [kg]
c_w	specific heat capacity of water, [J/kgK]
ΔT_{super}	amount of supercooling, $\Delta T_{super} = T_m - T_f$, [K]
T_m	liquid equilibrium freezing/melting temperature, [K]
$m_{i,d}$	mass of dendritic ice formed, [kg]
h_{if}	latent heat of fusion of ice, [J/kg]

From (5.18), a mass fraction of dendritic ice formed can be solved:

$$\chi_{mass,i,d} = \frac{m_{i,d}}{m_{tot}} = \frac{m_{i,d}}{m_{w,0}} = \frac{\rho_i V_{i,d}}{\rho_w V_{w,0}} = \frac{c_w \Delta T_{super}}{h_{if}} \tag{5.19}$$

ρ_w	density of water, [kg/m^3]
$V_{w,0}$	initial volume of water, [m^3]
ρ_i	density if ice, [kg/m^3]
$V_{i,d}$	volume of dendritic ice, [m^3]

To obtain volume fraction of dendritic ice, one must keep in mind that total volume of the system increases during ice formation and equals volume of dendritic ice formed plus volume of remaining water:

$$\chi_{vol,i,d} = \frac{V_{i,d}}{V_{tot}} = \frac{V_{i,d}}{V_{i,d}+V_w} = \frac{\frac{m_{tot}\chi_{mass,i,d}}{\rho_i}}{\frac{m_{tot}\chi_{mass,i,d}}{\rho_i}+\frac{m_{tot}\chi_{mass,w}}{\rho_w}} = \frac{\chi_{mass,i,d}}{\chi_{mass,i,d}+\frac{\rho_i}{\rho_w}\chi_{mass,w}} \tag{5.20}$$

By inserting $\chi_{mass,i,d}$ from (5.19) and utilizing that the mass fraction of remaining water must follow $\chi_{mass,w} = 1 - \chi_{mass,i,d}$, a final expression for volume fraction of the dendritic ice formed can be obtained:

$$\chi_{vol,i,d} = \frac{1}{1+\frac{\rho_i}{\rho_w}\left(\frac{h_{if}}{c_w \Delta T_{super}}-1\right)} \tag{5.21}$$

Equation (5.21) shows dependence between volume fraction of dendritic ice and supercooling which is illustrated by Figure 5.6. Physical properties used are evaluated for 0 °C from Fukusako and Yamada (1993), and Liley (2005).

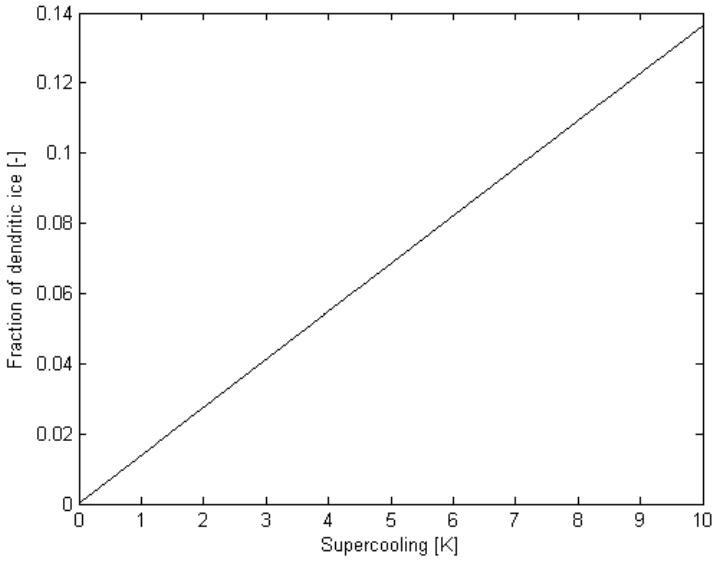

Figure 5.6 *Volume fraction of dendritic ice formed as a function of supercooling*

Gilpin (1977 b) actually does not use equation (5.21). Instead he neglects the volume expansion of the system due to formed ice; the volume fraction then becomes:

$$\chi_{vol,i,d} = \frac{\rho_w c_w \Delta T_{super}}{\rho_i h_{if}} \tag{5.22}$$

Use of this expression can be easily justified: deviation of (5.22) from (5.21) increases monotonously with supercooling and for a supercooling of – 10 °C, the fraction calculated with equation (5.21) is 98.9 % of fraction calculated with equation (5.22).

To use equation (5.21) and (5.22) the supercooling at nucleation must be known or measured. Gilpin (1977 b) have reported a nucleation range of – 6 °C to – 5 °C for water from hot water tap. For cold tap water a corresponding range of – 5 °C to – 4 °C seems to be reasonable. However, if the test pipe where filled with tap water from an open container, the supercooling obtained before nucleation was not more than – 3 °C. Gilpin (1977 b) made an attempt to explain this behaviour with so called heterogeneous theory of nucleation. According to this, nucleation ability of water is dependent on insoluble impurities picked up from the air e.g. dust particles which act as nucleation centers in water. Prolonged contact with water and particularly hot water destroys the efficiency of these impurities as nucleation agents which explains why water coming from different background conditions exhibits outlined nucleation behaviour.

With supercooling cancelled, no further dendritic ice formation occurs and solidification of remaining water proceeds in a less dramatic manner. Gilpin (1977 b) found that for quiescent water in a pipe, the solidification of water remaining in pipe after dendritic ice growth will be

completed mainly in an annular fashion. Thus, a complete solidification of quiescent water in a pipe follows a sequence of events showed in Figure 5.7.

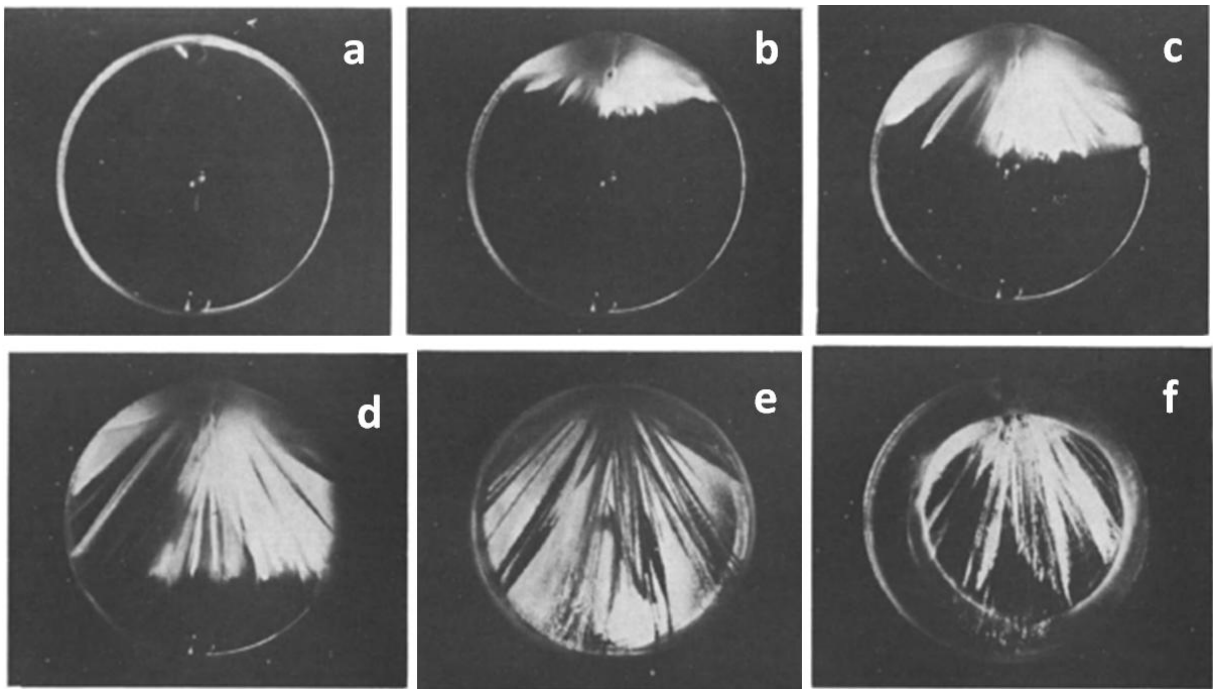

Figure 5.7 *Solidification of quiescent water in a pipe (a) before nucleation, (b)-(e) during dendritic ice growth, (f) during annular ice growth (after Gilpin (1977 a))*

The experiments of Gilpin (1977 b) were done with very slow rate of cooling to assure as homogenous temperature throughout the volume as possible. Some minor temperature differences will of course be present. As water density exhibits a maximum at 4 °C and thus increases with temperature below this point, in a quiescent volume of water with some temperature distribution and at temperatures lower than 4 °C, the coldest water will always be present at the top which explains why nucleation starts at the top of the pipe in Figure 5.7.

Gilpin (1977 b) also proposed an expression for calculating volume fraction of annular ice at any time between completion of dendritic ice growth and a throughout solidification within the pipe. The idea is that energy conducted through the solid annulus and further through the pipe during annular ice growth must be equal to the energy of fusion released by the annular ice that forms during the same time:

$$m_{i,a} h_{if} = \chi_{vol,i,a} L_{t=t_{a,1}} A \rho_i h_{if} = P \int_{t_{a,0}}^{t_{a,1}} L \dot{q} \mathrm{d}t \qquad (5.23)$$

$m_{i,a}$	mass of annular ice at time $t_{a,1}$, [kg]
$\chi_{vol,i,a}$	volume fraction of annular ice at time $t_{a,1}$, [-]
L	length considered, [m]
A	inner cross-sectional area of the pipe, [m^2]
P	inner perimeter of the pipe, [m]
$t_{a,0}$	start time for annular ice growth, [s]
$t_{a,1}$	arbitrary time point between $t_{a,0}$ and complete solidification of the pipe, [s]
$\dot{q}$	heat flux from the wall, [W/m^2]

The length L is here simply the instantaneous volume of the system at some time t divided by the inner, cross-sectional area of the pipe. Gilpin (1977 b) neglects the fact that this length increases in time due to expansion of the system by ice formation and he therefore lifts out L from the integral at the right hand side and set it equal to $L_{t=t_{a,1}}$ in order to obtain easy, explicit relation for $\chi_{vol,i,a}$:

$$\chi_{vol,i,a} = \frac{P}{\rho_i A h_{if}} \int_{t_{a,0}}^{t_{a,1}} \dot{q}\,\mathrm{dt} \tag{5.24}$$

The idea is thus to use heat flux measured at the pipe perimeter to estimate volume fraction of annular ice formed at some arbitrary time.

In equation (5.24), all ice formed is assumed to be of the annular mode. Gilpin (1977 b) observed actually some small changes in morphology of the dendritic ice occurring after its initial growth. Original highly branched structure with fern-like appearance was gradually replaced by thin, solid plates. This ice growth is judged to be of insignificant magnitude compared to the annular one.

Start-up pressure gradient in partially frozen pipes

The reason for Gilpin (1977 b) to deal with and quantifying ice formation in pipes with quiescent water is a want to clarify whether dendritic ice formation can result in a complete blockage of the pipe so that a subsequent start-up attempt fails. Gilpin's approach was to generate certain ice fraction (both dendritic and annular) in the pipe and compare it to the pressure gradient required to start up the flow in the partially frozen pipe.

Gilpin was interested in varying supercooling at which nucleation begun and thus (via equation (5.22)) fraction of dendritic ice $\chi_{vol,i,d}$. He discovered that he could initiate nucleation at arbitrary measured supercooled temperature (of course lesser than maximal naturally occurring one) by exposing the test pipe to a sharp blow. Subsequently he let annular ice be formed by waiting certain time and then $\chi_{vol,i,a}$ could be calculated from (5.24). Finally a pressure required to start up the flow through the pipe could be measured and divided by pipe length to obtain start-up pressure gradient.

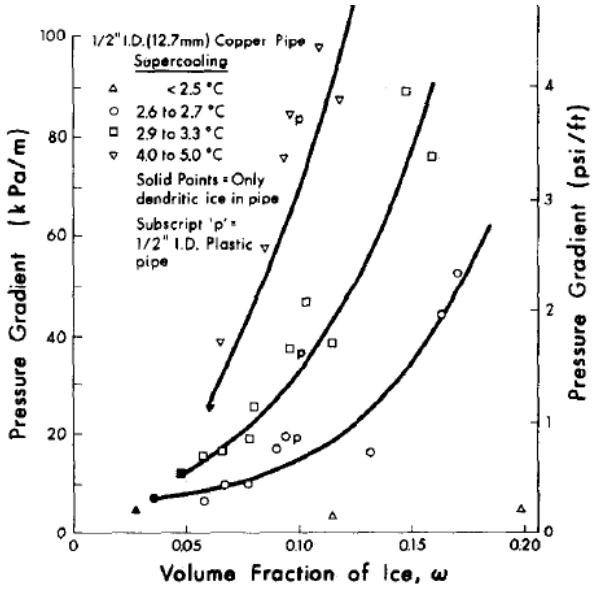

Figure 5.8 *Start-up pressure gradients as a function of volume fraction ice, after Gilpin (1977 b)*

The results obtained by Gilpin (1977 b) shows clearly that for a certain ice fraction in the pipe, the start-up pressure increases with increased amount of dendritic ice. For supercoolings less than 2.5 °C (i.e. $T_f \geq -2.5$ °C), no significant start-up pressure was measured. In Figure 5.8, the solid triangles represent experiments when only dendritic ice was present in the pipe while other data point represents combined dendritic and annular volume fraction of ice i.e. $\omega = \chi_{vol,i,d} + \chi_{vol,i,a}$ in accordance to nomenclature of Gilpin in Figure 5.8. Some experiments with plastic pipe do not exhibit any deviations from copper pipe tests. This is expected as we have to do with quasi-stationary process with very slow cooling of both pipe and water within it. Thus, a thermal contact problem applied by Gilpin (1981 b) does not fit here.

Figure 5.9 shows results extended to higher volume fractions of ice without such detailed distinction in amounts of supercooling as in Figure 5.8 with supercoolings less than 2.5 °C as natural exception.

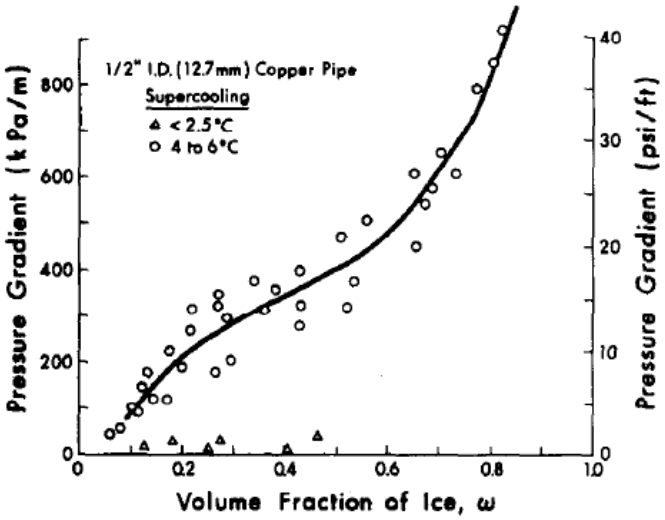

Figure 5.9 *Start-up pressure gradients as a function of volume fraction ice, after Gilpin (1977 b)*

The first sharp increase in pressure gradient depends probably on fact that the initial annular ice growth (recall from Figure 5.6 and later discussion that the highest volume fraction dendritic ice possible should hardly be greater than $\chi_{vol,i,a}(\Delta T_f = -6\,°C) = 0.08$) provides a bonding between wall and original dendritic ice matrix. Earlier discussed changes in dendritic ice morphology may also have some effect. Further increase in pressure required to start the flow depends on gradually blockage the core diameter free from annular ice.

Gilpin (1977 b) also made some experiments to check diameter dependence on results and generated following figure:

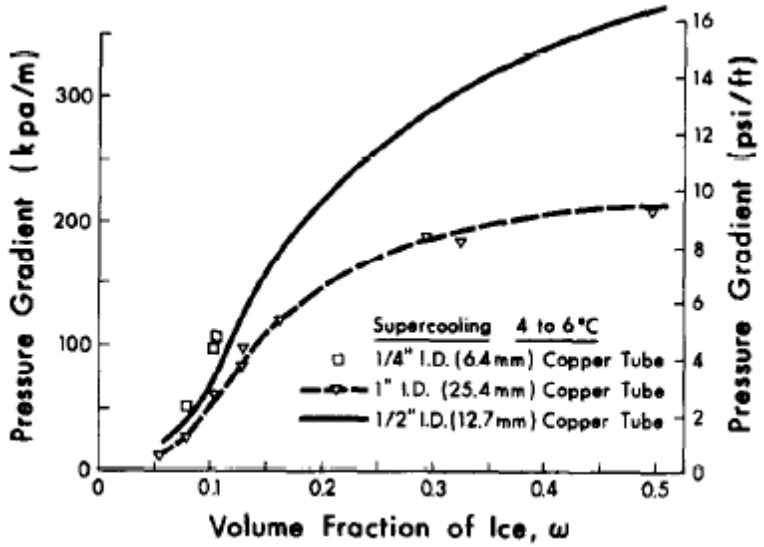

Figure 5.10 *Start-up pressures as a function of volume fraction ice for different diameters, after Gilpin (1977 b)*

Not surprisingly, start-up pressure gradient increases with decreasing diameter.

Gilpin (1977 b) did his research for quiescent water in pipe with very slow cooling rate. Gilpin (1977 a) wrote actually a contemporary paper regarding complete blockage by dendritic ice at finite cooling rates (less than 1 °C/min) of pipe containing quiescent water. Conclusion of Gilpin (1977 a) was that as a cooling rate increases, amount of supercooled water in the pipe decreases and is constrained to upper part of the pipe so that dendritic ice only fills the pipe partially and does not manage to completely block the pipe. As cooling rates increase, ice formation is finally reduced to the annular mode. Gilpin (1977 a) also presents a mathematic model making it possible to estimate risk for complete blockage of the pipe as a function of cooling rate.

Applicability to treated problem

Use of equation (5.21) or (5.22) to calculate volume fraction of dendritic ice in a supercooled volume ought to be valid as well at conditions of water flowing in a pipe. The things gets however a little bit complicated by fact that water penetrating an initially empty, cold sprinkler system will not have a homogenous temperature but a temperature distribution at least depending on coordinate *x* (Figure 4.1). Thus, in a water penetrating a cold pipe, supercooling of bulk volume needed for dendritic ice growth mode (Gilpin, 1981 b) would be a local phenomenon extending from water front (lowest temperature). In consequence, dendritic ice formation is likely to start at the water front and extend upstream to the point where no

supercooling exists. Temperature, and thus the amount of supercooling varies in supercooled volume and so will fraction dendritic ice that will form in accordance to:

$$\chi_{vol,i,d}(x) = \frac{\rho_w c_w}{\rho_i h_{if}} \Delta T_{super}(x) \tag{5.25}$$

Mean dendritic ice fraction formed in the supercooled volume could thus be expected to follow:

$$\overline{\chi_{vol,i,d}} = \frac{\rho_w c_w}{\rho_i h_{if}} \overline{\Delta T_{super}} = \frac{\rho_w c_w}{\rho_i h_{if}} \frac{1}{L_{super}} \int_{x(T_f=0)}^{x(T_f=T_n)} T_f(x)\mathrm{dx} \tag{5.26}$$

L_{super} length of supercooled volume i.e. $L_{super} = x(T_f = T_n) - x(T_f = 0\ °\mathrm{C})$

The reader must be aware of the fact that in flowing water, deviations from equation (5.26) are to be expected. Dendrites start to form at the wall and cannot be expected to instantaneously follow the flow while remaining rigidly in the original supercooled volume. Probably, they will be somewhat diluted while being break off the wall, as indicated by greater volume with dendritic ice compared to the initial supercooled volume in Figure 5.1 (D). On other hand, complete blockage process is certainly characterized by accumulation of dendrites.

To calculate dendritic ice fraction in accordance to (5.25) or (5.26) one must know the amount of supercooling at which nucleation starts. Gilpin's (1977 b) guidelines for normal supercoolings in water outlined earlier are valid for quiescent, slowly cooled water and are not necessarily valid at flow. Particularly for start-up of a flow in initially empty and cold pipe, Gilpin (1981 b) showed that dendritic ice formation is actually typical for negative Celsius temperatures rather close to the freezing point. If Gilpin (1981 b) showed experimentally that initial steel *pipe* temperature range – 4 °C to – 3 °C is the one with greatest risk for complete flow stoppage due to dendritic ice growth, there can be of course no question about supercooling of *water* to temperatures lower than these during such a process.

The amount of supercooling in forced turbulent flow inside circular tubes has been subject of interest of Arora and Howell (1973). They express supercooling at nucleation as a function of Reynolds number, inner diameter, local wall temperature and a dimensional constant C evaluated experimentally. The mathematical model of Arora and Howell (1973) takes into account that it is not enough if water is supercooled to the nucleation temperature within arbitrary small distance to the pipe wall. Indeed, a solid nucleus must exceed some critical size for a stable process of solidification to continue; otherwise it can be melted away (Callister, 2004). Thus, temperatures lower than nucleation temperature within this distance to the pipe wall is not enough for stable nucleation to begin.

Based on experimental observation, Arora and Howell (1973) assume that no supercooling is possible in laminar flow and set $\Delta T_{super}(\mathrm{Re} = 3000) = 0\ °\mathrm{C}$ while evaluating C. This gives an interesting implication; Gilpin's (1981 b) experiments with steel pipe of with inner diameter of 1 cm and flow velocity of 0.6 m/s gives a Reynolds number only slightly higher than 3000 and if the calculation in accordance with Arora and Howell (1973) is made for these conditions, negligible amount of supercooling (ca. 0.3 °C) and in consequence dendritic ice results. As dendritic ice managed to completely block the flow in Gilpin's experiments, predictions of Arora and Howell (1973) do not seem to be applicable to our problem and reason is possibly that they performed the experiments at established flow by submerging the test pipe section in the

coolant, thus omitting the temperature contact problem appearing in Gilpin's research with filling of a empty pipe in favour of regular temperature distribution in the fluid.

Consequently, it seems that supercooling at which nucleation and thus dendritic ice growth will begin cannot be predicted any further at the moment. The best estimation may probably be deduced from Gilpin's (1981 b) results; if most dendritic ice was formed at steel pipe temperatures around – 3 °C or – 4 °C, it is likely that water became supercooled to temperature slightly above these temperatures before nucleation occurred.

However, here arrives a new uncertainty: how long did water supercooled to almost T_p travel before nucleation? This question remains unanswered so far. Nevertheless, there is hope that this question may be answered in experimental manner. If – as it was outlined earlier – nucleation temperature range [– 7 °C; – 4 °C] is understood in such a way that probability for nucleation is high at – 7 °C and low at – 4 °C, this behaviour ought to be possible to describe statistically by e.g. probability distribution function. Analogically, at flow conditions, with sufficient experimental material one should be able to determine an expected value of penetration length at nucleation start for flow maintained at certain amount of supercooling.

Once dendritic ice growth begins in supercooled volume, it will proceed in a manner on which there seems to be a mutual agreement among the researchers i.e. in *fast* manner. How fast? Gilpin (1977 b) reported that once dendritic ice growth started, it was usually completed in about 30 s. However, this cannot be valid at flowing conditions with Gilpin (1981 b) as the best argument. Pressure traces corresponding to complete blockages in Figure 5.3 shows clearly that once the pressures traces start to deviate from normal one, revealing start of dendritic ice growth inside pipe, complete blockage occur in a matter of seconds. Fernandez and Barduhn (1967) made some experimental researches on growth rate of crystals in supercooled water but they deal only with growth of stationary crystals growing in upstream direction of the flow at very unpretentious supercoolings (0.02 °C – 0.6 °C) which makes their results fairly uninteresting to our problem. Thus, "seconds" is probably the best estimate.

Comparing pressure gradient with volume fraction ice is an approach that should be useful and practical also at pipe flow. The pressure gradient used at flow then should be the one needed to maintain the flow instead of Gilpin's (1977 b) start-up pressure. Figure 5.8 shows that dendritic ice itself is responsible for rather low magnitudes of start-up pressure. Gilpin pointed out also a trivial truth that a bond between the dendritic ice matrix and wall must be created to block flow effectively and that this bond consists of annularly grown ice. Can we perhaps describe this solid ice annulus according to Epstein et al. (1977)? Yes, we probably can. Indeed, the bulk water volume that was subjected to supercooling is at freezing temperature after completion of dendritic ice growth and thus fulfils requirement of Epstein's model. This procedure would then give us total volume fraction ice in the pipe which then could be compared to pressure gradient required to maintain the flow and finally, pressure at complete blockage. Is such a procedure reasonable? Indeed, Figure 5.1 shows that mixed mode of ice formation observed by Gilpin (1981 b) proceeds in similar manner. Gilpin (1981 b) does not mention explicitly any such observations at pure dendritic ice growth mode, but possible explanation is that very little of annular ice was needed to effectively bond dendritic ice to wall and cause stoppage. Finally, Gilpin's (1977 b) method with measuring the heat flux at the wall and using equation (5.24) may be used to verify this procedure to calculate annular ice growth.

To conclude, we did not succeed to present here a complete method for accounting for dendritic ice growth in pipes at start-up of the flow materialized as penetration lengths corresponding to expression (5.14). However, there is a perspective of advancing present knowledge in the field through experiments and this perspective will be discussed further in chapter 8.

5.2 Ice formation and complete flow blockage at an established flow

A literature survey revealed, that systematic description of internal ice formation in pipes with an established flow started with treatment of this phenomenon occurring at conditions of laminar flow and was developed later to include turbulent flow. This chronological as well as logical distinction will also be made in this thesis. In the literature regarding this topic, only annular ice formation mode was treated. The present section will thus consider mostly annular ice growth mode and some discussion regarding dendritic ice growth mode is dispatched to the end of this section.

5.2.1 Complete blockage at an established laminar flow

A pioneering work in the field seems to be a paper by Zerkle and Sunderland (1968), which theoretically determines the pressure distribution, heat transfer distribution and radius of the solid annulus at steady state conditions. However, we will concentrate mostly on the research of Des Ruisseaux and Zerkle (1969), which builds further on Zerkle and Sunderland (1968) and includes criteria for complete blockage – a perspective we always must keep in mind as it defines the core of subject of this thesis.

The seminal problem formulation of Zerkle and Sunderland (1968) inherited by i.a. Des Ruisseaux and Zerkle (1969) is outlined in Figure 5.11. In greater detail, the research is concerned with a liquid of an uniform temperature and a fully developed velocity profile at the thermal entrance i.e. at the entrance of the freezing section where the tube wall is maintained at a constant temperature lower than the liquid freezing temperature, to which it had been suddenly brought at time $t = 0$.

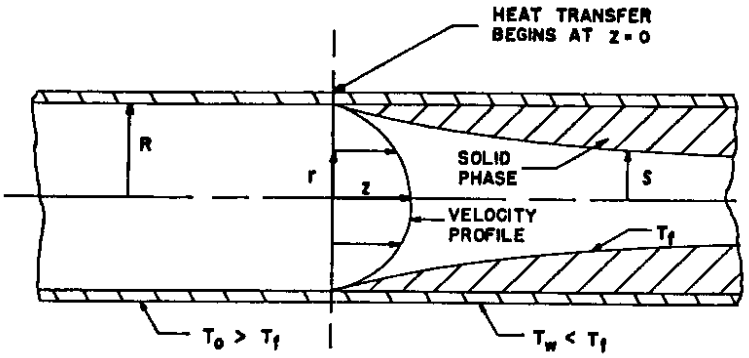

Figure 5.11 *Inlet of the freezing section (Zerkle and Sunderland, 1968)*

The assumptions made by Zerkle and Sunderland (1968) in their analytical investigation can be summarized as follows:

- Steady-state conditions
- Laminar flow everywhere in the pipe
- Uniform temperature at the thermal entrance
- Fully developed laminar velocity profile at the inlet of the freezing section

- Constant temperature at the solid-liquid interface equal to the freezing temperature
- Constant tube wall temperature
- Heat transfer only in radial direction
- Newtonian, incompressible and pure liquid
- Smooth, homogenous and isotropic solid-phase shell starting at the thermal entrance with monotonically increasing thickness

As the object of interest of Des Ruisseaux and Zerkle (1969) is a system rather than a pipe itself, further conditions are specified. They arrive from a qualitative discussion about nature of internal solidification in hydraulic systems which will be summarized here.

When the liquid enters the cooling section, it starts to freeze resulting in a solid annulus at the wall. The liquid is cooled down during its flow through the freezing section i.e. there is a heat transfer from the liquid to the solid annulus. This heat must be conducted through the solid annulus further to the pipe wall. However, the solid-liquid interface has a certain temperature – the liquid freezing temperature and the pipe wall is maintained at a constant temperature as well. This means that heat conducted through a solid annulus of certain thickness has a distinct value, independent of the heat conducted to the solid annulus from the liquid in the matter of convection. The energy balance is fulfilled by latent heat of fusion of formed ice. This means that if the heat conducted through the solid is greater than the heat transferred to the solid from the liquid, the ice crust is growing. Analogously, it shrinks if the heat transferred to the solid is greater than the heat conducted through the solid as the excess of energy which cannot be conducted through the solid annulus is absorbed during melting process. This helps us to understand what steady-state means; it is simply a case when the heat transferred from the liquid to the solid equals the heat conducted through the solid so that neither solidification nor melting occurs at the solid-liquid interface (Des Ruisseaux and Zerkle, 1969).

The behaviour of a system subjected to such an internal solidification will depend on the way in which the flow in the system is maintained. If a constant mass flow rate is forced through the system, a steady state configuration will exist regardless of severity of the temperature boundary conditions as the freeze shut is precluded by definition. The pressure required will of course increase as the steady-state solid annulus grows but still there will be a steady state (Des Ruisseaux and Zerkle, 1969).

More often, a pressure drop through the system will be limited. This will be the case with a flow between a reservoir with constant pressure head and the atmosphere. As outlined in section 3.5 a centrifugal pump delivers also limited pressure head dependent on flow extracted. This means that a proceeding solidification in a part of the system with resulting increasing pressure drop over the freezing section will be accomplished by a decrease in flow rate. This development may continue until the system is completely blocked by ice when the pressure head present do not manage to maintain any flow through the system. Otherwise, a steady state will be reached (Des Ruisseaux and Zerkle, 1969).

This helps us to understand why Des Ruisseaux and Zerkle (1969) use a model for analysis with a constant pressure drop summarized by the system in Figure 5.12.

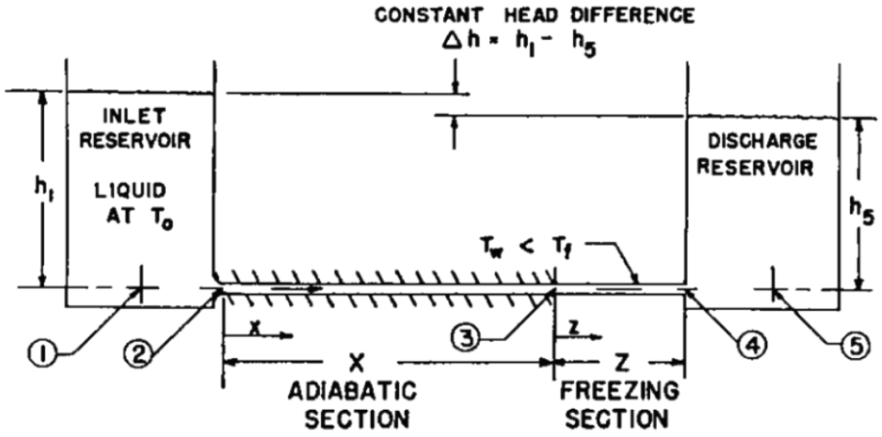

Figure 5.12 *Model of analysis of Des Ruisseaux and Zerkle (1969)*

Des Ruisseaux and Zerkle (1969) use the same basic assumption as those outlined by Zerkle and Sunderland (1968). This means that even if complete blockage occurs, it is assumed to be reached in a quasi steady-state process. An additional assumption which has to do with the proposed model of analysis (Figure 5.12) is made by Des Ruisseax and Zerkle (1969) and states that velocity in the reservoirs is negligible so that the head difference of the system is given by hydrostatic pressure difference between (1) and (5) in Figure 5.12.

This hydrostatic pressure difference can be determined from equation (3.2). To calculate f in eq. (3.2), Des Ruisseaux and Zerkle (1969) do not use eq. (3.3) but a variant of it which takes account for entrance effects in the pipe and results in the following expression for the hydrostatic pressure difference:

$$p_1 - p_5 = \rho g \Delta h = \frac{\rho V_0^2}{2}\left(2.28 + \frac{64X/D}{\mathrm{Re}_0} + \frac{64Z/D}{\mathrm{Re}_0}\right) \tag{5.27}$$

p_1 pressure at (1) in Figure 5.12, [Pa]
p_5 pressure at (5) in Figure 5.12, [Pa]
Δh head difference between the reservoirs, [m]
V_0 average velocity in the pipe prior to solidification, [m/s]
Re_0 Re based on V_0 and D, [-]
X length of the adiabatic pipe section, [m]
Z length of the freezing section, [m]
D pipe inner diameter, $2R_0$, [m]

With solidification occurring in the freezing section and steady state, the system pressure drop is described by expression (5.28) instead:

$$p_1 - p_5 = \rho g \Delta h = \frac{\rho V^2}{2}\left(2.28 + \frac{64X}{\mathrm{Re}D}\right) + (p_3 - p_5) \tag{5.28}$$

V average velocity in the adiabatic section after freezing reaches steady state in the freezing section, [m/s]
Re $\mathrm{Re}(V, D)$
p_3 pressure at the inlet of the freezing section (3) in Figure 5.12, [Pa]

To evaluate equation (5.28), one must determine the pressure drop through the freezing section, i.e. $p_3 - p_5$. Des Ruisseaux and Zerkle (1969) accomplish this by utilizing results of Zerkle and Sunderland (1968). Their methodology, which is quite similar to this of Epstein et al. (1977) outlined in section 5.1.3, will be summarized here only briefly. For detailed derivations the reader is recommended to consult Zerkle and Sunderland (1968).

Zerkle and Sunderland (1968) solve the velocity field in the freezing section of variable diameter (Figure 5.11) from continuity equation by incorporating appropriate basic boundary conditions and an assumption that the axial component of velocity retains its parabolic profile throughout the freezing section, which yields:

$$v_z(r,z) = 2V\left(\frac{R_0}{R}\right)^2\left[1-\left(\frac{r}{R}\right)^2\right] \tag{5.29}$$

$v_z(r,z)$ axial fluid velocity component, [m/s]
r radial coordinate, [m]
z axial coordinate in the freezing section, see Figure 5.12, [m]
R_0 radius of the pipe, [m]
R radius of solid-liquid interface, [m]

For discussion on the assumption of retained parabolic profile one is referred to Zerkle and Sunderland (1968). Utilizing (5.29) in an integral form of the axial momentum equation, one obtains an expression for dimensionless pressure drop across the cooling section, which takes following form:

$$\frac{p_3-p_5}{\frac{\rho V^2}{2}} = \frac{4}{3\delta_E^{*4}}\left(1-\delta_E^{*4}\right) + 16\mathrm{Pr}\int_0^{z^*}\frac{\mathrm{dz}^*}{\delta^{*4}} \tag{5.30}$$

δ^* dimensionless radius of the solid-liquid interface, R/R_0, [-]
δ_E^* δ^* at the freezing section exit, $\delta^*(z=Z)$, [-]
z^* dimensionless axial coordinate, $4\alpha_l z/VD^2$, [-]
α_l thermal diffusivity of liquid phase, see equation (5.11), [m²/s]

With velocity field known, the temperature field in the fluid and the radial location of solid-liquid interface can be determined from energy equation accompanied by boundary conditions and an additional relation describing energy balance at the solid-liquid interface. The expression relating δ^* to dimensionless fluid bulk temperature gradient and dimensionless wall temperature becomes as follows:

$$\delta^{*\frac{1}{T_w^*}} = e^{2\frac{dz^*}{dT_f^*}} \tag{5.31}$$

T_w^* dimensionless wall temperature, $k_s(T_m - T_w)/k_l(T_{f0} - T_m)$, [-]
T_m liquid freezing/melting temperature, [K]
T_{f0} initial temperature of liquid, [K]
k_s thermal conductivity of solid phase, [W/(mK)]
k_l thermal conductivity of liquid, [W/(mK)]
T_f^* dimensionless fluid bulk temperature, $(T_f - T_m)/(T_{f0} - T_m)$, [-]

Further, it is showed by Zerkle and Sunderland (1968) that the assumption of parabolic profile retained throughout the freezing section imposes that the heat transfer from the liquid to the solid is the same as it would be if the liquid flow occurred in a tube with constant, original diameter and a wall temperature equal to the liquid freezing temperature. This behaviour has been attributed to two counterbalancing phenomena coupled to decreasing flow diameter in the freezing section: increased radial heat flux at the solid-liquid interface due to acceleration of the liquid in the freezing section and simultaneous decrease of the liquid-solid surface area available for heat transfer.

This insight makes it possible to express the decrease in fluid temperature in the freezing section using theory outlined in chapter 4. Des Ruisseaux and Zerkle (1969) actually use expression (4.7) for this purpose, which with quantities defined in this section takes the following elegant form:

$$T_f^* = e^{-z^* \overline{Nu}_d} \tag{5.32}$$

Nusselt number in (5.32) is in turn calculated in accordance with eq. (4.12) which after inserting definition of z^* becomes only a function of z^*. Des Ruisseaux and Zerkle (1969) also uses an alternative expression for Nusselt number valid for combined forced and natural convection in order to obtain results both neglecting and taking into account participation of the natural convection.

$$\overline{\mathrm{Nu}} = 1.57 \left(\frac{\mu}{\mu_f}\right)^{0.14} \left[\frac{\pi}{z^*} + 5.6 \cdot 10^{-4} \left(\mathrm{ReGrPr}^2 \frac{\nu(T_0)}{\nu} \frac{z^*}{4}\right)^{0.4}\right]^{1/3} \tag{5.33}$$

With this, temperature as a function of coordinate z can be calculated. This is done in Figure 5.13 which presents the results in dimensionless manner with T_f^* (T_b^* in the figure) as a function of z^*.

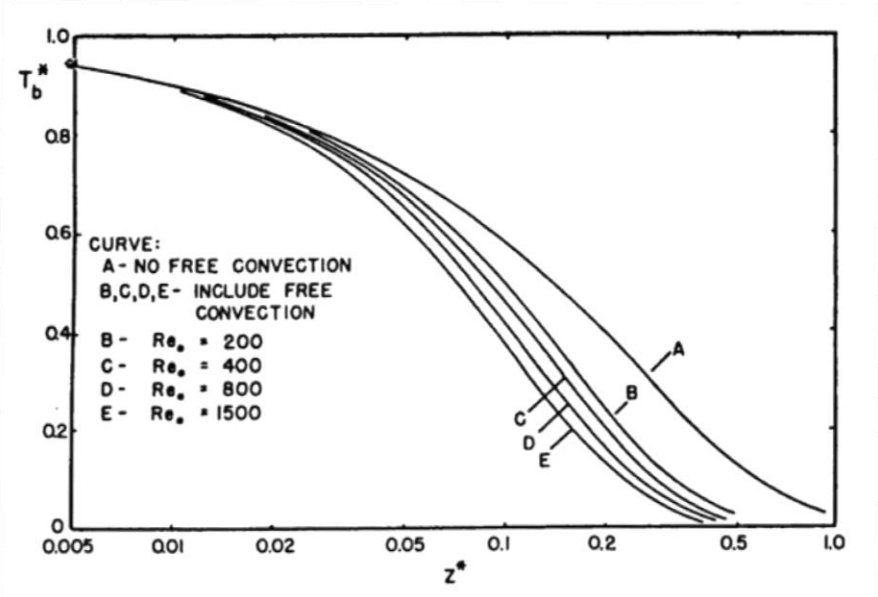

Figure 5.13 *Dimensionless temperature as a function of dimensionless coordinate, $T_{f0} = 26.7\ °C$ (Des Ruisseaux and Zerkle, 1969)*

With $T_f^*(z)$ known, radius of the solid-liquid interface can be determined from (5.31), Figure 5.14.

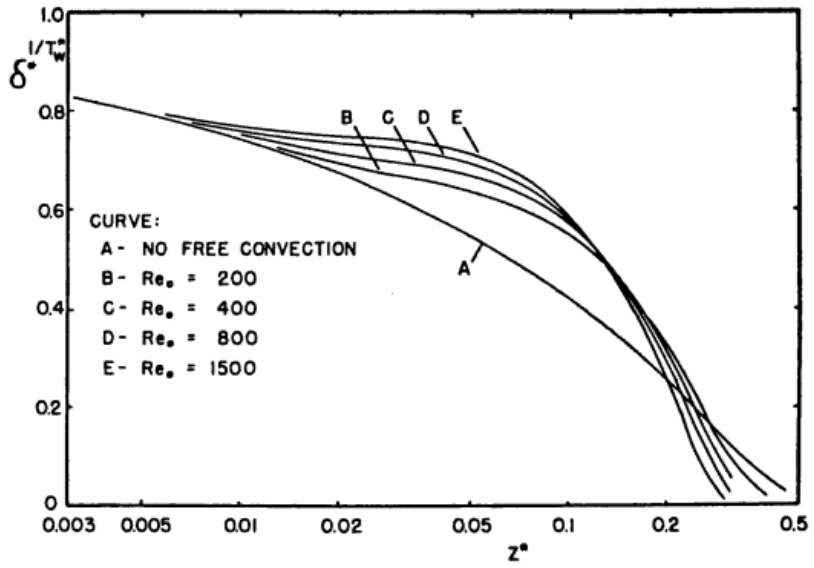

Figure 5.14 *Dimensionless radius of the solid-liquid interface as a function of dimensionless coordinate, $T_{f0} = 26.7\ °C$ (Des Ruisseaux and Zerkle, 1969)*

With δ^* determined, equation (5.30) can be solved after which it can be inserted in equation (5.28) giving the final results, Figure 5.15.

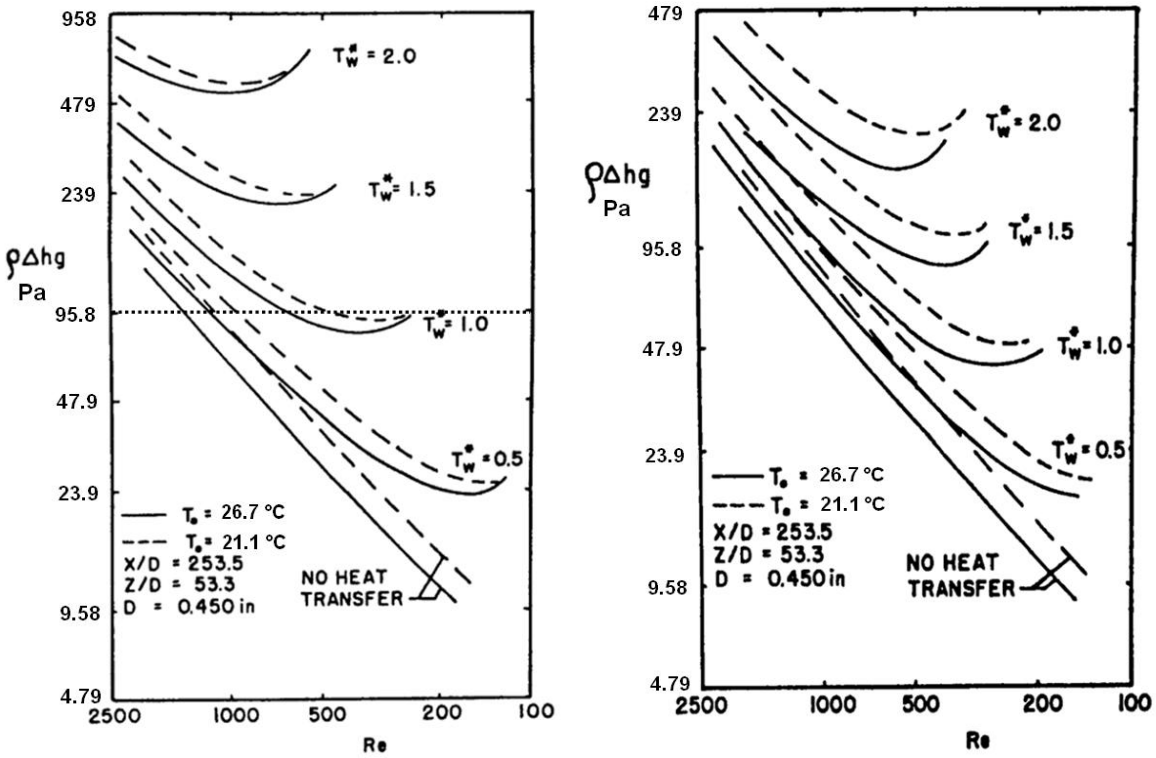

Figure 5.15 *Pressure drop in the system subjected to freezing as a function of steady-state Reynolds number in the adiabatic section calculated for forced convection (left) and combined forced and natural convection (right) respectively, adopted from Des Ruisseaux and Zerkle (1969)*

The interpretation of the results presented in 5.15 is that for a certain freezing condition expressed here as T_w^*, there exists a minimal pressure drop that must be maintained through the

system for steady state to be possible which is consistent with discussion outlined at the beginning of this section.

As example, study left diagram in Figure 5.15. For a system in accordance with Figure 5.12 with certain values of T_0, X/D, Z/D and D specified, one can read in the diagram that a system with e.g. pressure drop of 95.8 Pa (dotted line) and $T_0 = 26.7$ °C will give Reynolds number of approximately 1450 if no heat transfer occurs, i.e. before cooling conditions are imposed on the part of the system (solid line with no heat transfer). If the temperature of the wall in the freezing section is now suddenly lowered so that $T_w^* = 0.5$, a steady state will be established at Reynolds number of 1200 which can be read on the solid line corresponding to this dimensionless cooling temperature. One should be reminded that Reynolds number referred to are those in the adiabatic, constant flow diameter section. Thus a decreasing Reynolds number indicates decrease in flow at the same rate. If more severe cooling conditions are imposed and T_w^* becomes 1, the steady-state Reynolds number decreases to 670. Somewhere between $T_w^* = 1$ and $T_w^* = 1.5$ the minimal pressure drop required to drive flow through the system becomes higher than the available 95.8 Pa and complete blockage occurs in the system (Des Ruisseaux and Zerkle, 1969).

By comparing the two diagrams in Figure 5.15, it is seen that an analysis including free convection predicts lower minimum pressure drops required to prevent shut up at different dimensionless wall temperatures than the analysis concerning forced convection alone. Thus, for freeze shut, the wall must be cooled down more for complete blockage to occur if the natural convection is of significance (Des Ruisseaux and Zerkle, 1969).

Summarizing, for a certain flow rate and thus Re, the required pressure drop increases as the wall temperature in the freezing section decreases (T_w^* increases). The lowest pressure drop preventing freeze shut of the tube and associated flow rate increases also with increasing T_w^*. As expected, lowering inlet temperature has roughly the same influence on pressure drop curves as increasing T_w^*.

It should be noted that the theoretical pressure drop curves, having minima, indicate that there may be two steady-state Reynolds number. However, as the steady-state is approached from left in the figure (decreasing flow) the higher steady-state Reynolds number will be reached first (Des Ruisseaux and Zerkle, 1969).

Des Ruisseaux and Zerkle (1969) also present experimental results in order to verify their theoretical model. The experiments were set up in accordance with Figure 5.12, pipe inner diameter was 11.4 mm and cooling was provided by glycol circulating inside pipe enclosing the freezing section. Measured minimal steady-state system pressure drop required for preventing freeze shut was compared to dimensionless wall temperature so that data points corresponding to minima in Figure 5.15 was obtained and could be compared to these. A comparison presented in Figure 5.16 shows that minimal theoretical pressure drops calculated with and without taking account for free convection creates upper and lower bounds for the experimental data except perhaps for $T_w^* \leq 1$.

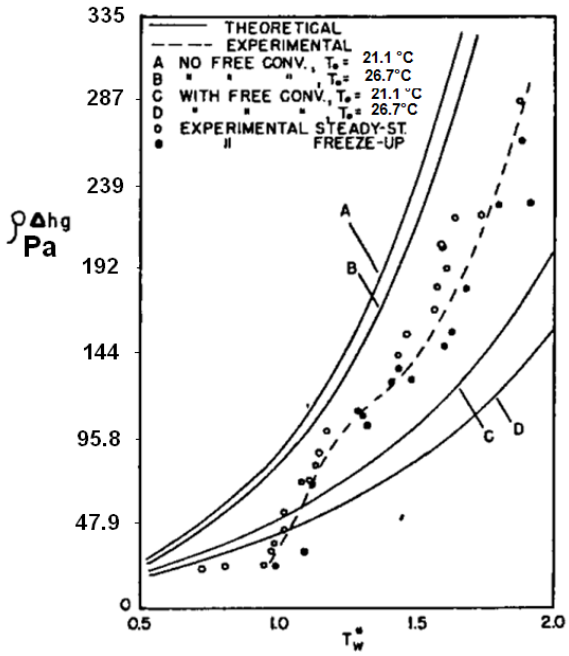

Figure 5.16 *Comparison between theoretical and experimental minimum system pressure drop as a function of dimensionless wall temperature, adopted from Des Ruisseaux and Zerkle (1969)*

Des Ruisseaux and Zerkle (1969) propose that the analytical method developed by them can be applied to systems more complex than the presented in Figure 5.12. The only difference in presenting the results for a pump-driven system will be that a suitable pump characteristic curve must be included. The principal appearance of such a diagram is showed in Figure 5.17. Observe that reverse appearance of required pressure drop curves has to do with flow rate increasing to the left in the figure, contrary to Figure 5.15. The steady-state will be given by intersection between the pump characteristic curve and the required pressure drop curve suitable for the actual cooling conditions, which is represented by points (1), (2) and (3) in Figure 5.17 (compare with Figure 5.15 where the dotted line can be seen as characteristic curve for the constant head system). Point (1) describes steady state at no solidification as the curve (A) is simply ordinary system curve. With this in mind, curves (B)-(D) may be interpreted as system curves modified by internal solidification in the system.

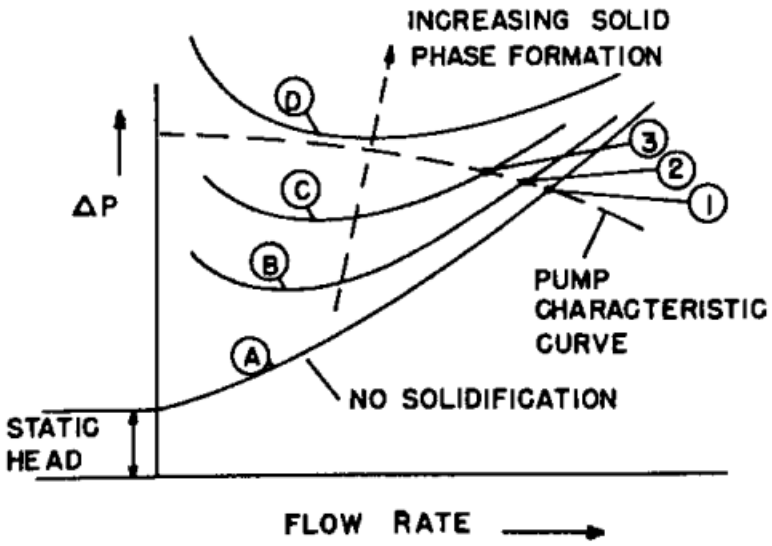

Figure 5.17 *Pump characteristic curve (dashed) and system curves for increasingly severe cooling conditions (A)-(D) giving different pump operation points (1)-(3), (Des Ruisseaux and Zerkle, 1969)*

In a similar way, complete blockage occurs when no intersection exists as for curve (D) in Figure 5.17. It is also straightforward to use the same approach for more complicated systems, i.e. with fittings, pipe elevation changes etc. as long as the freezing section in the system is a straight pipe, for which the present theory was developed.

The quasi-steady state approach of Zerkle and Sunderland (1968) and Des Ruisseaux and Zerkle (1969) is not the only possible method to handle internal solidification in laminar flow. The other principal different, theoretical method is by calculation of the solid crust thickness and flow rate as a function of time. Although it seems as a more intuitive way to handle such problems, one must have in mind that the mathematical complexity is increased by utilizing such a method. Özişik and Mulligan (1969) do it anyway but they only focus on steady state solutions and do not treat complete blockage problems. Complete blockage in this transient way is however treated by Martinez and Beaubouef (1972) as well as Sampson and Gibson (1980). Martinez and Beaubouef (1972) assume a linear pump characteristic and presents a model which degenerates to the one of Des Ruisseaux and Zerkle (1969) for steady state. Sampson and Gibson (1980) assume constant pressure drop across the freezing section and compares derived criteria for complete blockage with experimental results of Des Ruisseaux and Zerkle (1969). The results were found to be in good agreement with experiments of Des Ruisseaux and Zerkle (1969) providing safe criteria against complete blockage (Figure 5.18).

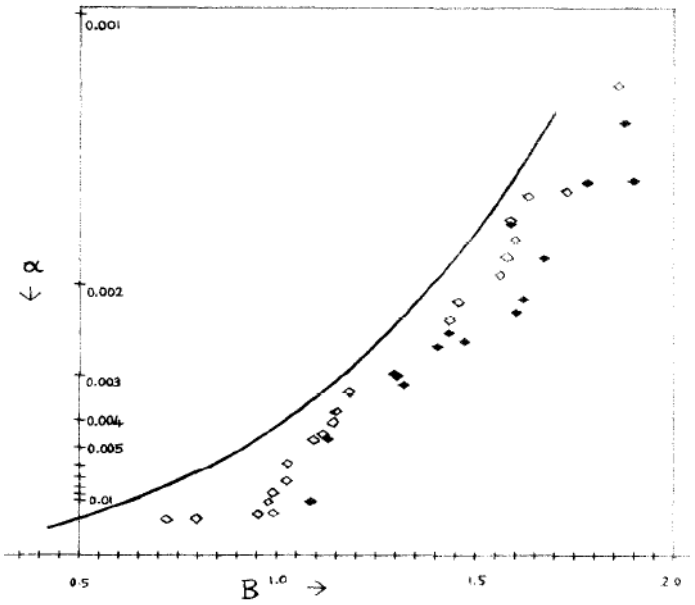

Figure 5.18 *Comparison between critical curve for complete blockage by Sampson and Gibson (1981) and experimental results of Des Ruisseaux and Zerkle (1969), alpha in the figure equals* $\alpha_l Z/(2\pi R_0^2 V_0)$ *and B equals* T_w^* *according to prior nomenclature, solid points represents complete blockage (Sampson and Gibson, 1981)*

A problem formulation identical to that of Zerkle and Sunderland (1968), outlined in connection with Figure 5.11 as well as the assumption on a parabolic velocity profile, is common for all these papers. Chida (1987) relaxes this restriction and by following mainly the approach of Des Ruisseaux and Zerkle (1969) he presents theoretical and experimental results which are with good agreement with each other and with Dus Ruisseaux and Zerkle (1969), Figure 5.19.

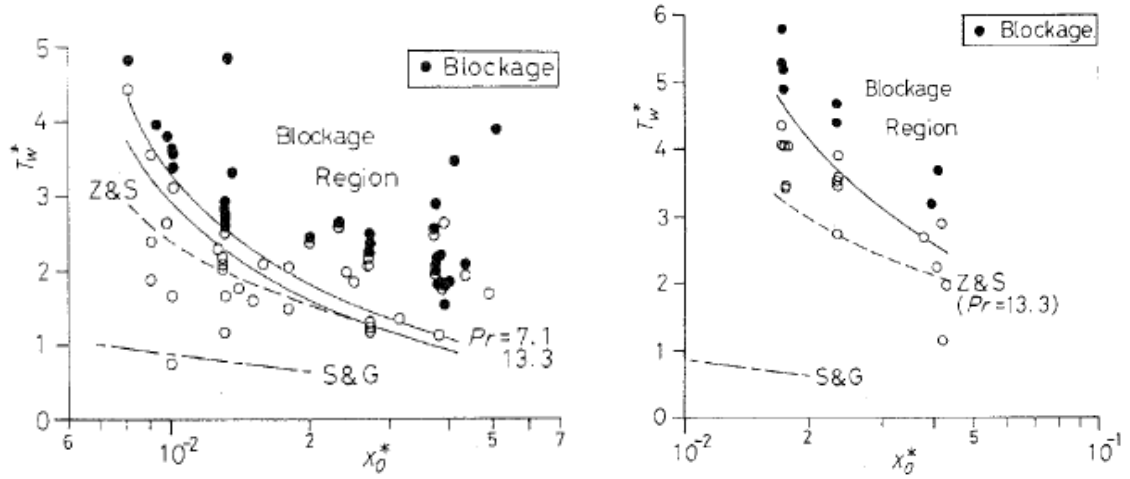

Figure 5.19 *Critical curves for complete blockage by Chida (1987) for constant head system (left) and the pump system compared with own experimental results and theoretical results of Zerkle and Sunderland (1969) and Sampson and Gibson (1981), Z&S and S&G respectively,* x_0^* *equals* $z^*(z = Z)$ *according to prior nomenclature, Chida (1987)*

Unfortunately, Chida (1987) does not present any further details on derivation of the theoretical critical curves for blockage.

5.2.2 Complete blockage at established turbulent flow

The problem statement of Zerkle and Sunderland (1968) is transferred to turbulent flow by Thomason et al. (1978). In a paper with a title confusingly like that of Zerkle and Sunderland (1969), Thomason et al. (1978) obtain analogous results for the turbulent case. This means that pressure, solid phase profile and heat transfer as a function of dimensionless coordinate in the freezing section are obtained at steady state for constant wall temperature. A transient approach is taken by Cho and Özişik (1979) who are interested in steady-state and Samson and Gibson (1982) who also concerns complete blockage. Criteria for complete blockage of turbulent flow derived in a quasi-steady state manner are of interest of Epstein and Cheung (1982). Gilpin (1981 a) discovered that smooth, monotonously increasing solid-liquid interface, as assumed by all these authors, is not the only possible scenario at conditions of established flow. So-called ice-band structure characterized by periodical variation in ice crust radius R along the freezing section sometimes occurs and may promote complete blockage of a pipe. Therefore both these modes have to be investigated.

Smooth solid-liquid interface

Epstein and Cheung (1982) use a quasi-steady state method analogous to that of Des Ruisseaux and Zerkle (1969). The derivation starts with a heat balance in the freezing section with solid annulus using equation (4.5). By inserting constant wall temperature condition ($h_o = k = \infty$ and $T_0 = T_w = T_m$ according to prior discussions), mass continuity relation in the freezing section (which becomes $V = V_0(R_0/R)^2$), definition of the local Nusselt and Prandtl numbers as well as Reynolds number evaluated at V_0 and R_0, equation (4.5) can be written as:

$$\frac{1}{2}\mathrm{Re}_0\mathrm{Pr}R_0\frac{dT_f}{dz} = -\mathrm{Nu}_\mathrm{d}\left(T_f - T_m\right) \tag{5.34}$$

Further, using equation (4.4), the radial temperature distribution in the ice crust can be determined. Invoking that for steady state all energy convectively transferred to the solid annulus must be conducted through it, one obtains:

$$\ln\left(\frac{R_0}{R}\right) = \frac{2T_w^*}{\mathrm{Nu}_\mathrm{d}}\frac{T_{f0}-T_m}{T_f-T_m} \tag{5.35}$$

Arguing that thermal entrance region is short in turbulent flow, Epstein and Cheung (1982) evaluate Nusselt number in expression (5.35) assuming a fully developed thermal profile. They use the following expression, similar to eq. (4.19):

$$\mathrm{Nu}_\mathrm{d} = 0.0155\mathrm{Re}^{0.83}\mathrm{Pr}^{0.5} = 0.0155\mathrm{Re}_0^{0.83}\mathrm{Pr}^{0.5}\left(\frac{R_0}{R}\right)^{0.83} \tag{5.36}$$

The last step is done inserting mass continuity relation so that Re, which is function of axial coordinate (due to flow area contraction in the freezing section), is replaced by the constant initial Re_0 multiplied with scaling parameter R_0/R.

By eliminating the bulk temperature between expressions (5.34) and (5.35), substituting (5.36) and integrating in *z*, Epstein and Cheung (1982) obtain a final, although somewhat cumbersome, expression for $R(z)$. This can be used to determine the axial pressure distribution. This is done by setting up a balance between pressure and frictional forces at an arbitrary location z in the freezing section, as follows:

$$\left(p+\frac{1}{2}\rho V^2\right)-\left(p_0+\frac{1}{2}\rho {V_0}^2\right)=\int_0^z \frac{2\tau}{R}\mathrm{dz} \tag{5.37}$$

Using $\tau = 0.5 C_f \rho V^2$and Blasius formula for the friction coefficient ($C_f = 0.0791(2VR/\nu)^{-0.25}$), Epstein and Cheung (1982) obtain an expression for pressure:

$$\frac{2(p_0-p)}{\rho V_0^2}=\frac{0.1582}{R_0 \mathrm{Re}^{0.25}}\int_0^z \left(\frac{R_0}{R}\right)^{19/4}\mathrm{dz}+\left(\frac{R_0}{R}\right)^4-1 \tag{5.38}$$

After integrating equation (5.38) using expression for $R(z)$, Epstein and Cheung (1982) can relate dimensionless pressure drop to Reynolds number and dimensionless wall temperature for certain dimensionless length of the freezing section, in complete analogy with Figure 5.15. However, Epstein and Cheung (1982) do not include such a diagram in their rapport, focusing instead directly on one comparable to Figure 5.16. Thus, in a Figure 5.20 minimal dimensionless pressure drop required for maintaining the flow ($2(p_0 - p)D_0^2/\rho\nu^2$) can be seen plotted as a function of dimensionless wall temperature T_w^* for different ratios between freezing section and pipe diameter (Z/D_0).

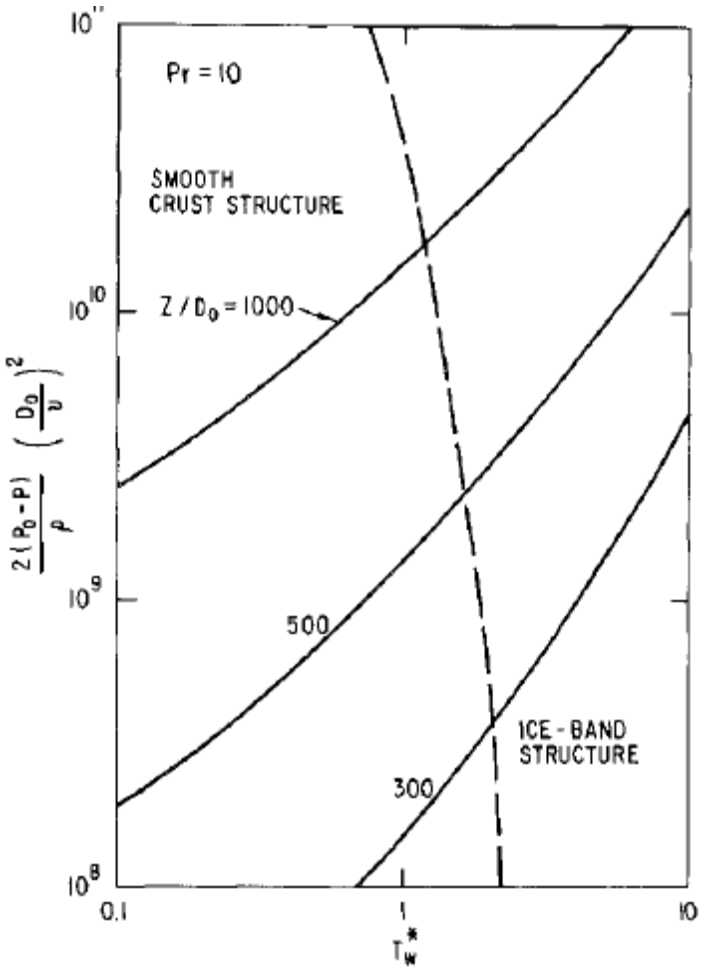

Figure 5.20 *Minimal dimensionless pressure drop as a function of dimensionless wall temperature for different dimensionless freezing section lengths (Epstein and Cheung, 1982)*

Epstein and Cheung (1982) draw a limitation curve in Figure 5.20 using a correlation developed by Gilpin (1981 a), $Z/D = 80[k_s/(k_l\, T_w^*)]^2 + 6$. On the right side of this curve, ice-band structure is predicted and the freeze-off criteria of Epstein and Cheung (1982) are not valid. Epstein and

Cheung (1982) points out however that Gilpin's expression have been derived from experimental results obtained for $Z/D < 40$, the curve drawn in Figure 5.20 may thus constitute a heavy extrapolation.

Ice-band structure of the solid-liquid interface

It has been observed by Gilpin (1981 a) that ice growth in a pipe containing a water flow in transition regimes produces an ice-band structure (Figure 5.21) rather than the uniformly tapered flow area assumed so far.

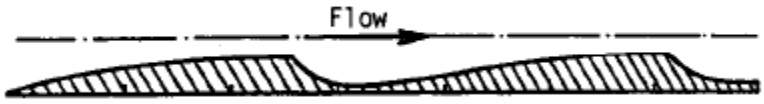

Figure 5.21 *Ice-band structure i.e. periodical thickness variation of the solid annulus, (adopted from Hirata and Ishihara (1985))*

Gilpin (1981 a) noticed that the ice-band structure leads to very high pressure drop in the freezing section which is natural if we consider that structure from Figure 5.21 creates several minor losses due to the sudden expansions, in addition to ordinary frictional drag at the solid-liquid interface. The models predicting complete blockage outlined so far were all based on calculations taking account only for pressure loss due to viscous drag. Due to this fact, the predicted minimal pressure drop over the freezing section needed for preventing a freeze off is underestimated if applied for conditions which results in ice-band structure and following additional minor pressure losses. Thus, freeze-off conditions must be re-examined which is done by Hirata and Ishihara (1985) for steady-state conditions.

For this purpose, Hirata and Ishihara (1985) conduct a series of experiments in copper pipes with inner diameters of 16.6 mm and 19.9 mm and 1.1 mm wall thickness, which constituted a 697 mm long freezing section inserted in a larger tube where the coolant circulated. The freezing section was removable so that the ice could be taken out for investigation. Numerous observations of ice-band structures resulting from different cooling conditions, allowed Hirata and Ishihara (1985) to correlate steady-state spacing between two neighbouring ice bands to the cooling conditions as follows:

$$\frac{S}{D} = \frac{75}{\theta^{3/5}} + 4.5 \qquad (5.39)$$

$1.6 \leq \theta \leq 31$

S	spacing between two neighboring ice bands at steady state, see Figure 5.22, [m]
θ	cooling temperature ratio, $(T_m - \overline{T_w})/(\overline{T_f} - T_m)$, [-]
$\overline{T_w}$	mean measured wall temperature in the freezing section, [K]
$\overline{T_f}$	mean fluid temperature in the freezing section, [K]

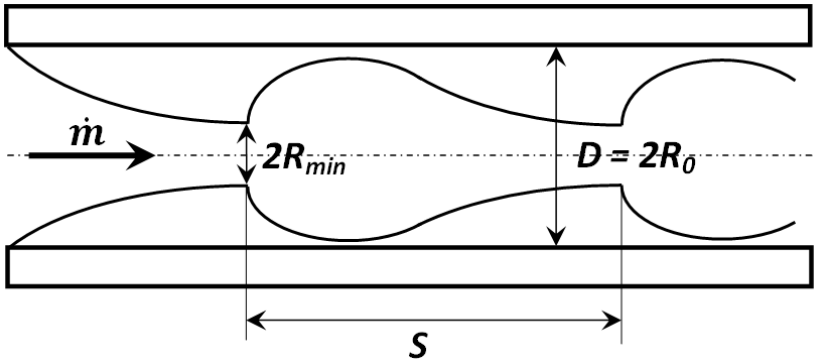

Figure 5.22 *Ice-band spacing S*

At this point it is interesting to emphasize the different way of Hirata and Ishihara (1985) to specify cooling conditions if compared to previous authors. The mean wall temperature $\overline{T_w}$ is obtained as an average value of temperatures measured at three positions along the freezing section while $\overline{T_f}$ is simply taken as the average between water inlet and outlet temperatures which both lies in narrow range of water freezing temperature.

The absence of a Reynolds number dependency in equation (5.29) may be somewhat surprising, however it is also confirmed by Gilpin (1981 a) who relates this behavior to fact that Re loses its importance in the strongly accelerating and decelerating flow through a developed ice-band structure. At the same time, the range of Reynolds numbers possible also becomes implicitly restricted by the presence of ice bands.

At steady state conditions on which present calculations are based, heat conducted through the solid annulus (equation (4.1)) must equal heat transferred to the solid annulus by convection. This heat balance at the narrowest passage in Figure 5.22 becomes:

$$2\pi R_{min} h_i\left(\overline{T_f} - T_m\right) = 2\pi k_s \frac{T_m - \overline{T_w}}{\ln(R_0/R_{min})} \tag{5.40}$$

By using definition of Nusselt number in the narrowest passage ($\mathrm{Nu}_{Rmin} = 2h_i R_{min}/k_f$), above equation can be written as:

$$\mathrm{Nu}_{Rmin} = \frac{-2k_s\theta}{k_f \ln(R_{min}/R_0)} = \frac{-2k_s\theta}{k_f \ln R^*} \tag{5.41}$$

The last step in expression (5.41) defines the dimensionless solid-liquid interface radius R^*. Hirata and Ishihara (1985) could evaluate Nu_{Rmin} for different steady-state configurations after measuring corresponding R_{min} and by plotting the calculated Nusselt number as function of Reynolds number also evaluated at R_{min}, they established following relation between these quantities:

$$\mathrm{Nu}_{Rmin} = 0.0045\mathrm{Re}_{Rmin} \tag{5.42}$$

$$1.6 \leq \mathrm{Re}_{Rmin} \leq 3.0 \cdot 10^4$$

Taking into consideration that the ice bands appear one after the other in the whole length of the pipe, Hirata and Ishihara (1985) conclude that contribution of the viscous drag to the total pressure loss in the freezing section can be neglected. It is quite easy to justify if we emphasize that pressure drop in a pipe with ice-band is between 10 and 100 greater than in the smooth

pipe. Pressure loss is thus assumed to be exclusively due to flow area expansions that ice-band structure produces. Hirata and Ishihara (1985) approximate each such expansion with sudden expansion (compare with sudden contraction in Figure 3.1) which allows corresponding minor pressure loss (eq. (3.6)) to be expressed in accordance with e.g. White (2008):

$$\Delta p_m = \frac{\rho V_{Rmin}^2}{2} K_m = \frac{\rho V_{Rmin}^2}{2} \left(1 - R^{*2}\right)^2 \tag{5.43}$$

To evaluate Δp_m, Hirata and Ishihara (1984) use V_{Rmin} which is mean velocity at R_{min}. Hirata and Ishihara (1985) wish to express equation (5.43) in terms of friction factor, which is possible using definition of friction factor in equation (3.2) and becomes for *n* number ice bands in a pipe:

$$f = \frac{n\Delta p_m}{\frac{\rho V^2}{2}\frac{L}{D}} \tag{5.44}$$

Here in contrast, as whole freezing section is considered, V_0 is used. After utilizing that $n = L/S$ as well as equations (5.39) and (5.43), expression (5.44) becomes:

$$f\left(\frac{75}{\theta^{3/2}} + 4.5\right) = \frac{1-\left(R^{*2}\right)^2}{R^{*4}} \tag{5.45}$$

At the same time, after inserting equation (5.42) and continuity relation $\mathrm{Re_D} = \mathrm{Re}_{Rmin} R^*$ in expression (5.41), it becomes:

$$\frac{\mathrm{Re_D}}{\theta} = -\frac{2\left(k_s/k_f\right)}{0.0045}\frac{R^*}{\ln R^*} \tag{5.46}$$

By eliminating R^* in the two last expressions, the friction factor can be expressed as function of $\mathrm{Re_D}$ and compared with experimental data, which is done in Figure 5.23.

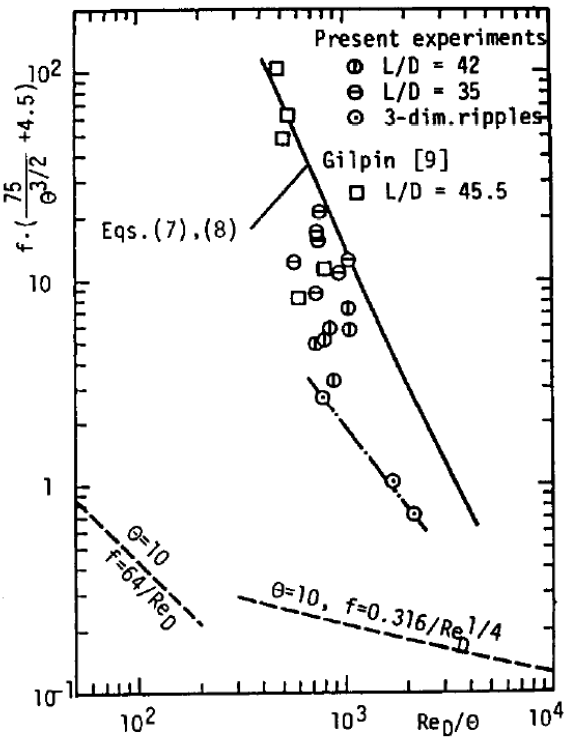

Figure 5.23 *Calculated friction factors over ice-band structure compared with experimental data, (Hirata and Ishihara, 1985)*

As seen in Figure 5.23, the theoretically calculated friction factors give upper limit values for those measured in experiments. Deviation from experimental results seems to increase with increasing values of $\mathrm{Re_D}/\theta$, which Hirata and Ishihara (1985) relate to fact that $\mathrm{Re_D}/\theta$ is mainly proportional to the diameter of flow passage. The expansion angle has been observed to decrease with increasing flow diameter which means that when the flow passage becomes greater, expression (5.43) grossly overestimates the minor pressure loss over the ice band.

Using equation (3.1), the relation between mean velocity at the contraction region V_{Rmin} and inlet pressure can be written as follows (Hirata and Ishihara, 1985):

$$\Delta p - n\Delta p_m = \frac{\rho V_{Rmin}^2}{2} \tag{5.47}$$

By substituting eq. (5.43) in expression (5.47), one obtains:

$$V_{R,min} = \sqrt{\frac{2\Delta p/\rho}{1+n\left(1-R^{*2}\right)^2}} \tag{5.48}$$

Eq. (5.47) can be used to express the Reynolds number at the maximal contraction as follows:

$$\mathrm{Re}_{Rmin} = \frac{R^*}{\sqrt{1+n\left(1-R^{*2}\right)^2}}\mathrm{Re_p} \tag{5.49}$$

$\mathrm{Re_p}$ is called the modified Reynolds number, defined as (Hirata and Ishihara, 1985):

$$\mathrm{Re_p} = \frac{D}{\nu}\sqrt{\frac{2\Delta p}{\rho}} \tag{5.50}$$

It should be emphasized that the modified Reynolds number in eq. (5.50) is also used by Epstein et al. (1977), eq. (5.15) and by Epstein and Cheung (1982), Figure 5.20. After using equations (5.41) and (5.42) in eq. (5.49), the following expression is obtained.

$$\mathrm{Re_p} = -\frac{2(k_s/k_f)\theta}{0.0045}\frac{\sqrt{1+n\left(1-R^{*2}\right)^2}}{R^*\ln R^*} \tag{5.51}$$

If eq. (5.39) is utilized, n in eq. (5.51) can be eliminated yielding a relation between θ and R^* for a certain $\mathrm{Re_p}$ (Figure 5.24).

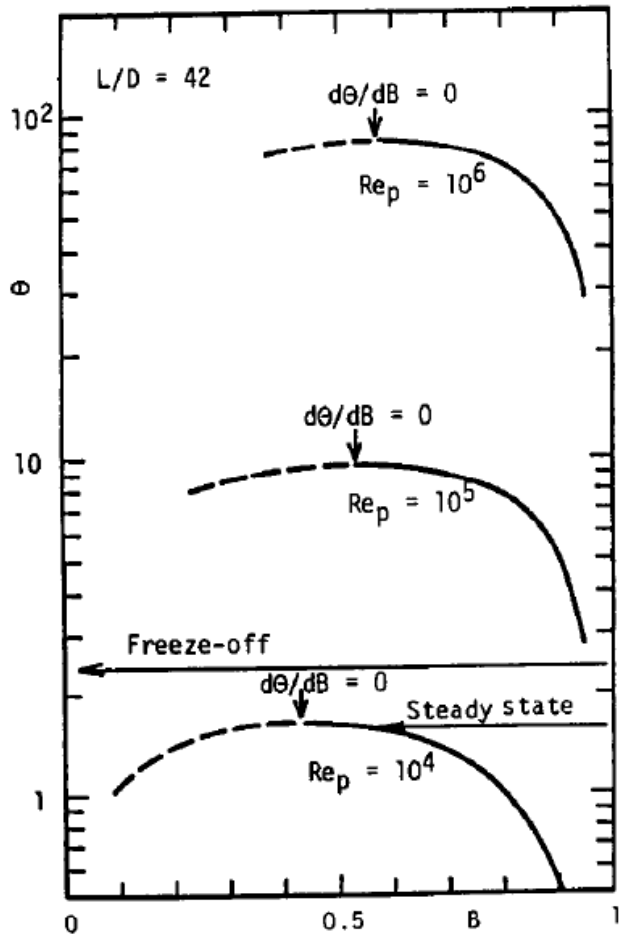

Figure 5.24 *Cooling temperature ratio θ as a function of dimensionless crust radius ($B = R^*$), (Hirata and Ishihara, 1985)*

With guidance from Figure 5.24, Hirata and Ishihara (1985) concludes that steady-state condition must be given from $\mathrm{d\theta/dR^*} = 0$, i.e. that R^* remains constant for certain θ and $\mathrm{Re_p}$. As indicated in Figure 5.24, if steady-state value of θ i.e. $\theta(\mathrm{d\theta/dR^*} = 0)$ is exceeded for certain $\mathrm{Re_p}$, complete blockage occurs. By differentiating eq. (5.51) with respect to R^* and introducing $\mathrm{d\theta/dR^*} = 0$, the steady state number of ice band can be expressed as:

$$n = -\frac{1+\ln R^*}{\left(1-R^{*2}\right)^2+\left(1-R^{*4}\right)\ln R^*} \tag{5.52}$$

$R^* > 0.368$ or $n > 0$

Be eliminating n and R^* in (5.51) and (5.52) using eq. (5.39), the final condition for complete blockage can be obtained and compared with experimental data (Figure 5.25).

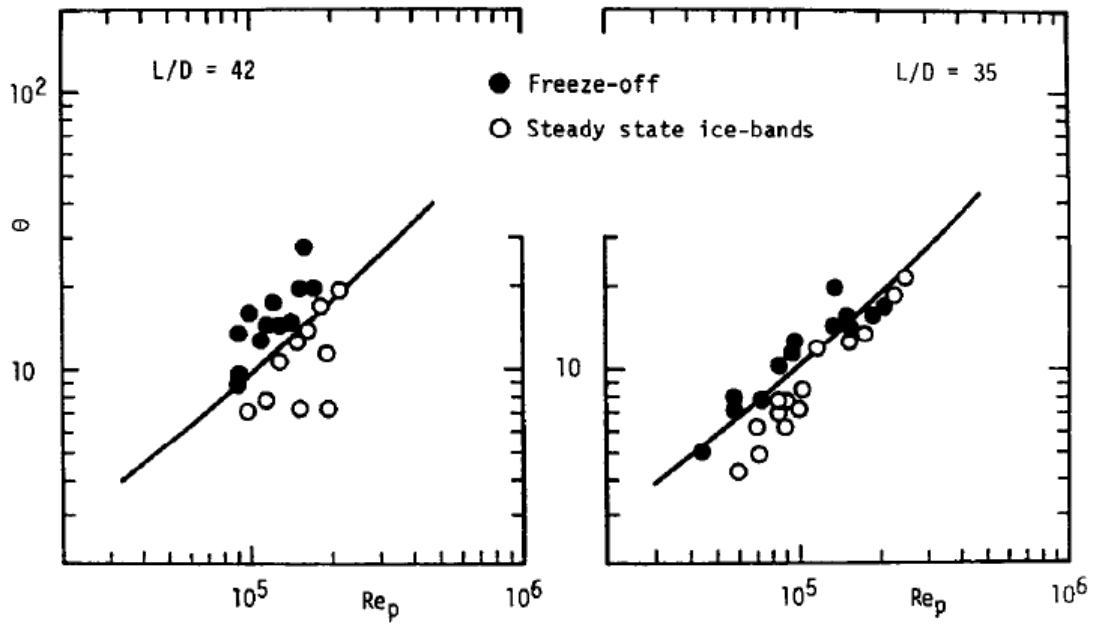

Figure 5.25 *Freeze-off conditions in a pipe containing ice bands (lines) compared with experimental data, (Hirata and Ishihara, 1984)*

Some further discussion about nature of ice-band structure is presented in Hirata and Matsuzawa (1987). The occurrence of ice bands is attributed to transitions in the flow due to presence of the internal solidified layer. A flow is accelerated by presence of an ice layer with monotonously increasing thickness. An initially laminar flow may thus experience transition to turbulent flow resulting in melting of the solid annulus due to enhanced heat transfer. This can produce a sudden expansion in the ice crust as indicated in Figures 5.22 and 5.23. The expansion creates a local flow separation which means that transition to turbulence may occur in a very short distance. The high heat transfer in the separate flow region will melt away rear face of the step until heat balance and thus steady state are established. An initial turbulent flow may as well lead to ice-band structure due to firstly laminarization and subsequent return to turbulence (Hirata and Matsuzawa, 1987).

5.2.3 Relaxing constant wall temperature assumption

Recalling the definition of dimensionless temperature given by Hirata and Ishihara (1985), eq. (5.39), we see that constant wall temperature assumption is relaxed in favor of measured average wall temperatures. This relaxation is however mostly an illusion, because it means that one has nothing else to do than assume some wall temperature, if no experiments on the interesting system are conducted and truly, by using some calculation method we want actually to avoid experiments.

Thomason (1986) is aware that applicability of the theories named so far is restricted due to assumption on constant wall temperature. According to Thomas (1986), a statement that wall temperature is constant during internal solidification process is a poor description of, not least, experimental reality regardless all endeavours to maintain wall temperature constant by coolants. This is especially true when we come to thicker ice layers, as those developing during complete blockage process (Thomason, 1986). To remedy this deficiency, Thomason (1986)

conducted an experimental study aimed to clarify the way in which the external convective condition affects the internal solidification of flowing water. For this purpose he used an experimental set-up quite similar to model in Figure 5.12 with an outer tube enclosing freezing section to make coolant circulation possible. Cooling conditions in terms of coolant temperature and Re was varied and so were inlet conditions of water by varying initial Re between 4000 and 10 000. To present his results, Thomason (1986) defines a dimensionless temperature:

$$T^* = \frac{k_s}{k_l}\frac{T_m - T_c}{T_{f0} - T_m} \tag{5.53}$$

This quantity is almost identical to T_w^* of Des Ruisseaux and Zerkle (1969) with coolant temperature T_c replacing wall temperature as the difference intended to push the dimensionless temperature in the direction of describing outer convection, which is an unique approach when compared to previous authors. The second quantity defined by Thomason (1986) is dimensionless coordinate:

$$Z^* = \frac{\mathrm{Re_0 Pr}}{\mathrm{Re_c Pr_c}}\frac{D}{4L} \tag{5.54}$$

Also here the cooling conditions are present in terms of Reynolds and Prandtl number for coolant in the denominator (and of course water in the nominator). By plotting these defined quantities, Thomason (1986) arrived at the following figure:

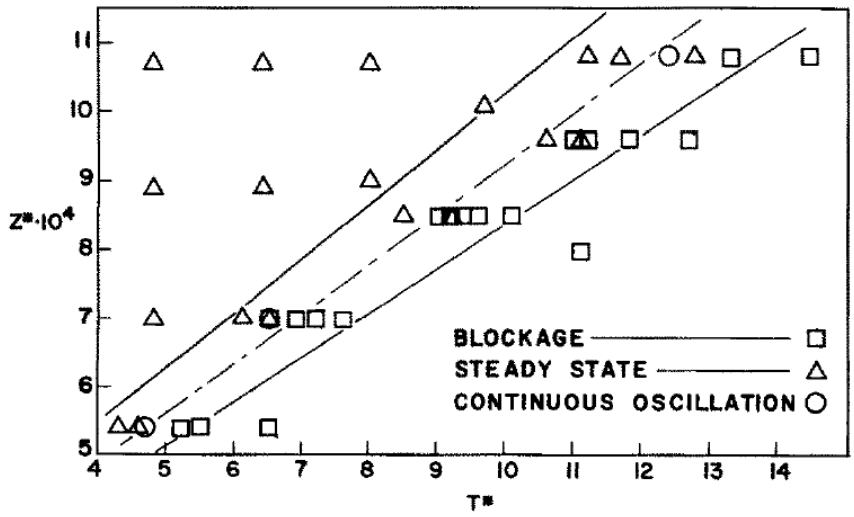

Figure 5.26 *Effects of T^* and Z^* on freezing section response, (Thomason, 1986)*

As seen in Figure 5.26, the experimentally derived complete blockage criterion is basically a linear relationship between quantities defined in expressions (5.53) and (5.54). By continuous oscillation occurring sometimes in the region within the two solid lines in Figure 5.26 it is meant a state where neither steady state nor blockage but continuously oscillating solid annulus occurs.

Sadeghipour et al. (1984) make an effort to include external convection in theoretical model of internal solidification in turbulent, established pipe flow. However, they focus on only steady-state solutions and thus not complete blockage.

5.2.4 Some notes on dendritic ice growth mode

Dendritic ice formation mode in established pipe flow is totally absent in both experimental results and theoretical reflection of the authors named so far. This is however hardly surprising because if Arora and Howell (1973) are correct, the amounts of supercooling to be expected at established flow are quite modest, *vide* our discussion in section 5.1.5. With this in mind, once more pointing out that no author named so far in connection to established flow reported dendrites in experiments, we leave them in peace.

5.2.5 Applicability of the presented models to the treated problem

The obvious weakness of all theoretical models presented here is constant wall temperature assumption, which is rather unlikely valid at established flow in a sprinkler system for other than very short durations. This is also supported by Gilpin's (1981 b) observations which show that no continuous annular ice is to be expected along whole freezing section at conditions realistic for activating sprinkler. Any usage of these models applied to whole pipe length as freezing section must be hence viewed as hardly rewarding and very conservative. Moreover, the annular freezing risk in sprinkler systems after establishment of the flow through the system must be considered as non-existing. Nevertheless, if length of the instantaneous solid annulus as observed in Figure 5.1 (A) could be expressed in some way (based on empirical observation), one should regard possibility of describing its behaviour considering only pipe section when this annular ice shell is present as freezing section. It seems tempting, but as conditions required for such an annular freeze-off is believed to be rather severe and the process sudden, one must consider if the outlined methods apply to this problem. This is due to fact that Zerkle and Sunderland (1968), Epstein and Cheung (1982) and Hirata and Ishihara (1984) use quasi-steady solution methods. At the same time, the researchers taking a transient approach also often assume slowly growing ice profile which does not need to be valid here.

Probably the most fundamental concept presented in this section is that system response to internal solidification can be expressed and visualized in terms of Figure 5.17. Although the curve expressing required pressure drop for certain freezing condition may alter depending on, freezing section length, calculation method etcetera, the basic approach of comparing this curve to pump performance curve must be considered to be very general. Reminding that dendritic ice growth impact on pipes with great possibility also can be expressed in terms of required pressure head to drive the flow, there is a chance for both ice formation modes to be expressed in this straightforward way which is very familiar for the sprinkler industry.

At the same time, review of the work done within this field provides many implications on how the knowledge may be advanced. This regards possible measures regarding both theory and experiments. Just like things were done earlier, steady-state model of Sadeghipour et al. (1984), which accounts for external convection may be possibly extended to include complete blockage criteria. Many hints are provided from the authors who conducted experiments and this considers both dealing with obtained data and purely practical advices. We have so far deliberately restricted description of experimental set-up details. Further discussion on details interesting for our problem will be provided in chapter 8. On presenting results in fruitful and meaningful way, plenty of elegant dimensionless quantities have been provided by our honourable predecessors, Thomason's (1986) convection-including quantities seems especially promising for our problem (after slight modifications), which will be further discussed in chapter 8.

5.3 Further reading

Comprehensive review of ice formation in flows inside pipes and ducts is provided by Weigland et al. (1997). A wider compilation including freezing in other systems than pipe with flow can be found in review of Fukusako and Yamada (1993). Akyurt et al. (2002) describes freezing phenomena more generally while Liley (2005) presents tables with thermophysical properties of ice, liquid water and steam between – 20 ˚C and 50 ˚C.

6. Special interest features of sprinkler systems

Theories and experiments regarding ice formation in pipes, as outlined in the previous chapter, are all concerned with ice growth in a straight pipe section. Thus, they are not representative for sprinkler systems. This is also true for the approach of Des Ruisseaux and Zerkle (1969); although the method is essentially system-oriented with comparing pump characteristic curve with system curve (Figure 5.17), the authors presume a straight freezing section in calculations. In reality, a hydraulic system will of course differ from a straight pipe in several aspects, which reduces the applicability of the presented complete blockage criteria.

6.1 Components generating minor losses

As outlined in section 3.1, the total pressure loss in a system is a sum of wall friction loss and minor losses that can be described by eq. (3.6). The latter are created by all kind of deviations from a straight pipe system: pipe entrance and exits (e.g. nozzles), expansions and contractions (sudden or gradual), bends, elbows, tees and all other fittings. These components complicate of course description of internal solidification in sprinkler systems. Moreover, in this context and research-wise, they have received only limited attention.

6.1.1 Flow contractions

Due to the way in which the water is discharged from sprinkler systems, pipe contractions are commonly present, as seen in Figure 3.6. While significance of contraction as such for the ice growth, either dendritic or annular, is difficult to estimate and account for (see next section), it seems possible to account for subsequent flow velocity changes in ice formation calculations.

6.1.2 Other components

Chida and Tajima (1988) consider *Laminar Flow Blockage in 90° Bend*, as stated by the title. Some results are presented and plotted in dimensionless form; however, the author cannot take part of the results in greater detail because the paper is in Japanese, except abstract and some annotations in the figures. Weigand et al. (1997) review papers concerning freezing in rectangular curved channel sections but the complete blockage problem is ignored. Freezing in diverging rectangular channel without complete blockage seems to constitute a limit regarding geometrical complexity for these problems, which is not surpassed by the existing papers (Weigand et al., 1997). Somewhat general description of freezing process in valves and more complicated nozzles (as water mist nozzles) is hardly imaginable taking into account geometrical complexity and endless possible designs of these components.

Regarding analytical approaches, as assumption of straight freezing section without minor losses in various components therefore seems to be the only way out of this problem. Experimental outlooks will be discussed in chapter 8.

6.2 Water mist systems

Certain characteristics of water mist systems are so extreme compared to water supply systems or other “ordinary” hydraulic systems more or less presumed by the authors, that there arise doubts if, or to which extent, the presented theories can be applied to such systems.

6.2.1 High pressure systems

According to definitions from section 2.3, high pressure water mist systems are systems where the highest pressure occurring in the piping exceeds 34.5 bar (NFPA, 2003), but it should be emphasized that high pressure water mist nozzles operating at 100 bar (10 MPa) are also common (e.g. nozzles in Figure 2.6 & 2.7) which in turn mean even higher pressure in the piping. Presence of pressure of those magnitudes must be viewed in light of the fact that both dendritic and annular ice growth can be viewed as phenomena creating additional pressure drop in the system which result in complete blockage if the resulting total pressure drop exceeds pump head. In other words, complete blockage of high pressure system at reasonable temperature conditions is hardly imaginable.

The decrease in water freezing temperature due to pressure of those magnitudes will be negligible; neither any ice phase other than "ordinary" ice will form, which is realized by studying phase diagram of ice and water, Figure 6.1.

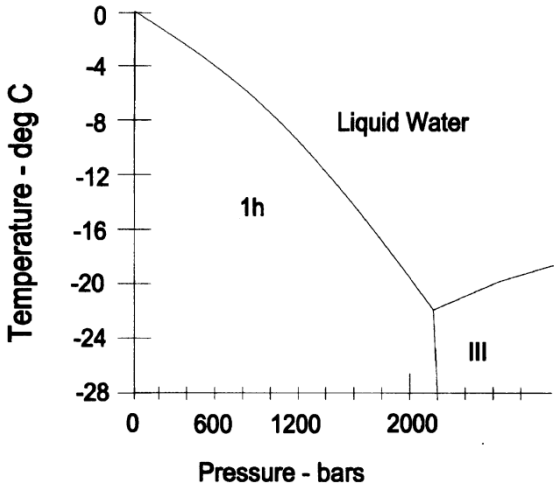

Figure 6.1 *Water-ice phase diagram, after Akyurt et al. (2002)*

At first sight, it is therefore difficult to find anything that may render the presented theories inapplicable at such fundamental level, but we identify at least one "trap" by comparing compressive strength of ice with pressure magnitudes occurring in high pressure systems.

Compressive strength of ice exhibits a strain-rate dependence common for many materials i.e. it increases with increasing strain-rate. Ice failure stresses between 1 MPa and 15 MPa are reported in the literature, for strain-rates ranging between 10^{-6}/s and 10^{1}/s (Kim and Keune, 2007). These values are supported by Schulson (1999) who compiles compressive strength of freshwater ice obtained experimentally by different researchers at approximately – 10 °C, with 9 MPa as the maximum value reported in vicinity of 10^{-3}/s. Values for iceberg ice reported by Jones et al. (2003) are less than 10 MPa observed at the high strain rate of 10^{1}/s. The impact problem (e.g. in studying iceberg-ship collision), which is described by these higher strain-rates, has however nothing to do with pressure build-up ending in (relatively) steady pressure which ice formed in a sprinkler system will be exposed to. Thus, the interesting magnitude of compressive strength of ice is for us a few MPa rather than 10 MPa, which means that it is lower than pressures observed in many high pressure mist systems.

This consideration provides interpretation difficulties. What is to be expected if an ice mode predicted at some pressure and temperature by water-ice diagram, has lower compressive strength than this particular pressure? Will the ice literally be crushed? Anyway, it will hardly disappear or be annihilated. However, for annular ice growth, deviation from regular solid annulus as "peeling off" of ice fragments may be expected.

Insights on dendritic ice blockage during filling may be obtained if the strength of the bonding between the slush-ice matrix and pipe wall is considered. This cannot of course be given a general value, but it is reasonable to assume that strength of the bonding between solid ice and pipe wall consist an upper limit value. U.S. Army Corps of Engineers (2003) conducted experiments in order to determine shear strength of the bond between ice and different materials. The experimental set-up consisted of a vertical pipe with a cylinder piston inside (diameters 30.5 mm and 25.4 mm respectively). The gap between pipe and piston was filled with water which was allowed to solidify and reach a temperature of −10 ˚C before forced was applied on the piston until fracture occurred. The values for bare carbon steel were found in the range between approximately 0.8 MPa and 2.4 MPa with 1.5 MPa as mean value. The values obtained for bond between ice and bare stainless steel, which is the actual material in high pressure systems, were much more gathered and were all in vicinity of 0.5-0.6 MPa.

Let us now assume that hypothetical ice plug of length L_{ip} is instantaneously placed on the way of advancing water front in a high pressure system pipe and also instantaneously creates bond of strength 0.5 MPa with the pipe wall. The piston pump encountering so abrupt resistance will rapidly build up pressure in the pipe until safety valve preventing pump damage activates; let us assume conservatively that pressure at this moment is 160 bar which is normal working pressure for pumps in such applications. By equaling force created due to bond between ice-plug and the wall ($\pi d L_{ip} \tau_{bond}$) with force acting on the ice plug on water side ($\pi (d/2)^2 p_{pump,max}$), we can express required solid ice-plug length required to resist known maximal pressure of the pump for certain inner pipe diameter and bond shear strength:

$$L_{ip} = \frac{p_{pump,max} d}{4 \tau_{bond}} \tag{6.1}$$

L_{ip} length of hypothetical solid ice plug, [m]
$p_{pump,max}$ maximal static pressure than the pump can provide, [Pa]
τ_{bond} shear strength of bond between ice and pipe wall, [Pa]

Using values presented above, the solid ice-plug lengths become 96 mm for 12 mm pipe, 176 mm for 22 mm pipe and 224 mm for 28 mm pipe (inner diameters). In reality, formation of dendritic slush-ice plug at the advancing water front can in no way be compared in severity to the scenario calculated for above using equation (6.1) wherefore analogous lengths of dendritic ice-plugs should be much greater. At the same time, the obtained lengths are considerable and should be compared to at most 50 mm long slush-ice plugs of *dendritic* ice observed by Gilpin (1981 b) in his steel pipe experiments. Thus the possibility of dendritic ice blockage in pipe during filling of a high-pressure water mist system must be assessed as very small. This would not need to apply to bends and contractions if we had to do with the hypothetical solid ice plug, but the real dendritic ice plug must be assessed as rather flexible in comparison.

Recalling Figure 5.1, realistic annular ice growth during filling of a pipe consists of an annular ice shell of some length. If complete blockage occurs due to final contraction of such shell, the values calculated recently can be seen as minimal shell lengths required for complete blockage to not risk be dismissed by slip at the wall. In this case, no judgment can be done considering only this particular phenomenon.

6.2.2 Dry pipe system filling process

Activation of a dry pipe sprinkler system leads to releasing of the enclosed compressed gas (air or nitrogen) through the activated nozzle with resulting decrease in gas pressure in the whole system. This in turn will lead to partial filling of not activated branches, which is schematically shown in Figure 6.2. For configuration in this figure, the degree of water filling of the branches is expected to increase with decreasing distance to the activated sprinkler, as more gas can be evacuated from them prior to arrival of the advancing water front which entraps the remaining gas in the branch. Once the water flow between supply main and the sprinkler is established, a steady state is reached and water flow to sprinkler occurs as indicated with arrow in Figure 6.2. For the partially water-filled branches it means that pressure of the entrapped gas in the branches balances static water pressure in the same branch which in turn must equal pressure of flowing water in cross main just outside the branch.

At the same time as partial filling of inactive branches consumes water during the filling process, the advancing water front still encounter “resistance” from the pressure of the evacuating air. This may be especially apparent in water mist systems due to small flow area of the nozzle restricting gas evacuation and fact that this flow cannot occur at supersonic speeds, assuming the nozzle to be convergent.

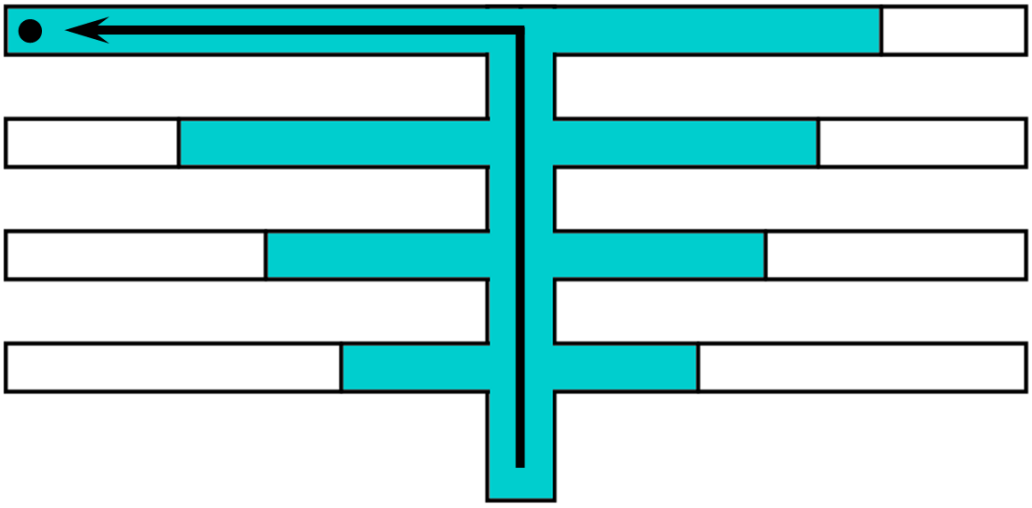

Figure 6.2 *Partially water filled branches after activation of a dry pipe sprinkler system; activated sprinkler uppermost to the left*

These theoretical considerations have very practical implication: arrival of water to the active sprinkler is delayed and thus undesirable and, what is more important, it is difficult to describe analytically.

6.2.3 Nozzles

Conventional fire sprinklers do not appear to cause additional problems to analytical approach as they basically constitute pipe outlets. The way in which flow if "post-processed" by deflector, after leaving the pipe, does not seem to affect the pipe flow and thus internal ice formation significantly. However, this cannot be said about water mist nozzles inside which the water flow pattern deviates greatly from pipe flow, before it is finally discharged. Flow through concentric annuli (i.e. annular space between two concentric cylinders) and subsequent rectangular channels of varying size (down to diameters of fraction of millimetre) are examples of such a flow pattern. The general appearance of water mist nozzles i.e. rather big steel volume compared to small flow area seems risky from the freezing point of view but this risk is hardly analytically accounted for due to this complex flow pattern inside nozzle and is leaved aside here. Usage of equation (6.1) for calculating smallest hypothetical solid ice plug needed to counterbalance the pump pressure gives results of magnitude of few millimetres but there arise uncertainties regarding value of bonding shear strength when we come to such very small dimensions. With such a rough estimation we cannot do any detailed judgment and e.g. question what happens when the flow tries to force a dendritic slush ice through the nozzle remain unanswered.

Of course, complete ice blockage of a heat activated automatic nozzle is very unlike but one cannot forget that there exist open nozzles that are not heat activated. Some experimental and numeric outlooks will be raised in chapters 8 and 9.

7. Complete-blockage calculations

In order to assess freezing risk in sprinkler systems, earlier discussions will be in this chapter complemented with calculations in consistency with previously presented models and representative for sprinkler systems. Recalling incompleteness of these models with respect to our problem, the results presented here must be seen more as platform for further insights than directly applicable guidelines.

7.1 Complete blockage during start-up of a dry pipe sprinkler system

As stated earlier, complete blockage during filling of an initially empty pipe may occur due to dendritic or (more unlikely) annular ice formation (Gilpin, 1981 b). The blocking mechanism of dendritic ice growth at flow conditions has been found to be rather difficult to describe analytically. However, according to our discussion in section 5.1.5, dendritic ice growth as such occurs very fast and therefore this problem will be reduced here to calculation of pipe length required to cool down the flowing water to a temperature range representative for dendritic ice formation resulting in complete blockage. On other hand, by calculating the pipe length required to cool down water flow to freezing point and combine this with model of Epstein et al. (1977), a final penetration length of water front before annular complete blockage will be obtained.

Assuming that the filling process is properly described by a constant wall temperature assumption, equation (4.7) is believed to be valid. Associated Nusselt number correlations ought to be eq. (4.12) for laminar flow and (4.17) otherwise; however, one should have in mind that these are valid for established flow. No Nusselt number correlations valid for penetrating flow conditions have been found in literature. This is possibly explained by very limited interest of this penetration problem as attention in e.g. industry is rather directed towards established, steady-state flow. Nevertheless, one can assess deviation of results obtained by applying correlations (4.12) and (4.17) to pipe filling process by comparison with experimental observations of Gilpin (1981 b).

Figure 7.1 shows calculated water temperature profiles T_f as a function of penetrated distance in the pipe x for different T_p calculated with equation (4.7) using Nusselt numbers according to eq. (4.17). Calculations where done for the four cases where complete blockage occurred in Gilpin's (1981 b) experiments using details provided by Gilpin i.e. flow velocity 0.6 m/s, inner diameters 10 mm and 12.7 mm for steel and plastic pipe respectively, initial pipe temperatures as presented in Figure 7.1 and initial water temperature of 1 °C. Physical properties of water used were those at 0 °C provided by Liley (2005).

Complete blockage occurred 18 m into steel pipe for $T_p = -3$ °C (uppermost curve in Figure 7.1) according to Gilpin (1981 b). A little more severe freezing conditions ($T_p = -4$ °C) gave flow stoppage after 15 m instead. The corresponding, theoretical water temperatures at these locations can be read in Figure 7.1 and are – 3 °C and – 4 °C respectively. According to our previous discussion in section 5.1.5, these temperatures can be seen as reasonable for those when dendritic ice formation is believed to start. This could be seen as a sign that eq. (4.17) predicts Nusselt number correctly for the penetration problem; however, such conclusions cannot be drawn based on only two experiments.

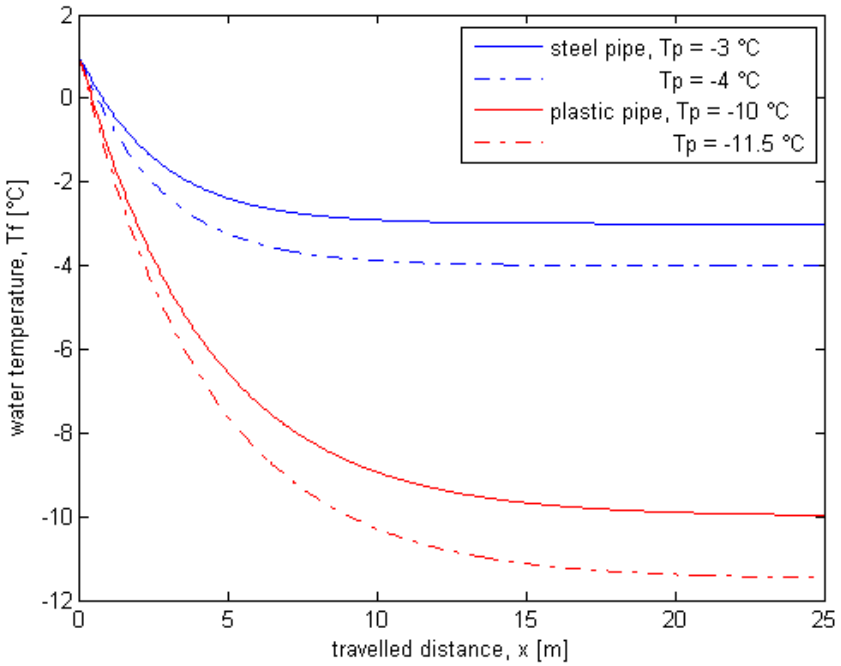

Figure 7.1 *Calculated temperature profiles for Gilpin's (1981 b) experiments resulting in complete blockage of the pipe*

For plastic pipe experiment at $T_p = -10$ °C , complete blockage was observed after 17 m, predeceased by a large amount of dendritic ice formation between 11 and 14 meters into pipe. At $T_p = -11.5$ °C, large amount of dendritic ice was formed between 8 and 11 meters into pipe, however, the final blockage did not occur until $x = 27$ m. Visual observations of Gilpin (1981 b) provides here valuable data and provides information on where the first dendritic ice is observed. As seen in Figure 7.1, predicted water temperatures corresponding to these locations (11 and 8 meters) are –9.5 °C and – 9 °C respectively. These values are hardly any realistic estimation of true water temperature at these locations as water is believed to nucleate at $T_f \geq -4$ °C according to Gilpin (1981 b), if dendritic ice growth is observed. This would indicate that calculations based on equations (4.7) and (4.17) overestimates cooling of water in plastic pipe. A possible explanation may be that constant wall temperature assumption is poor even during filling process of if a pipe is plastic. However, plastic pipes are not interesting for our sprinkler problem and will not be studied any further here.

7.1.1 Dendritic complete blockage

Gilpin (1981 b) observed thus that complete blockage may occur several meters from the site where first dendritic ice started to form. The location of this site is not easily predicted even if we would possess absolute certainty about temperature distribution because it is somewhat random. This means that once water attains (almost) pipe temperature which in the case with steel pipe is equal to higher nucleation point of water, it is not possible to say in deterministic way how long the water front will continue to move before nucleation starts. And if we in some way succeed to predict this, we are not able to judge whether stoppage will occur or not, as we did not succeed to find a sufficient support in former researchers to describe the complete blockage mechanism at dendritic ice growth mode. To that should be added doubtfulness regarding validity of known Nusselt number correlations at filling process and even uncertainty

on flow itself, due to air evacuation problem encountered during start-up of a dry pipe sprinkler system as outlined in chapter 6.

Thus, the results presented below are at best to be seen as rough estimation.

In Table 7.1, we present distances to dendritic ice formation calculated with equation (4.7) using (4.17) to evaluate Nusselt number. Physical properties of water are taken from Liley (2005) and evaluated at 0 °C. Dendritic ice formation is assumed to start at $T_f = -3.9$ °C i.e. in close vicinity of pipe temperature, as deduced from Gilpin's (1981 b) experiments with steel pipe. Table 7.1 presents results representative for flows and diameters in water mist systems.

Table 7.1 *Distances to dendritic ice formation representative for water mist systems,* $T_{f0} = 5$ °C *and* $T_w = -4$ °C

Inner diameter [mm]	Pipe distance to – 3.9 °C (to 0 °C with brackets) [m]		
	Flow rate 8 l/min	**Flow rate 16 l/min**	**Flow rate 24 l/min**
12	18 m (3 m)	19 m (3 m)	18 m (3 m)
22	33 m (6 m)	33 m (6 m)	34 m (6 m)
28	44 m (8 m)	42 m (7 m)	42 m (8 m)

In Figure 7.2, some of results are presented graphically as to remind the reader that the values presented in Table 7.1 are not carved in stone as the temperature becomes almost constant after some penetrated distance making prediction of distance at which dendritic ice formation begins much more difficult. The author takes also opportunity to show that the inlet temperature loses significance quite rapidly with penetration distance as water approaches the wall temperature.

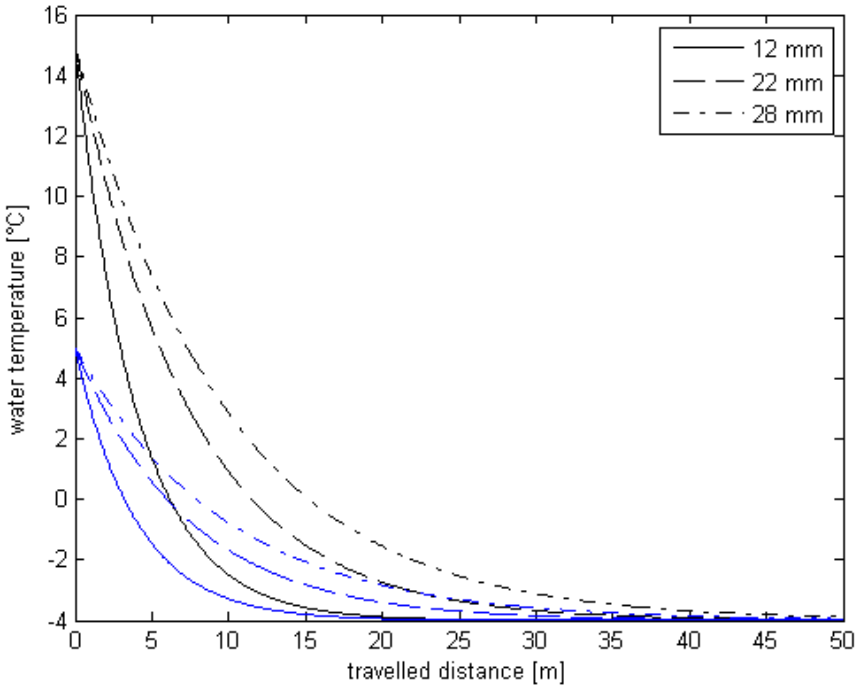

Figure 7.2 *Water temperature as a function of penetrated distance in the pipe at flow rate 8 l/min*

Inlet temperature 5 °C is routinely chosen in calculations as one expected for water from water supply system in Sweden at winter.

Table 7.1 shows similar data for flow rates and diameters encountered in conventional sprinkler systems.

Table 7.2 *Distances to dendritic ice formation representative for water mist systems,* $T_{f0} = 5$ °C *and* $T_w = -4$ °C

Inner diameter [mm]	Pipe distance to – 3.9 °C (to 0 °C with brackets) [m]		
	Flow rate 100 l/min	**Flow rate 200 l/min**	**Flow rate 400 l/min**
25	44 m (8 m)	48 m (9 m)	52 m (9 m)
32	55 m (10 m)	60 m (11 m)	65 m (12 m)
50	83 m (15 m)	89 m (16 m)	96 m (17 m)
65	104 m (18 m)	110 m (20 m)	121 m (22 m)
100	153 m (27 m)	163 m (29 m)	176 m (32 m)
150	223 m (40 m)	234 m(42 m)	250 m (45 m)

7.1.1 Annular complete blockage

In accordance with theory presented and confirmed by experiments by Gilpin (1981 b), the dendritic ice formation mode is expected at very narrow ranges of initial steel pipe temperatures. Especially the interval where complete blockage is to be feared is so constricted that practically only one value of T_w is needed to be considered in previous section. Coming to annular ice formation mode we leave this peculiar behaviour and results will be presented for freezing conditions of increasing severity.

In Table 7.3 we present results of penetration distances representative for water mist systems and calculated using method of Epstein et al. (1977) for wall temperature $T_w = -10$ °C and inlet water temperature as previous. All results presented in the rest of this chapter are based on pressure values needed to maintain an initial flow of stated magnitudes. This is because a more sophisticated approach would require knowledge of pump characteristic and render results less general and less conservative. As Epstein's method presume liquid at its freezing temperature, the results in Table 7.3 consist of penetration lengths calculated with eq. (5.14) added to distances needed to cool down water from 5 °C to 0 °C calculated with equations (4.7) and (4.17). This means that for 8 l/min in 12 mm pipe in Table 7.3, 1.6 m is needed to bring water to its freezing point and further 10 m until complete blockage occurs i.e. 11.6 m in total.

Table 7.3 *Penetration distances at complete blockage according to Epstein et al. (1977) representative for water mist systems,* $T_{f0} = 5$ °C *and* $T_w = -10$ °C

Inner diameter [mm]	Pipe distance to complete blockage (to 0 °C with brackets) [m]		
	Flow rate 8 l/min	**Flow rate 16 l/min**	**Flow rate 24 l/min**
12	11.6 m (1.6 m)	18.2 m (1.7 m)	24 m (1.8 m)
22	14.7 m (3 m)	22.5 m (3 m)	29.1 m (3 m)
28	16.5 m (4 m)	24.5 m (3.7 m)	31.7 m (3.8 m)

The next two tables present similar results but for lower wall temperatures.

Table 7.4 *Penetration distances at complete blockage according to Epstein et al. (1977) representative for water mist systems,* $T_{f0} = 5$ °C *and* $T_w = -20$ °C

Inner diameter [mm]	Pipe distance to complete blockage (to 0 °C with brackets) [m]		
	Flow rate 8 l/min	**Flow rate 16 l/min**	**Flow rate 24 l/min**
12	7.4 m (0.9 m)	11.7 m (0.9 m)	15.5 m (1.0 m)
22	9.4 m (1.7 m)	14.3 m (1.6 m)	18.8 m (1.7 m)
28	10.4 m (2.2 m)	15.7 m (2.1 m)	20.4 m (2.1 m)

Table 7.5 *Penetration distances at complete blockage according to Epstein et al. (1977) representative for water mist systems,* $T_{f0} = 5$ °C *and* $T_w = -40$ °C

Inner diameter [mm]	Pipe distance to complete blockage (to 0 °C with brackets) [m]		
	Flow rate 8 l/min	**Flow rate 16 l/min**	**Flow rate 24 l/min**
12	4.7 m(0.5 m)	7.7 m (0.5 m)	10.1 m (0.5 m)
22	6.0 m (0.9 m)	9.4 m (0.9 m)	12.2 m (0.9 m)
28	6.7 m (1.2 m)	10.1 m (1.1 m)	13.2 m (1.1 m)

In the following three tables, analogical results are presented for flow and pipe diameters more representative for conventional sprinkler systems.

Table 7.6 *Penetration distances at complete blockage according to Epstein et al. (1977) representative for conventional sprinkler systems,* $T_{f0} = 5$ °C *and* $T_w = -10$ °C

Inner diameter [mm]	Pipe distance to complete blockage (to 0 °C with brackets) [m]		
	Flow rate 100 l/min	**Flow rate 200 l/min**	**Flow rate 400 l/min**
25	80.4 m (4.0 m)	131 m (4.3 m)	214 m (4.7 m)
32	86.6 m (5.0 m)	141 m (5.4 m)	230 m (5.8 m)
50	99.5 m (7.3 m)	161 m (7.9 m)	261 m (8.6 m)
65	108 m (9.3 m)	174 m (10.0 m)	282 (10.9 m)
100	125 m (13.7 m)	199 m (14.6 m)	321 m (15.8 m)
150	144 m (20 m)	227 m (21 m)	364 m (22.6 m)

Table 7.7 *Penetration distances at complete blockage according to Epstein et al. (1977) representative for conventional sprinkler systems,* $T_{f0} = 5\ °C$ *and* $T_w = -20\ °C$

Inner diameter [mm]	Pipe distance to complete blockage (to 0 °C with brackets) [m]		
	Flow rate 100 l/min	**Flow rate 200 l/min**	**Flow rate 400 l/min**
25	52.1 m (2.2 m)	85.1 m (2.4 m)	139.7 m (2.6 m)
32	56.2 m(2.8 m)	91.5 m (3.0 m)	149.7 m (3.2 m)
50	64.4 m (4.0 m)	104.3 m (4.4 m)	170.1 m (4.7 m)
65	69.9 m (5.1 m)	112.8 m (5.5 m)	183.7 m (6 m)
100	80.4 m (7.5 m)	128.7 m (8 m)	208.5 m (8.7 m)
150	92.4 m (11 m)	146.4 m (11.6 m)	235.6 m (12.4 m)

Table 7.8 *Penetration distances at complete blockage according to Epstein et al. (1977) representative for conventional sprinkler systems,* $T_{f0} = 5\ °C$ *and* $T_w = -40\ °C$

Inner diameter [mm]	Pipe distance to complete blockage (to 0 °C in brackets) [m]		
	Flow rate 100 l/min	**Flow rate 200 l/min**	**Flow rate 400 l/min**
25	34.2 m (1.1 m)	56.2 m (1.3 m)	92.3 m (1.4 m)
32	36.9 m (1.4 m)	60.3 m(1.6 m)	98.9 m (1.7 m)
50	42.1 m(2.1 m)	68.6 m (2.3 m)	112 m (2.5 m)
65	45.7 m(2.7 m)	74.1 m (2.9 m)	121 m (3.2 m)
100	52.4 m(4 m)	84.3 m (4.2 m)	137 m (4.6 m)
150	59.8 m (5.8 m)	95.6 m (6.1 m)	155 m (6.6 m)

The results for conventional systems presented in Tables 7.6 – 7.8 indicate that annular ice blockage during start-up of such systems must be considered to be extremely unlike as the obtained penetration lengths to complete blockage are large even at considerably severe temperatures despite the fact that Epstein's model assumes constant wall temperature at whole penetrations length which must give exceedingly conservative complete blockage criteria. Thus it should not be viewed as a constraint if future research in this context was restricted to dendritic ice formation mode alone.

Such definitive judgment cannot be done for water mist systems as we cannot quantify a safety margin provided by using the conservative model of Epstein et al. (1977). Certainly, in light of the research of Gilpin (1981 b) and capacity of pumps used in such a systems, this possibility seems to be small but still we do not possess enough knowledge to totally neglect it.

7.2 Established flow

For a constant wall temperature system, it is of course possible that initial establishment of water flow throughout the system succeeds but that complete blockage occurs after that. This cannot be viewed as a reasonable scenario for a sprinkler system at activation. As long as the system it is cooled externally in a freely convective manner, constant wall temperature is very poor assumption as the pipe in reality will be gradually warmed up by the flowing water. But, in

order to deepen "feeling" and insight about the problem, it is anyway rational to do some calculation representative for real sprinkler systems. Tables below present results obtained using model of Epstein and Cheung (1982).

Table 7.9 *Critical constant wall temperatures for 6 m pipe section representative for water mist systems,* $T_{f0} = 5$ °C

Inner diameter [mm]	Critical constant wall temperature (for 6 m section) [°C]		
	Flow rate 8 l/min	**Flow rate 16 l/min**	**Flow rate 24 l/min**
12	−0.9 °C	−2.9 °C	−5.1 °C
22	−0.1 °C	−0.5 °C	−1.3 °C
28	0 °C	−0.2 °C	−0.5 °C

Table 7.10 *Critical constant wall temperatures for 6 m pipe section representative for water mist systems,* $T_{f0} = 5$ °C

Inner diameter [mm]	Critical constant wall temperature (section length in brackets) [°C]		
	Flow rate 100 l/min	**Flow rate 200 l/min**	**Flow rate 400 l/min**
25	−7 °C (6 m)	−18 °C (6 m)	−27 °C (6 m)
32	−7 °C (12 m)	−18 °C (12 m)	−27 °C (12 m)
50	−1.6 °C (6 m)	−4 °C (6 m)	−11 °C (6 m)
65	−0.9 °C (6 m)	−2.2 °C (6 m)	−7 °C (6 m)
100	−0.2 °C (6 m)	−0.9 °C (6 m)	−2.2 °C (6 m)
150	−1.4 °C (3.6 m)	−0.2 °C (6 m)	−0.9 °C (6 m)

Results presented in Tables 7.9 and 7.10 are obtained using Figure 5.20 and simplify usage of these figure, we have used freezing section of varying length, as indicated in brackets.

8. Proposed experimental activities

Many researchers studying internal solidification used experiments in order to confirm their theories or as a step in developing them. The experimental set-ups consisted in the vast majority of cases of heat-exchanger-inspired equipment with external cooling of the freezing section by moving coolant in order to maintain a (nearly) constant wall temperature as assumed in the theories. Of the approaches taken by the researches mentioned in this thesis, there are basically two exceptions from this template: Gilpin (1981 b) and Thomason (1987). Gilpin (1981 b) formulates a problem very representative for start-up of a dry pipe sprinkler systems but has no ambition to develop any general complete blockage criteria. Thomason (1987) establishes such criteria for established flow in purely empirical way, but forced outer convection with flowing coolant is assumed (although no assumption of wall temperature as such is made). We believe that these approaches could be combined to possibly provide further insights in the field.

8.1 Experimental set-up

Naturally, we would like to highlight the experimental set-up of Gilpin (1981 b) as one most representative for testing start-up properties of sprinkler systems at low temperatures (Figure 8.1).

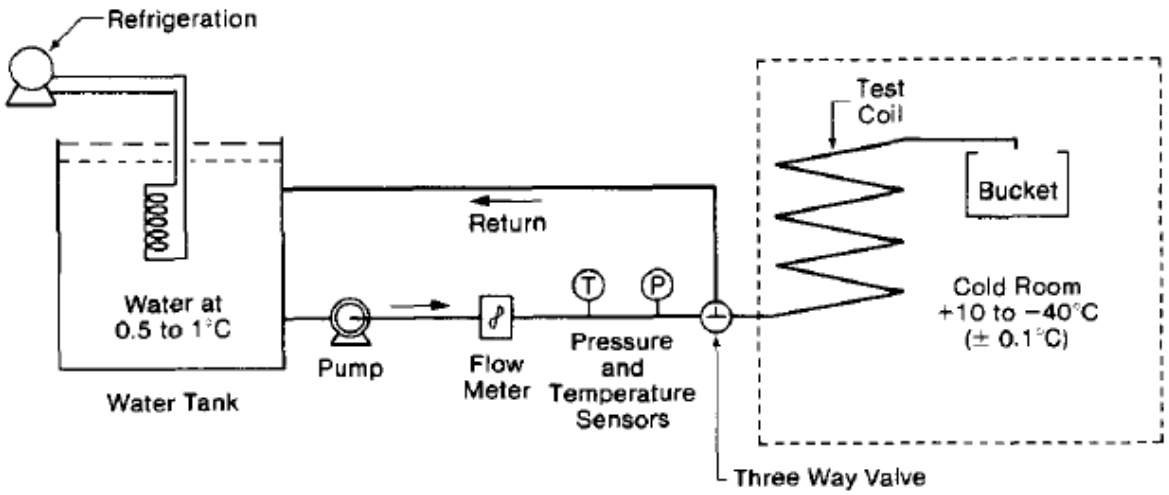

Figure 8.1 *Experimental set-up of Gilpin (1981 b)*

Even if the single pipe (test coil in Figure 8.1) is a rather simplistic representation of real sprinkler systems, it is desirable at least at the beginning as we still cannot definitely predict or dispatch complete blockage for certain freezing conditions. In addition to this, it is quite obvious that the experimental set-up should be assembled from elements that build up real sprinkler systems of the kind one are interested in. This may be especially true for water mist systems that deviate from conventional systems on so many points. However, in this context, the experimental approach should be subject of careful consideration. For example, the presence of water mist nozzle at the end of the test pipe may complicate general observations as the compressed air evacuation phenomenon arises. On other hand this phenomenon must be studied closer if a correct judgment on freezing risk during start-up of water mist systems is to be done. Possibly the best solution is to increase complexity from a set-up almost identical to that of Gilpin (1981 b) to set-ups more and more similar to real sprinkler systems. At the same time, one should consider separate experiments focused on possibility of nozzle complete blockage.

8.2 Measured quantities

Through the prism of Gilpin's (1981 a) observation that the test pipe entrance pressure traces tell the story about ice formation mode inside the test pipe, the presence of pressure sensor at this location is obvious just like the presence of a flow meter.

8.1.1 Temperature measurement and problems associated to it

As to clarify the cooling and freezing process in greater detail, we believe that temperature measurements inside the test pipe are necessary. However, one should have in mind that this is no trivial thing to do in high pressure water mist systems. The thermocouples themselves must be customized for high pressure applications and the same applies to fittings needed to fix it in a robust way. The author assured himself on availability of such integral solutions on the market. As thermal properties of pipe material have very important impact on ice growth mode expected, misgivings should arise before inserting plenty of thermocouples with other properties into the pipe. Let us consider this issue.

By assuming that water has a higher nucleation temperature $T_{n,higher}$ equal to −4 ˚C and that dendritic ice growth results when contact temperature between pipe and penetrating supercooled water is equal to $T_{n,higher}$, Gilpin (1981 b) could calculate that dendritic ice growth mode is to be expected at initial pipe temperatures greater than −4.5 ˚C. The contact temperature becomes so close to the pipe temperature because of superior thermal effusivity of water (equation 5.1). For even better thermal conductors as copper, the contact temperature will be practically equal to the pipe temperature, wherefore Gilpin (1981 b) predicts dendritic ice growth in copper pipes for $T_p > 4$ °C. This means, that as contact temperature between penetrating water and copper thermocouples will be slightly lower than contact temperature between water and steel pipe material, nucleation is to be expected to false start at slightly higher bulk water temperature than if only steel was present inside pipe. However, as difference between steel and copper is little in this context and as thermocouple material will not be continuously present along the pipe length but only at certain locations, it is possible that influence of it will be negligible and undetectable. Copper was taken as example of thermocouple material due of its extreme effusivity ($185 \cdot 10^3$ compared to $11.6 \cdot 10^3$ of steel and $1.54 \cdot 10^3$ of water) but this reasoning will of course apply to all materials with values of effusivity in between those of steel and copper.

On other hand, if we insert into the steel pipe a material with lower value of effusivity than that of steel (e.g. polyethylene), no influence at all on dendritic ice formation will occur, as dendritic ice growth will be induced at contact between water and steel which gives lowest contact temperature. Thus, whether thermocouple itself or material used in associated seals etc. has lower thermal effusivity than water, no influence on dendritic ice growth is to be feared.

If contact temperature between penetrating water and pipe material is $T_{n,lower}$ (assumed −7 ˚C for water) or lower, annular ice growth mode results i.e. a solid ice annulus forms at wall without any supercooling of bulk water volume. Presence of objects inside steel pipe with other thermal properties than steel will not influence this behaviour more than solid ice crust may form around them earlier or later than at the pipe wall depending whether the inserted body has higher or lower thermal effusivity than steel.

Ice crust forming around thermocouples is of course a problem that cannot be neglected due its potential to make measurement of temperature inside pipe impossible in favour of measuring

temperature of solid ice surrounding it. Measuring negative temperatures in supercooled flowing water should not be a problem, so long as nucleation does not start and as we argued before, regarding steel as pipe material, nucleation is not believed to start considerably earlier at thermocouples even if they consist of copper. However, as soon as dendrites start to grow from walls and thermocouples, the bulk temperature measurements in this region lose credibility. But still, we believe that we can map temperature distribution in the penetrating water when dendritic ice formation mode is to be expected, at least until nucleation begins. On other hand, at initial pipe temperatures when the annular ice growth mode is to be expected, solid annulus should form immediately also around the thermocouples if their effusivity is not considerably lower than that of water, which disables temperature measurements of flowing water until the crust is melted away.

The reader should note that reasoning above regards exclusively steel as pipe material. Greater complications may arise if one wishes to insert into a plastic pipe objects with much greater thermal effusivity as they will effectively false start nucleation at degrees of supercooling lower than occurring if only plastic is present inside pipe.

8.3 Experiments

The experiments should primarily focus on possibility of dendritic ice blockage of the system which for steel pipe mean a narrow range of weakly negative Celsius temperatures of the ambient. For high pressure systems where complete dendritic blockage in the pipe is rather unlike, these experiments are still valuable in order to answer the question what can happen if dendritic slush ice is tried to be forced through the nozzle.

The first issue could be to clarify whether equation (4.7) and Nusselt number correlation (4.17) describes properly cooling of the penetrating water front. This can be done at positive Celsius temperatures in order to avoid inevitable delays (i.e. costs) which arise when the system is completely blocked and must be cleared either by rising temperature in the cold room above freezing point or by lifting out whole system outside. Instead, by keeping these initial tests at positive temperatures, the system may be quickly used again after being thoroughly drained and dried by air provided by a compressor. In addition, by using ambient cold room air for this purpose, the system will return rapidly to desirable temperature.

Regarding the “real” experiments focused on dendritic ice blockage, if one wishes physical insights, bulk water temperature at initiation of dendritic ice formation should receive attention as well as time until dendritic ice formation is completed. Presumed that mean temperature in the supercooled volume extending from water front can be determined e.g. through use of equations (4.7), (4.17), mean dendritic ice fraction there should be possible to determine using equation (5.26) which we derived earlier. This fraction could be in turn compared to pressure required to drive the flow. Preferably, this pressure should be expressed in some dimensionless form e.g. that from Figure 5.20, at least to begin with, as it is favourable if both annular and dendritic blockage could be expressed in similar way.

Possibility of annular ice blockage should not be totally neglected, especially not in the water mist nozzles. If studies on it are to be conducted experimentally, one should consider using Thomason’s (1987) way in correlating experimental data, equation (5.53) and (5.54). As with our experimental set-up we have to do with free convection of cooling air rather than with

forced convection of flowing coolant, one should consider if Reynolds number in denominator of eq. (5.54) could not be replaced by Grashof number.

If complete blockage occurs, one can make use of ingenuity of Epstein et al. (1977) to determine penetration distance. These authors did it by simply measuring the weight of the empty pipe and comparing it to weight after occurrence of complete blockage in order to calculate penetration distance using density. Nevertheless, for accurate result, throughout solidification within pipe would be required which is unrealistic and undesirable at experiments of this kind. Therefore, time integrated results from flow meter is possibly the best option.

After every such complete blockage, actually after every test at subfreezing temperature, measures must be taken to render the pipe clean and empty again, let us illustrate this by quotation from Gilpin (1981 b):

> After each test the cold room was allowed to warm to +20 °C while the pipe was thoroughly dried with warm, dry air. Before the next test the pipe was allowed to stand at least two hours at the desired temperature.

This means quite huge effort and costs but it is absolutely necessary if it is to be guaranteed that no ice that can false start nucleation is present in the pipe before the next test begins. One should be also aware of possibility of contamination of the interior of the pipe (e.g. during montage) as impurities introduced may act as nucleation agents modifying nucleation temperature interval of water. Gilpin (1981 b) experimented with silver iodide as nucleation agent in order to move nucleation temperature range closer to equilibrium freezing point and discovered that this effect remained even after dozens of pipe start-ups and did not disappear until several treatment with diluted nitric acid. This illustrates the efficiency of small amounts of particular impurities in changing nucleation behaviour and should urge for high level of laboratory “hygiene.”

Much easier experimental set-up can be used for studying complete blockage at water mist nozzle itself. With this, piping inside cold room can be reduced to rather short pipe with nozzle at the end of it. The temperatures considered should include both those associated with dendritic and annular ice blockage. Regarding dendritic ice blockage, the pipe inside cold room should be sized to order to achieve different supercoolings at the nozzle as we assume that attempts to drive water supercooled at rest, in advance through the pump must fail. This easy set-up should allow possibility of quite extensive tests.

Summarizing, it seems clear that experimental procedure is cumbersome and time-consuming. Hence, attention should be paid to careful planning. In order to shorten the total action time of the climate chamber, it is not impossible that it may be justifiable with two similar systems (i.e. test coils) used parallel so that preparations for next experiments can start at the same time, when the pipe used in previous experiment is disconnected from the water supply and lifted out of the climate chamber for “recovery”. As to end up with optimistic observation, it should be pointed out that the costs of experiments will be clearly influenced in positive direction by fact, that dendritic ice formation mode that seems most crucial, occurs at rather high temperatures which diminishes need and costs of achieving extreme low temperatures in the climate chamber.

9. Conclusion

The conclusion of this thesis is that internal ice formation in a sprinkler system during activation at subfreezing temperatures may occur due to two ice formation modes: the dendritic and the annular one. Of them two, it is the dendritic ice formation mode at moderate subfreezing ambient temperatures in proximity of –4 °C (in steel pipes) that has the greatest potential to cause complete blockage during filling process of a sprinkler system. On contrary, start-up of a system at lower temperatures with resulting annular ice formation mode is believed to be successful. This counterintuitive behaviour depends on fact that large amounts of dendritic slush ice that has been found crucial for flow stoppage during filling of cold pipes is coupled to the phenomenon of supercooling of the flowing water which occurs quite near the freezing point. At the same time, annular ice formation mode results in a wall-bounded ice shell which is continuously melted away and occupies only fraction of the total length penetrated by water front at certain time.

Quantification of pipe freeze-off due to dendritic ice formation mode has been found to be principally straightforward but complicated due to a series of unknowns regarding the dendritic ice growth mechanism i.e. nucleation temperature, time to finished dendritic ice formation and finally creation of bonding with wall resulting in complete blockage. This means that we for certain system cannot with certainty predict whether complete blockage due to dendritic ice growth will happen or not. We managed to demonstrate, that this stoppage mechanism is extremely unlike to occur in a *piping* of a high pressure water mist system, but still not much can be said about possibility of similar stoppage at the *nozzles*. Thus we propose further experiments in order to gather additional insights.

Much literature has been found on annular ice formation mode but applicability to the present problem was heavily restricted by the fact that the authors in general assumed constant wall temperature and established flow. The result was prediction of annular ice behaviour greatly diverging from experimental observations at the filling process. Despite the fact that these assumptions simplify the theoretical analysis, the final results are usually noy in form of any easy expressions and numerical solution procedures are required. This indicates that if theoretical description of the annular ice formation in a pipe during filling process with not constant wall temperature succeeds, the only possible implementation to hydraulic design is a numerical one. So far, we propose experiments. Irrespectively of the fact that annular complete blockage in pipes is unlikely to occur at realistic temperatures, it may still occur in water mist nozzles. At the same time the annular blockage will actually constitute a lower temperature limit of certain sprinkler system operation and it may hence be interesting to clarify this limit for the sake of insight even if it lies at temperatures well below those actual for dry pipe sprinkler operation at severe conditions.

Regarding alternative approaches to this problem, we believe that an analysis using Computational Fluid Dynamics may be successful regarding those cases when annular ice formation mode is to be expected. However, it is a totally different thing when we come to dendritic ice formation mode. There, both temperature at nucleation and model describing formation of dendrites must be included. Moreover, it may be necessary to include a constitutive model of the dendrites in order properly model blockage mechanism with colliding and cumulating dendrites, which means that the approach will impose need of simultaneous CFD and

FEM (Finite Element Method) solution, so called Fluid-Structure Interaction (FSI). The implementation would hence demand so extensive fundamental research work on dendritic ice formation at flow condition that it would most likely be enough to properly describe complete blockage due to dendritic ice formation in simplified analytical way.

Thus, the experimental/analytical continuation of this work is the one recommended by the author as most promising endeavour towards sprinkler systems operable at any conditions.

References

Akyurt M., Zaki G., Habeebullah B. (2002) Freezing phenomena in ice-water systems, *Energy Conversion and Management*, Vol. 43, pp. 1773-1789

Arora A. P. S. & Howell J. R. (1973) An investigation of the freezing of supercooled liquid in forced turbulent flow inside circular tubes, *International Journal of Heat and Mass Transfer,* Vol. 16, pp. 2077-2085

Arvidson M. (2006) *An overview of fire protection of Swedish wooden churches*, SP Report 2006:42, SP Fire Technology, Technical Research Institute of Sweden, Borås, Sweden

Arvidson M. (2008) *The history of the development of modern water mist system technology in Sweden*, SP Fire Technology, Technical Research Institute of Sweden, Borås, Sweden

Arvidson M. & Hertzberg T. (2001) *Släcksystem med vattendimma – en kunskaps-sammanställning*, SP Rapport 2001:26, SP Brandteknik, SP Sveriges Provnings- och Forskningsinstitut, Borås, Sweden (in Swedish)

Bryan J. L. (1990) *Automatic Sprinkler and Standpipe Systems*, NFPA, USA

Callister W. D. Jr. (2004) *Fundamentals of Materials Science and Engineering: An Integrated Approach*, 2nd edition, John Wiley & Sons, USA

CEN, European Committee for Standardization (2004) *Fixed firefighting systems – Automatic sprinkler systems – Design, installation and maintenance*, CEN

Chida K. (1987) Blockage of laminar pipe flow in a piping system by internal fluid solidification, *Heat Transfer: Jap. Res.*, Vol. 15 , pp. 75-87

Chida K. & Tajima M. (1988) Solidification Blockage of Laminar Flow in 90° Bend, *Trans. Japanese Society of Mechanical Engineers*, Vol. 54, pp. 163-171 (in Japanese)

Chul Cho & Özişik M. N. (1979) Transient Freezing of Liquids in Turbulent Flow inside Tubes, *Journal of Heat Transfer*, Vol. 101, pp. 465-468

Chyr P. L. (1998) Limitations and Proper Use of the Hazen-Williams Equation, *Journal of Hydraulic Engineering*, Vol. 124, No. 9, pp. 951-954

Des Ruisseaux N. & Zerkle R. D. (1969) Freezing of Hydraulic Systems, *The Canadian Journal of Chemical Engineering*, Vol. 47, pp. 233-237

Eckert E. R. G. & Drake R. M. JR. (1972) *Analysis of Heat and Mass Transfer*, McGraw–Hill, Tokyo, Japan

Epstein M. & Cheung F.B. (1982) On the prediction of pipe freeze-shut in turbulent flow, *Journal of Heat Transfer*, Vol. 194, pp. 381-384

Epstein M., Hauser G. M. (1977) Freezing of an Advancing Tube Flow, *Journal of Heat Transfer*, Vol. 99, pp. 687-689

Epstein M., Yim A., Cheung F. B (1977) Freezing-Controlled Penetration of a Saturated Liquid Into a Cold Tube, *Journal of Heat Transfer*, Vol. 99, pp. 233-238

Fernandez R. & Bardhunt (1971) The growth rate of ice crystals, *Desalination*, Vol. 3, pp. 330-342

Fukusako S. & Yamada M. (1993) Recent Advances in Research on Water-Freezing and Ice-Melting Problems, *Experimental thermal and Fluid Science 1993*, Vol. 6, pp. 90-105

Gilpin R. R. (1977 a) The Effect of Cooling Rate on the Formation of Dendritic Ice in a Pipe With No Main Flow, *Journal of Heat Transfer*, Vol. 99, pp. 419-424

Gilpin R. R. (1977 b) The effects of dendritic ice formation in water pipes, *International Journal of Heat and Mass Transfer*, Vol. 20, pp. 693-699

Gilpin R. R. (1981 a) Ice Formation in a Pipe Containing Flows in the Transition and Turbulent Regimes, *Journal of Heat Transfer*, Vol. 103, pp. 363-368

Gilpin R. R. (1981 b) Modes of ice formation and flow blockage that occur while filling a cold pipe, *Cold Regions Science and Technology*, Vol. 5 , pp. 163-171

Gordon J. R. (1996) *An Investigation into Freezing and Bursting Water Pipes in Residential Construction*, University of Illinois, Illinois, USA

Hirata T. & Ishihara M. (1985) Freeze-off conditions of a pipe containing a flow of water, *International Journal of Heat and Mass Transfer*, Vol. 28, No. 2, pp. 331-337

Hirata T. & Matsuzawa H. (1987) A Study of Ice-Formation Phenomena on Freezing of Flowing *Water in a Pipe*, *Journal of Heat Transfer*, Vol. 109, pp. 965-970

Holman J. P. (1997) *Heat Transfer*, 8th edition, McGraw –Hill, USA

Isman K. E. (2010) Does Velocity Matter?, *Journal of the National Fire Sprinkler Association*, No. 162, pp. 15-19

Jensen L. (2001) *Dimensionering av sprinklersystem*, Lunds Tekniska Högskola, Lunds Universitet, Lund, Sweden (Swedish)

Jones S. J., Gagnon R. E., A. Derradji A. & Bugden A. (2003) Compressive strength of iceberg ice, *Canadian Journal of Physics*, Vol. 81(1-2), pp. 191–200

Kim H. & Keune J. N. (2007) Compressive strength of ice at impact strain rates, *Journal of Materials Science*, Vol. 42 (8), pp. 2802-2806

Liley P. E. (2005) Thermophysical properties of ice/water/steam from -20 °C to 50 °C, *International Journal of Mechanical Engineering Education*, Vol. 32/4, pp. 45-50

Martinez E. P & Beaubouef (1972) Transient Freezing in Laminar Tube-Flow, *The Canadian Journal of Chemical Engineering,* Vol. 50, pp. 445-449

NFPA, National Fire Protection Association (2003) *NFPA 750: Standard on Water Mist Fire Protection Systems,* NFPA, USA

NFPA, National Fire Protection Association (2007) *NFPA 13: Standard for the Installation of Sprinkler Systems,* NFPA, USA

Özişik M. N. & Mulligan J. C. (1969) Transient Freezing of Liquids in Forced Flow Inside Circular Tubes, *Journal of Heat Transfer*, Vol. 91, pp. 385-390

Quentin B. & Larry W. Mays (2007) Relationship between Hazen-William and Colebrook-White Roughness Values, *Journal of Hydraulic Engineering*, Vol. 133, No. 11, pp. 1270-1273

Sadeghipour, M. S., Özişik M. N., Mulligan, J. C (1984) The effect of external convection on freezing in steady turbulent flow in a tube, *International Journal of Engineering Science,* Vol. 22, No. 2, pp. 135-148

Sampson P. & Gibson D. (1981) A Mathematical Model of Nozzle Blockage by Freezing, *International Journal of Heat and Mass Transfer*, Vol. 24, pp. 231-241

Sampson P. & Gibson D. (1982) A Mathematical Model of Nozzle Blockage by Freezing – II, Turbulent Flow, *International Journal of Heat and Mass Transfer*, Vol. 25, No. 1, pp. 119-126

Schulson E. M. (1999) The Structure and Mechanical Behavior of Ice, *The Member Journal of the Minerals, Metals and Materials Society (JOM)*, Vol. 51 (2), pp. 21-27

Sundén B. (2006) *Värmeöverföring*, Studentlitteratur, Lund, Sweden (Swedish)

Särdqvist S. (2006) *Vatten och andra släckmedel*, Räddningsverket, Kalmar, Sweden (Swedish)

Thomason S. B. (1987) Experimental evaluation of parameters affecting turbulent flow freeze blockage of a tube, *International Journal of Heat and Mass Transfer*, Vol. 30, No. 10, pp. 2201-2205

Thomason S. B., Mulligan J. C., Everhart J. (1978) The Effect of Internal Solidification on Turbulent Flow Heat Transfer and Pressure Drop in a Horizontal Tube, *Journal of Heat Transfer*, Vol. 100, pp. 387-394

U.S. Army Corps of Engineers (2003), *Progress in Evaluating Surface Coatings for Icing Control at Corps Hydraulic Structures*, U.S. Army Engineer Research and Development Center, Cold Regions Research and Engineering Laboratory, Technical Note 03-4, Hanover, New Hampshire, USA

Weigand B., Braun J., Neumann S. O., Rinck K. J. (1997) Freezing in forced convection flows inside ducts: A review, *Heat and Mass Transfer*, Vol. 32, pp. 341–351

White F. M. (2008) *Fluid Mechanics*, 6th edition, McGraw-Hill, New York, USA

Williams G. S., and Hazen A. (1933) *Hydraulic tables*, 3rd edition, Revised, Wiley, New York, USA

Zerkle R. D. & Sunderland J. E. (1968) The Effect on Liquid Solidification in a Tube Upon Laminar-Flow Heat Transfer and Pressure Drop, *Journal of Heat Transfer*, Vol. 90, pp. 183-190